NTNU

Norwegian University of
Science and Technology

Homogenizing metamaterials by the plane wave expansion method

Haakon Aamot Haave

Master of Science in Electronics
Submission date: January 2017
Supervisor: Johannes Skaar, IES
Co-supervisor: Christopher A. Dirdal, IET
Hans Olaf Hågenvik, IET

Norwegian University of Science and Technology
Department of Electronic Systems

Abstract

Increasingly complex metamaterial structures has revitalized the interest in homogenization and effective medium theories, with the intention of finding better ways to model and understand their electromagnetic complexity. This thesis describes an implementation of the plane wave expansion method in MATLAB, employed for simulating the electric field inside one- and two-dimensional periodic metamaterial unit cells. The electric field is excited by an unlocalized plane wave source, and is used to determine the significance of higher order multipoles of the averaged microscopic polarization density through a scheme that employs two different source polarizations. The simulated electric fields in three different unit cells are discussed, and the significance of the simulated higher order terms is interpreted in context of this discussion. The simulations that have been performed in this thesis is used to argue that higher order terms are significant, and have been used in an article that was submitted to Phys. Rev. B in January 2017. The effective permeabilities obtained from two different homogenization formalisms are simulated for two unit cells and used to support the previous results suggesting that higher order terms are significant.

Sammendrag

Den økte kompleksiteten i nyere metamaterialstrukturer har fornyet interessen for homogenisering og effektiv-medium teori, for å forsøke å finne bedre måter å forstå deres elektromagnetiske kompleksitet på. Denne masteroppgaven beskriver en implementasjon av planbølge-ekspansasjons metoden, som blir brukt til å simulere det elektriske feltet i en- og to-dimensjonale metamaterial enhetsceller. Det elektriske feltet blir eksitert av en ulokalisert planbølgekilde, og blir brukt til å bestemme signifikansen til høyere ordens multipoler av den midlede mikroskopiske polariseringstettheten ved å bruke to forskjellige kilde-polariseringer. Det simulerte elektriske feltet i tre forskjellige enhetsceller blir diskutert, og signifikansen av høyere ordens multipol-ledd blir tolket i denne sammenhengen. Simuleringene som har blitt utført i denne masteroppgaven blir brukt til å argumentere for at disse høyere ordens multipol-leddene er betydlige, og har blitt brukt i en artikkel som er innsendt til Phys. Rev. B i januar 2017. Den effektive permeabiliten har blitt beregnet for to enhetsceller, ved å anvende to homogeniseringsformalismer som blir brukt til å understøtte argumentet om at høyere ordens multipol-ledd er betydelige.

Preface

This thesis was written for my master degree in Nanoelectronics and Photonics at NTNU in Trondheim, during the fall semester of 2016. It contains the theoretical background for developing a numerical method for simulating electric fields in periodic metamaterial unit cells, that was created during a preliminary project in the spring semester of 2016. During the course of the master thesis, this numerical method has been thoroughly tested and expanded. The method has later been used to investigate the significance of higher order terms in metamaterial homogenization theory, and contributed with simulation results to the article in appendix B. Due to the close connection between my work and this article, much of the theory in my thesis can also be found in the article.

Since my master thesis has been heavily influenced by the work of my preliminary project, I have included this theory here in order for my thesis to be self-contained and for the report to follow a chronological progression. The process of working with both the preliminary project and my master thesis over the last year has taught me so much, and I feel it is right that the lessons I obtained from both are included here.

I would like to offer my sincere gratitude to my supervisor Johannes Skaar, who has devoted so much of his time and effort to me and my work over the last year. He has taught me alot, and inspired me to work hard. I would also like to extend my gratitude to my co-supervisors Christopher A. Dirdal and Hans Olaf Hågenvik for their guidance and cooperation. They have together contributed with helpful discussions, debugging and proof-reading to my thesis. I feel incredibly lucky to have had such good supervisors for my thesis. I would also like to offer my deepest gratitude to my family and friends for their support throughout my time at NTNU.

Trondheim,
11 of January, 2017

Haakon Aamot Haave

List of Figures

Nomenclature

CSRC Copper split-ring cylinder

DC Direct Current

DFT Discrete Fourier Transform

FFT Fast Fourier Transform

IFFT Inverse Fast Fourier Transform

PWEM Plane Wave Expansion Method

USRR U-shaped split-ring resonator

Contents

1 Introduction

The recent discoveries of novel photonic properties in artificially structured materials along with the capabilities of modern semiconductor manufacturing technology, have given rise to a new paradigm for the design and realization of functional materials with desired photonic properties that are not found in nature. Over the last 20 years, the fields of homogenization and effective medium theories have been revitalized due to the necessity of finding better ways to model the increasingly complex artificially structured materials. In the limit where the structures in such materials become smaller than the wavelength of the radiation propagating within them, artificially structered materials become what is known as metamaterials, allowing the medium to be regarded as one effective substance. The expression *metamaterial* comes from the inherent properties of these materials, some of which cannot be found in nature. The word *meta* itself, is described as a prefix added to the name of something that is analyzed at a higher level [34].

In 1968, V. G. Veselago explored the theoretical consequences of electromagnetic fields propagating in a medium exhibiting a negative refractive index [2], something that was mostly considered as a peculiarity at the time. It was not until around 2000, when J. B. Pendry et al. re-examined the negative refractive index in context of artificially structured media and suggested a possible way to manufacture such a material [13], that the interest for metamaterials started growing. In recent years there have been several improvements of the theoretical treatment of the electromagnetics of metamaterials, taking into account the effects of spatial dispersion, with the intent of understanding metamaterials and beeing able to exploit this knowledge for creating new and exciting photonic effects.

Computational simulations are valuable assets in the development of homogenization and effective-medium theory, since they offer a level of control and accuracy that can be difficult to reproduce in practical experiments. Electromagnetic fields are elusive, and it is often difficult to grasp the completeness of their behaviour in metamaterials analytically.

It is desirable to have a simulation tool that allows the user to define a specific simulation in one end, and obtain a result of the simulation in the other end. For electromagnetic problems, such a tool would have to utilize Maxwell's equations to solve the electric and magnetic fields in a particular system, and output the resulting solutions. The process of constructing such a simulation tool requires an accurate theoretical treatment of the electromagnetic theory, which can later be translated into to a numerical algorithm. When the theory is implemented into a working program, it is necessary to make considerations regarding digital signal processing, numerical calculations and time-effectiveness for optimal performance. The result is a convenient simulation tool that can be used in the process of improving the understanding of the elusive electromagnetic fields in metamaterials.

The objective of this thesis is to improve a simulation software for metamaterials that was implemented in a preliminary project during the spring semester in 2016, in order to both optimalize and expand it for the purpose of investigating the higher order multipoles of the averaged microscopic polarization density obtained from the Landau-Lifshitz averaging-formalism. The simulation software that has been developed in this thesis features a user-defined and unlocalized plane wave source, and also allows the user to define different unit

cells as input.

The scope of this report is to provide a thorough description of the simulation software, as well as present and discuss simulation results. A brief introduction of metamaterials, interesting properties and potential applications will be the main topic of chapter 2, while chapter 3 will present general electromagnetic theory. Chapters 4 and 5 will specialize on electromagnetic theory in metamaterials, and introduce Russakoff-Jackson homogenization [1, 8] along with Casimir and Landau-Lifshitz formulations of effective parameters [6, 7, 9]. The theory presented in chapters 4 and 5 will also closely follow the theory introduced in an article submitted to Phys. Rev. B in January 2017 attached in Appendix B. Chapters 6, 7 and 8 will explain the algorithm for solving the inhomogeneous wave equation in one- and two-dimensional metamaterial unit cells, and provide a detailed description of the implementation in MATLAB. Chapter 9 describes the algorithm and implementation that allows for simulating the higher order multipoles of the averaged microscopic polarization density. Simulation results and discussions are provided in chapter 10, while the concluding remarks are given in chapter 11.

2 Metamaterials

A metamaterial can be described as a medium consisting of functional structures much smaller than the wavelength of incident electromagnetic radiation, such that the medium as a whole can be regarded as one effective medium. Metamaterials are interesting because they can under certain circumstances exhibit properties that are not found in nature. A thorough understanding of metamaterials rely heavily on principles of homogenization- and effective medium theory, which provides the tools of determining the electromagnetic fields propagating inside metamaterials. Before delving into electromagnetic theory, it is useful to develop a basic understanding of what exactly metamaterials are in general, and it will therefore be the objective of this section to provide a conceptual introduction of metamaterials and their usage.

2.1 Conceptual description

At the most fundamental level, all matter consist of an infinite number of atoms. In this microscopic world, atoms may be situated in molecular arrangements and lattices, or floating around arbitrarliy entirely independent from each other [1]. It is the compositition of various atoms that determines if the material is a solid, gas or a liquid, an insulator or a conductor. The entire nature of a material, and especially its electromagnetic properties, can be traced back to its atomic composition [1].

Now consider a medium comprising microscopical structures instead of atoms. For the time beeing, it is ample to limit the description of these structures only to stating that they may be arranged arbitrarily as long as they are *sufficiently small* in size. Given that this requirement is fulfilled, these structures could be made out of any type of matter and have any type of geometric shape. It turns out that these structures are also able to determine the electromagnetic properties of the material, much like the way the atomic composition does for a regular material.

It is beneficial to return to the atomic-level analogy to explain the requirement of having sufficiently small structures. The atom consists of electrons, protons and neutrons which are in an uninterrupted oscillating condition due to thermal agitation, orbital motion and zero-point vibration [1]. The oscillation of these charged particles are the origin of the electromagnetic fields. With this in mind, it seems reasonable that the detectable electromagnetic fields must pertain to the rapid oscillation of the charged particles in the atom. This is however not the case.

Upon closer inspection, it is found that the spatial oscillations occur at distances less than $1\,[\text{nm}]$ and that the temporal oscillations occur in periods shorter than $1\,[\text{ps}]$ [1, p. 249]. Such small variations are not present in any detectable signal because the transition from the atomic scale to the detection scale effectively averages the electromagnetic fields, leaving only a smoothly varying envelope of the original field [1].

In a metamaterial, the exact same effect occurs when the detection scale is significantly greater than the size of the structures that it is comprised of. If an electromagnetic wave of wavelength λ propagates through a metamaterial containing structures shorther in length than the distance a, it can be argued that the averaging of the electromagnetic fields will occur in the *long wavelength limit*, where $\lambda \gg a$.

2.2 Metamaterial properties and potential applications

Metamaterials are interesting because they under certain circumstances feature remarkable electromagnetic properties, which cannot be found in natural materials. This section will briefly highlight some of these properties, and describe some potential applications.

2.2.1 Negative refractive index

Metamaterials are capable of having negative refractive indices. The physical consequences of a negative index material was first investigated by V. G. Veselago in 1968 [2], while J. B. Pendry published an article in 2000 which discussed applications of such a material in greater detail [13] . The effect of a negative index metamaterial can be exemplified by using Snell's law

$$n_1 \sin(\theta_1) = n_2 \sin(\theta_2), \tag{1}$$

describing the refraction of a ray of light through a planar interface from a medium with refractive index n_1 to a medium with refractive index n_2, where θ_1 and θ_2 are the angles of incidence respectively [5]. If $n_1 = 1$ and $n_2 = -1$, it can be seen by inserting into equation (1) that

$$\theta_2 = \arcsin(-\sin(\theta_1)) = -\theta_1 \tag{2}$$

which means that the ray of light is refracted in the opposite direction. The general effect of the negative refractive index can be seen by considering figure 1, where it is seen that rays of light can be refocused by inserting a negative index medium on the optical axis.

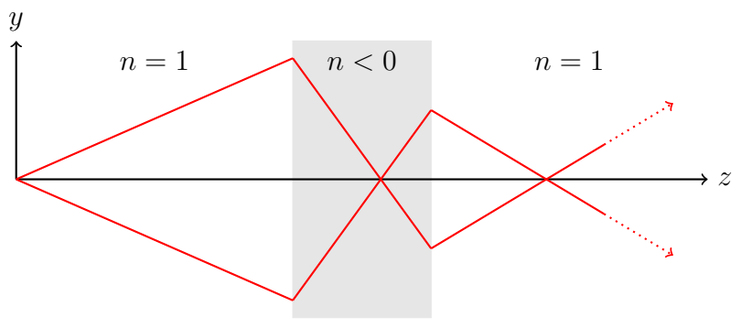

Figure 1: Refraction of light rays in a medium with $n < 0$ [13].

It has been shown by J. B. Pendry in [13] that a negative refractive index $n = \sqrt{\epsilon\mu}$ arises from an effective permittivity $\epsilon = -1$ and an effective permeability $\mu = -1$, and consequently that negative index media is able to amplify evanescent waves such that sub-wavelength imaging is made possible. Such metamaterials can potentially be employed to improve the resolution in microscopes, which could be highly beneficial for the semiconductor industry.

2.2.2 Anisotropic metamaterials

An Anisotropic material is characterized by having a permittivity ϵ and permeability μ that are dependent on the direction of incoming electromagnetic radiation [5]. Metamaterials offer the possibility of controlling the effective permittivity ϵ and permeability μ, and can therefore be used exploit their anisotropic properties to create interesting effects.

One way to make such an effect, is to create ϵ and μ such that they introduce a coordinate transform in the effective material. A coordinate transform can be regarded as a distortion of the coordinate system, such that a straight arrow in the original coordinate system, becomes a crooked arrow in the transformed coordinate system. A commonly used coordinate transform is one that maps a point in a two-dimensional plane onto a disc of a inner radius $\hat{R}_1$ an outer radius $\hat{R}_2$ outside the point itself [30, 31]. This coordinate transform can be expressed as

$$\hat{\mathbf{r}} \rightarrow \hat{\mathbf{r}}'(\hat{\mathbf{r}}, \hat{\theta}) = \hat{R}_1 + \frac{\hat{R}_2 - \hat{R}_1}{\hat{R}_2}\hat{\mathbf{r}}, \tag{3}$$

where $\hat{\mathbf{r}}$ is the radial coordinate and $\hat{\theta}$ is the azimuthal coordinate [32]. The effect of this coordinate transform is that it will manipulate an incident electromagnetic field into propagating around the region where $\hat{\mathbf{r}} < \hat{R}_1$, thus isolating this region from electromagnetic radiation [30, 32].

If ϵ and μ exhibit this behaviour for frequencies in the visible spectrum, this device will basically function as an invisibility cloak for objects located in the region where $\hat{\mathbf{r}} < R_1$ [32]. For other frequencies, this device can possibly function as a radiation shield since it diverts incident radiation away from the center region. Anisotropic metamaterials can therefore arguably offer interesting applications in both space- and military related technologies.

3 Theory

This section will introduce the microscopic electromagnetic theory, providing the basis for the remainder of this thesis.

3.1 Maxwell's equations

The propagation of microscopic electromagnetic fields are governed by the microscopic Maxwell equations, which are given by [4, p. 399]

$$\nabla \times \mathbf{e} = i\omega \mathbf{b} \qquad \text{Faraday's Law,} \tag{4a}$$

$$\nabla \times \mathbf{b} = \mu_0 \mathbf{j} - i\omega\varepsilon\mu_0 \mathbf{e} \qquad \text{Ampere's Law,} \tag{4b}$$

$$\nabla \cdot \mathbf{e} = \frac{\rho}{\varepsilon} \qquad \text{Gauss's Law,} \tag{4c}$$

$$\nabla \cdot \mathbf{b} = 0 \qquad \text{No Isolated Magnetic Charge,} \tag{4d}$$

in a linear, isotropic and non-magnetic medium [1], where

- $\mathbf{e}$ is the microscopic electric field intensity $[\mathrm{V\,m^{-1}}]$,
- $\mathbf{b}$ is the microscopic magnetic flux density $[\mathrm{N\,A^{-1}\,m^{-1}}]$,
- ρ is the microscopic charge density $[\mathrm{C\,m^{-2}}]$,
- $\mathbf{j}$ is the microscopic current density $[\mathrm{A\,m^{-2}}]$,

and a harmonic time-dependence $\exp(-i\omega t)$ has implicitly been assumed. All charges are directly included into $\mathbf{j}$ and ρ [1, p. 251-258]. These four equations provide a starting point for solving any microscopic electromagnetic problem, and form the foundation for the theory that will be presented in the subsequent chapters.

3.2 The wave equation in homogeneous media

Maxwell's microscopic equations in (4) completely determine how the microscopic electric and magnetic fields traverse through space and time. The microscopic electric field $\mathbf{e}$ and the microscopic magnetic field $\mathbf{b}$ are coupled to each other through Faraday's law (4a) and Ampere's law (4b), enabling the possibility of solving for one of them if the other one is known. It is however, often desirable to be able to solve for only $\mathbf{e}$ or $\mathbf{b}$ at a given time. This section will suggest a remedy for this problem by combining Faraday's law with Ampere's law.

If the medium in question is assumed to be a homogeneous medium described by a constant microscopic permittivity ε and a microscopic permeability μ_0, it follows that equation (4b) can be expressed as

$$\nabla \times \mathbf{b} = -i\omega\varepsilon\mu_0\mathbf{e}, \tag{5}$$

where it has been assumed that the current density $\mathbf{j} = 0$. Taking the curl on both sides of equation (4a) and inserting equation (5) yields

$$\nabla \times \nabla \times \mathbf{e} = \omega^2\varepsilon\mu_0\mathbf{e}. \tag{6}$$

By employing the vector identity, $\nabla \times \nabla \times \mathbf{A} = \nabla(\nabla \cdot \mathbf{A}) - \nabla^2\mathbf{A}$ [4, p. 335], and using that the surface charge density $\rho = 0$, the equation for $\mathbf{e}$ can be written

$$\nabla^2\mathbf{e} + \omega^2\varepsilon\mu_0\mathbf{e} = 0, \tag{7}$$

where the wavenumber $k = \omega\sqrt{\varepsilon\mu_0}$ is defined. Equation (7) is known as Helmholtz equation, and is a special case of the wave-equation resulting from the assumed harmonic time-dependence. In this equation $\varepsilon\mu_0 = \frac{1}{v^2}$, where v is the speed of the wave in the medium characterized by ε and μ_0. In the special case where $\varepsilon = \epsilon_0$ and $\mu = \mu_0$, the speed will identical to the speed of light in vacuum, such that $v = c = \frac{1}{\sqrt{\mu_0\epsilon_0}}$. Inserting the speed v in equation (7) yields

$$\nabla^2\mathbf{e} + \frac{\omega^2}{v^2}\mathbf{e} = 0, \tag{8}$$

An analogous relation can also be obtained for $\mathbf{b}$ by substituting into equation (4b), and using the same procedure as the one above,

$$\nabla^2\mathbf{b} + \frac{\omega^2}{v^2}\mathbf{b} = 0. \tag{9}$$

Not only does equations (8) and (9) allow for solving for $\mathbf{e}$ and $\mathbf{b}$ seperately, given a microscopic permittivity ε, but they also establish that electromagnetic fields are essentially propagating waves. The latter fact will become useful in the subsequent chapters. It can quickly be verified that a solution that satisfies equation (9) is a travelling plane wave

$$\mathbf{c}_{\text{pw}} = \hat{\mathbf{c}}\exp\left(i\mathbf{k}\cdot\mathbf{r}\right) \tag{10}$$

where $\hat{\mathbf{c}}$ is a constant amplitude, the wavevector $\mathbf{k} = k_x\hat{\mathbf{x}} + k_y\hat{\mathbf{y}} + k_z\hat{\mathbf{z}}$, and that an analogous solution also exist for $\mathbf{b}$ in equation (9) [4, 5].

3.3 Skin depth in conducting materials

Helmholtz equation in (7) can also be expressed as

$$\nabla^2 \mathbf{e} + k^2 \mathbf{e} = 0, \tag{11}$$

where $k = \omega\sqrt{\varepsilon\mu_0}$. The wavenumber k is generally a complex quantity [4, p. 367], which allows expressing $k = k' + ik''$. It follows that k can be written as a general complex number

$$k = k' + ik'' = i\omega\sqrt{\epsilon_0\mu_0 \cdot \big(1 + \frac{\sigma}{i\omega\epsilon_0}\big)}, \tag{12}$$

where σ is the electrical conductivity measured in [S/m] [4, p. 367]. Conducting materials such as Cu, Au and Ag are characterized by having very good conductivities σ, with numerical values well beyond 10^6 [S/m] [4, 27]. It will will be the objective to explore the wavenumber in a conducting material in the following.

By assuming that $\frac{\sigma}{\omega\epsilon_0} \gg 1$, it is possible to neglect the contribution of 1 to the sum under the square root in equation (12). The wavenumber k can then be expressed

$$k \simeq i\omega\sqrt{\mu_0\epsilon_0}\sqrt{\frac{\sigma}{i\omega\epsilon_0}} = \sqrt{i}\sqrt{\omega\mu_0\sigma} = \frac{1+i}{\sqrt{2}}\sqrt{\omega\mu_0\sigma}, \tag{13}$$

such that

$$k = k' + ik'' \simeq (1+i)\sqrt{\pi f\mu_0\sigma}, \tag{14}$$

where it is used that $\omega = 2\pi f$ and where the relation $\sqrt{i} = \exp(i\pi/2) = (1+i)/\sqrt{2}$ has been employed [4, p. 369]. It is seen from equation (14) that $\mathrm{Re}[k] = \mathrm{Im}[k] = \sqrt{\pi f\mu_0\sigma}$ [4, p. 369]. In order to appreciate the significance of this result, it is necessary to consider the solution of Helmholtz equation in equation (10), which suggests that the solution $\mathbf{e} = e_x\hat{\mathbf{x}}$ of equation (11) can be written

$$e_x = \hat{c}_x \exp(i(k' + ik'') \cdot x) = \hat{c}_x \exp(-k''x) \cdot \exp(+ik'x). \tag{15}$$

The exponential factor in e_x now has two equally important terms. The factor $\exp(+ik'x)$ signifies a travelling plane wave in complex notation, analogous to equation (10). The other factor, $\exp(-k''x)$, is not a complex number, and will approach zero when x increases. For good conductors, it follows that a high conductivity σ results in a high numerical value of k''. The amplitude of the electric field therefore undergoes an exponential decay with increasing values of x. It is convenient to define a parameter that describes how quickly the electric field decays in a conducting material. This is done by considering the distance δ that the electric field must propagate within a material before the amplitude decreases by a factor of $\exp(-1)$. This distance δ is given by

$$\delta \equiv \frac{1}{k''} = \frac{1}{\sqrt{\pi f\mu_0\sigma}}, \tag{16}$$

and is known as the skin depth of the conducting material and is measured in meters [4, p. 370]. Equation (16) illustrates that the skin depth decreases as the conductivity increases. Although equation (16) is only accurate for travelling plane waves of the form given in equation (10), the skin depth is an important characteristic of all conducting materials, and will be employed later in this thesis.

3.4 Inhomogeneous media

An inhomogeneous medium is a medium that comprises several sub-media, which exhibit different electromagnetic properties Inhomogenious media are characterized by a position dependent microsopic permittivity $\varepsilon(\mathbf{r})$, which implies that an electromagnetic wave travelling in an inhomogeneous medium will experience a different permittivity at different positions $\mathbf{r}$. The wave equation for inhomogeneous media can be obtained by taking the curl of equation (4a) and inserting equation (4b) and $\varepsilon = \varepsilon(\mathbf{r})$, such that

$$\nabla \times \nabla \times \mathbf{e} - \frac{\omega^2}{c^2}\varepsilon(\mathbf{r})\mathbf{e} = i\mu_0\omega\mathbf{j}. \tag{17}$$

All materials are essentially inhomogeneous due to the spatial variations of the atomic structure. However, for wavelengths that are sufficiently larger than the interatomic distance, say 10 times larger or more, the radiation will average the effects of the rapid variations in space and the material will appear to be homogeneous [6]. This means that the $\mathbf{r}$ dependence of ε can be neglected, and that the permittivity can be considered as constant throughout the medium. For structures where the wavelength of the incident radiation is approaching the characteristic length of the structure itself, it is still necessary to solve equation (17) in order to determine the electric and magnetic fields. In the case where there is an external source $\mathbf{j}_{\text{ext}}$ exciting the electric field, equation (17) can be written as

$$\nabla \times \nabla \times \mathbf{e} - \frac{\omega^2}{c^2}\varepsilon(\mathbf{r})\mathbf{e} = i\mu_0\omega\mathbf{j}_{\text{ext}}. \tag{18}$$

Solving equation (18) can often be quite difficult, since it includes a forcing term on the right side. The solution to the wave-equation in a specific type of inhomogeneous medium will be described in the following subsection.

3.4.1 Solutions in periodic inhomogeneous media

It is not uncommon that inhomogeneous media are arranged in periodic structures, instead of beeing randomly placed throughout space. The periodicity of the medium proves to be important for the solutions of the electromagnetic fields that can propagate inside it. For the electric field $\mathbf{e}(\mathbf{r})$ in a non-magnetic dielectric inhomogeneous medium, the periodicity of the medium will manifest itself through a microscopic permittivity $\varepsilon(\mathbf{r})$ that is periodic with period $\mathbf{T}$, such that $\varepsilon(\mathbf{r} + \mathbf{T}) = \varepsilon(\mathbf{r})$.

It can be shown that a solution that satisfies equation (17) is,

$$\mathbf{e}(\mathbf{r}) = \mathbf{V}(\mathbf{r}) \cdot \exp\left(+i\mathbf{k} \cdot \mathbf{r}\right), \tag{19}$$

where the function $\mathbf{V}(\mathbf{r})$ is also periodic, such that $\mathbf{V}(\mathbf{r} + \mathbf{T}) = \mathbf{V}(\mathbf{r})$ [5, 14, p. 265,p. 167]. The period of $\mathbf{V}(\mathbf{r})$ will be the same as the period of the microscopic permittivity $\varepsilon(\mathbf{r})$.

The theory presented in this section is a part of Bloch's theorem and the solution given in (19) is known as a Bloch, or Floquet solution [14, 15]. This type of solution is used to describe the periodic potential in atomic lattices [14], and the propagation of electromagnetic radiation in photonic crystals [5].

3.5 Dispersive media

Dispersion is a phenomenon in electromagnetic theory that involves scattering of the electromagnetic radiation. Dispersion manifests itself in two ways: In temporally dispersive media, the material exhibits a lag between an applied electric field and a resulting polarization density, indicating a material-memory [5, p. 160]. In spatially dispersive media the electric field at a point in space will depend on the fields in the surrounding points in space, suggesting a certain coupling in the material [12]. The first part of this section will briefly explain temporal dispersion and motivate the use of Fourier theory in order to describe the second part, which will focus on describing spatial dispersion in greater detail.

3.5.1 Temporally dispersive media

A temporally dispersive medium exhibits a delay in the response of the polarization density to a applied electric field. More precisely, the polarization density $\mathbf{p}(t)$ at a given time t can be expressed as a weighted sum of the electric field $\mathbf{e}(t)$ at other times [3, p. 100]. Mathematically this is written as a convolution between the two fields [5, p. 161], such that

$$\mathbf{p}(t) = \epsilon_0 \int_{-\infty}^{\infty} \chi(t - t')\mathbf{e}(t')dt'. \tag{20}$$

where $\chi(t) = \varepsilon(t) - 1$ is the time-dependent electric susceptibility [4, p. 110]. The response of a polarization density $\mathbf{p}(t)$ to an applied electric field $\mathbf{e}(t)$ can be regarded as a linear system. By transforming $\mathbf{e}(t)$, $\mathbf{e}(t)$ and $\chi(t)$ into the Fourier domain it is found that

$$\mathbf{p}(\omega) = \epsilon_0 \chi(\omega) \cdot \mathbf{e}(\omega), \tag{21}$$

by applying the convolution theorem [11, p. 249]. This linear system is described by a transfer function $\epsilon_0\chi(\omega)$ that produces an output $\mathbf{p}(\omega)$ when an input $\mathbf{e}(\omega)$ is applied. The Fourier transform $\mathbf{e}(\omega)$ is determined from [5, p. 1122],

$$\mathbf{e}(\omega) = \int_{-\infty}^{\infty} \mathbf{e}(t) \exp{(i\omega \cdot t)} dt, \tag{22}$$

where similar transforms also exist for both $\epsilon_0\chi(\omega)$ and $\mathbf{p}(\omega)$.

The application of the one-dimensional Fourier transform enables the use of a multiplication instead of a convolution, which can simplify equation (20) considerably. The temporal dispersion of the microscopic permittivity is not the topic of this thesis, but is included here in order to motivate the use of the Fourier transform. It is also important to keep in mind that all media generally will exhibit temporally dispersive properties, and that neglecting this can be a source of error in any analysis.

3.5.2 Spatially dispersive media

In the previous section, the nonlocal time dependence between the microscopic polarization density $\mathbf{p}(t)$ and the microscopic electric field $\mathbf{e}(t)$ was described, and it was found through Fourier theory that they could be related through a convolution. The very same analogy will be applied in this section to describe the phenomena of spatial dispersion. It will be assumed that the electromagnetic fields are functions of both $\mathbf{r}$ and t, and it is also assumed that the temporal Fourier transform in equation (20) has already been performed, such that $\mathbf{e} = \mathbf{e}(\mathbf{r}, \omega)$ and $\varepsilon = \varepsilon(\mathbf{r}, \omega)$.

A spatially dispersive medium is a medium where the spatial dependence between $\mathbf{p}$ and $\mathbf{e}$ is nonlocal [1, 6, 12]. This means that the value of $\mathbf{p}$ at a given point in space does not only depend on $\mathbf{e}$ at the same point, but also on $\mathbf{e}$ in the points in a surrounding neighborhood [1, 6, 12]. Similarly to the temporally dispersive medium, the relation between $\mathbf{p}$ and $\mathbf{e}$ in a spatially dispersive medium can be written as [12]

$$\mathbf{p}(\mathbf{r}, \omega) = \int \epsilon_0(\varepsilon(\mathbf{r} - \mathbf{r}', \omega) - 1)\mathbf{e}(\mathbf{r}', \omega)d^3\mathbf{r}', \tag{23}$$

where $\varepsilon(\mathbf{r}, \omega) = (\chi(\mathbf{r}, \omega)+1)$. Equation (23) is a three-dimensional convolution, which implies that the microscopic polarization $\mathbf{p}(\mathbf{r}, \omega)$ is a weighted sum of the electric field $\mathbf{e}(\mathbf{r}, \omega)$ in all of the points $\mathbf{r}'$ surrounding $\mathbf{r}$. In order to determine $\mathbf{p}(\mathbf{r}, \omega)$, all of the contributions from the electric field intensity in the surrounding region must be added. The integration limits are limited to a surrounding region V, including all possible contributions to $\mathbf{p}(\mathbf{r}, \omega)$. In order to apply the convolution theorem [11] on equation (23), the spatial Fourier transforms $\mathbf{e}(\mathbf{k}, \omega)$ and $\varepsilon(\mathbf{k}, \omega)$ is determined from [5, 12],

$$\mathbf{e}(\mathbf{k}, \omega) = \int \mathbf{e}(\mathbf{r}, \omega) \exp(-i\mathbf{k} \cdot \mathbf{r})d^3\mathbf{r}, \tag{24a}$$

$$\varepsilon(\mathbf{k}, \omega) = \int \varepsilon(\mathbf{r}, \omega) \exp(-i\mathbf{k} \cdot \mathbf{r})d^3\mathbf{r}, \tag{24b}$$

with a similar expression for the microscopic magnetic field [5, p. 44]

$$\mathbf{b}(\mathbf{k}, \omega) = \int \mathbf{b}(\mathbf{r}, \omega) \exp(-i\mathbf{k} \cdot \mathbf{r})d^3\mathbf{r}, \tag{25}$$

The wavevector is a vector in reciprocal space, also referred to as k-space, and denotes the direction of propagation for the electromagnetic wave. It is emphasized that any field displaying a $\mathbf{k}$ dependence in the following sections must be considered as having undergone a Fourier transformation analogous to the ones in equation (24). Inserting the Fourier transforms into equation (23) and applying the convolution theorem [11, 12], yields the relation between $\mathbf{p}$ and $\mathbf{e}$ for spatially dispersive media in Fourier space

$$\mathbf{p}(\mathbf{k}, \omega) = \epsilon_0(\varepsilon(\mathbf{k}, \omega) - 1) \cdot \mathbf{e}(\mathbf{k}, \omega). \tag{26}$$

It is worth emphasizing that $\mathbf{k}$ and ω must be regarded as two independent variables [6, 12], and that the general relation $k = \frac{2\pi}{\lambda} = \omega\sqrt{\mu_0\varepsilon}$ is no longer necessarily valid. Although equation (26) completely describes the relation between $\mathbf{p}$ and $\mathbf{e}$ in a spatially dispersive medium, the subsequent derivations in this thesis will assume that the media included within the metamaterial does not exhibit spatial dispersion. The relation between the microscopic polarization and the microscopic electric field in a non-spatially dispersive medium simplifies into

$$\mathbf{p} = \epsilon_0 \chi \mathbf{e}, \tag{27}$$

which is what will be used in the following sections. The discussion of spatially dispersive media is included here because metamaterials will generally be spatially dispersive at a macroscopic level, as will be explored later in this thesis.

The application of the Fourier analysis that has been shown in this section is very convenient when solving electromagnetic problems. In addition to providing convenient tools for analyzing dispersive materials, it also offers an interpretation of electromagnetic fields as sums of plane waves containing different spatial frequencies. The latter is not only a valuable way of understanding electromagnetism, but also a mathematical consequence that will be employed extensively later in this thesis.

3.5.3 Expressing fields in k-space

In the previous section it was shown that it is convenient to express electromagnetic fields as sums of plane waves containing different spatial frequencies, in what was referred to as k-space. It is advantageous to develop expressions for Maxwells equations (4a) - (4d) in k-space. In order to express equations (4a)- (4d) in k-space, it is necessary to determine the corresponding curl and divergence operators. This can be done by assuming that the fields are plane waves of the form given in equation (10), and inserting into Maxwells equations. The curl and divergence operators in k-space are found in the two steps below.

- **Curl operator in k-space**

  Assuming an electric field $\mathbf{e}$ of the form given in equation (10) having components e_x, e_y, e_z, and inserting into the left side of equation (4a) yields,

  $$\nabla \times \mathbf{e} = \hat{\mathbf{x}}\left(\frac{\partial e_z}{\partial y} - \frac{\partial e_y}{\partial z}\right) + \hat{\mathbf{y}}\left(\frac{\partial e_z}{\partial x} - \frac{\partial e_x}{\partial z}\right) + \hat{\mathbf{z}}\left(\frac{\partial e_y}{\partial x} - \frac{\partial e_x}{\partial y}\right). \tag{28}$$

  Differentiating with respect to x,y and z in each component, yields

  $$\nabla \times \mathbf{e} = i\Big(\hat{\mathbf{x}}\big(k_y e_z - k_z e_y\big) + \hat{\mathbf{y}}\big(k_x e_z - k_z e_x\big) + \hat{\mathbf{z}}\big(k_x e_y - k_y e_x\big)\Big), \tag{29}$$

  from which it can be seen that

  $$\nabla \times \mathbf{e} = i\mathbf{k} \times \mathbf{e}. \tag{30}$$

- **Divergence operator in k-space**

  Assuming the same electric field $\mathbf{e}$ of the form given in equation (10), and calculating the left side of equation (4c) yields

  $$\nabla \cdot \mathbf{e} = ik_x e_x \hat{\mathbf{x}} + ik_z e_y \hat{\mathbf{y}} + ik_z e_z \hat{\mathbf{z}}, \tag{31}$$

  where it is seen that the following relation must hold,

  $$\nabla \cdot \mathbf{e} = i\mathbf{k} \cdot \mathbf{e}. \tag{32}$$

The two steps above show that the nabla operator $\nabla = i\mathbf{k}$ in k-space, such that the microscopic Maxwell equations now can be expressed as

$$i\mathbf{k} \times \mathbf{e} = i\omega\mathbf{b}, \tag{33a}$$

$$i\mathbf{k} \times \mathbf{b} = \mu_0\mathbf{j} - i\omega\varepsilon\mu_0\mathbf{e}, \tag{33b}$$

$$i\mathbf{k} \cdot \mathbf{e} = \frac{\rho}{\varepsilon}, \tag{33c}$$

$$i\mathbf{k} \cdot \mathbf{b} = 0. \tag{33d}$$

3.6 Low-pass filtering and windowing

When performing numerical calculations involving Fourier transforms on a computer, it might in some cases be necessary to reduce the amount of Fourier coefficients of a given quantity in order to make the simulation more time-efficient. A convenient way of reducing the number of Fourier coefficients is by employing a low-pass filter. If a function $F(x_m)$ and its Fourier transform $F(k_m)$ is represented digitally by an integer number M data points, it is possible to reduce number of Fourier coefficients by applying a filter

$$W(k_m) = \begin{cases} 1 & \text{if} \quad k_m \leq k_{filter}, \\ 0 & \text{if} \quad k_m > k_{filter}. \end{cases} \tag{34a}$$

The application of this filter is depicted in figure 2, where it is seen that every component of $F(k_m)$ for k_0 up to k_{filter} is extracted.

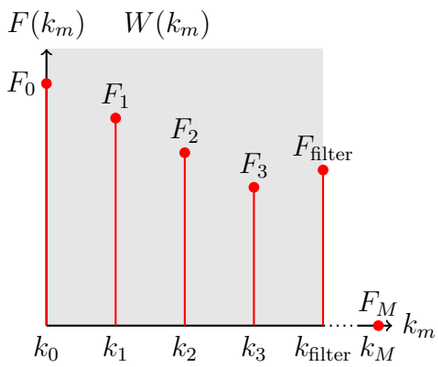

Figure 2: Coefficients of $F(k_m)$.

Figure 2 describes a typical low-pass filter, which is a rudimental yet very effective method for reducing the amount of Fourier coefficents in $F(k_m)$ [11, 24]. This low-pass filter signifies a typical trade-off, since the abrupt removal of higher order harmonic coefficients results in a deterioration of the original function $F(x_m)$ [11, 24].

The filter described above multiplies $[F_1, .., F_{\text{filter}}]$ by a factor of 1, and the coefficients $[F_{\text{filter}+1}, ..., F_M]$ by a factor of 0. By applying the convolution theorem, it can be argued that the multiplication of $F(k_m)$ and $W(k_m)$ corresponds to a convolution between $F(x_m)$ and the function $W(x_m)$ in the real domain, where $W(x_m)$ is the inverse Fourier transform of $W(k_m)$ [11, 24]. It can be shown that $W(x_m)$ is in this case a sinc-function, that slowly oscillates towards zero and therefore deteriorates the signal [26, 33].

It is possible to minimize the deterioration from the filter by employing a modified version of $W(k_m)$, which multiply higher order harmonics with an increasingly smaller amplitude, such that the inverse transform $W(x_m)$ becomes a function of finite extent in the real domain. Figure 3 depicts the application of a simple triangular function $W_{\text{triangular}}(k_m)$ which will gradually reduce the amplitudes of higher order Fourier coefficients and reduce the deterioration of the original function $F(x_m)$ [24].

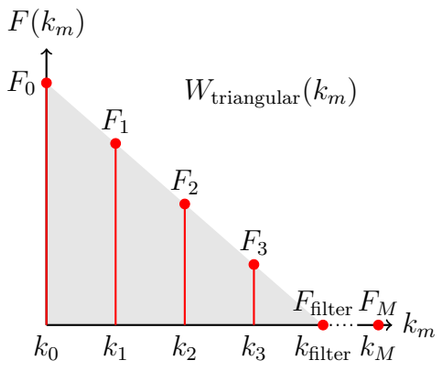

Figure 3: Coefficients of $F(k_m)$ after applying a triangular window $W_{\text{triangular}}(k_m)$.

This process is frequently used in digital signal theory, and is known as windowing [24]. The triangular window function depicted in figure 3 is intended only as a simple example, and it is worth mentioning that windowing functions that are similar to Gaussian or Lorentzian functions are more commonly used in real applications [24].

4 Homogenization of electromagnetic fields in metamaterials

The electric and magnetic fields in equation (4) that have been used to describe various electromagnetic phenomena so far, are accurate and expressive when it comes to describing microscopic electromagnetism. The propagation of electromagnetic radiation in metamaterials however, require a slightly different approach. The theory that is introduced in this chapter will be based on the homogenization approach suggested by G. Russakoff [8] and J. D. Jackson [1], and closely follow the derivations provided in the article in Appendix B.

If the microscopic electromagnetic radiation within the metamaterial is assumed to be well into the long wavelength regime, it follows that the effective macroscopic field that propagate inside the metamaterial becomes the average of the microscopic field. The average $\langle F(\mathbf{r})\rangle$ of a spatially varying function $F(\mathbf{r})$ is selected such that it is defined by

$$\langle F(\mathbf{r})\rangle = \int f(\mathbf{r}')F(\mathbf{r}-\mathbf{r})d^3\mathbf{r}', \tag{35}$$

where $f(\mathbf{r})$ is a nonzero test function, e.g. a Gaussian, and its integral over the entire space is unity [1, 6, 7]. The averaging integral in (35) is only over the spatial coordinates $\mathbf{r} = x\hat{\mathbf{x}} + y\hat{\mathbf{y}} + z\hat{\mathbf{z}}$ and not over the temporal variable t. The reason for this is because the spatial variations of the charged particles are considerably larger than their temporal variations, resulting in the latter beeing washed out by the spatial averaging [1]. By inserting the derivative operator $\frac{\partial}{\partial \mathbf{r}}$ into the integral in (35), can be seen that

$$\frac{\partial}{\partial \mathbf{r}}\langle F(\mathbf{r},t)\rangle = \int f(\mathbf{r}')\frac{\partial}{\partial \mathbf{r}}F(\mathbf{r}-\mathbf{r}')d\mathbf{r}' = \langle \frac{\partial}{\partial \mathbf{r}}F(\mathbf{r})\rangle, \tag{36}$$

indicating that the derivatives of the macroscopic fields are simply the average of the derivatives themselves [1]. The averaging procedure that has been described here is at the core of the Russakoff-Jackson homogenization theory, and can be employed for several types of metamaterials [1, 6]. The objective of the following section will now be to derive the macroscopic Maxwell's equations by applying the averaging in equation (35) to the Maxwell's microscopic equations in (4).

4.1 Maxwell's equations in periodic metamaterials

Having introduced the theory required to obtain the solutions of the electromagnetic fields inside a general metamaterial, the next task at hand is to derive the macroscopic Maxwell equations. The following discussion will specialize to periodic metamaterials, where the periodic structures can be broken down into identical unit cells. It will for the remainder of this thesis be assumed that the unit cells are cubic, and that the inclusions contained in these unit cells are linear, isotropic and non-magnetic. The fields that propagate inside the metamaterial are assumed to be excited by the externally applied source $\mathbf{J}_{\text{ext}}$, containing only a single spatial Fourier component:

$$\mathbf{J}_{\text{ext}} = \bar{\mathbf{J}}_{\text{ext}} \exp(i\mathbf{k}\cdot\mathbf{r}), \tag{37a}$$

$$\rho_{\text{ext}} = \bar{\rho}_{\text{ext}} \exp(i\mathbf{k}\cdot\mathbf{r}), \tag{37b}$$

where $\mathbf{J}_{\text{ext}}$ and ρ_{ext} are the source current and charge densities, and $\overline{\mathbf{J}}_{\text{ext}}$ and $\overline{\rho}_{\text{ext}}$ are constants. The source is assumed to be controllable and purely macroscopic. Since the metamaterial is periodic, it follows that the solution of the microscopic electromagnetic fields can be described as Floquet waves $F(\mathbf{r})$ of the form

$$F(\mathbf{r}) = V(\mathbf{r}) \exp(i\mathbf{k}\cdot\mathbf{r}), \tag{38}$$

where $V(\mathbf{r})$ is the periodic modulation function included in the microscopic fields, and share the same periodicity as the metamaterial [23, 14]. Considering that both the source $\mathbf{J}_{\text{ext}}$ and the microscopic field solutions $\mathbf{e}$ and $\mathbf{b}$ are Floquet waves, it is argued by Silveirinha in [6, 7] that the averaging procedure in equation (35) can now be written as

$$\langle F(\mathbf{r})\rangle = \bar{F} \exp(i\mathbf{k}\cdot\mathbf{r}), \tag{39}$$

where,

$$\bar{F} = \frac{f(\mathbf{k})}{V} \int_V F(\mathbf{r}) \exp(-i\mathbf{k}\cdot\mathbf{r}) d^3\mathbf{r}, \tag{40}$$

where $f(\mathbf{k})$ is the fourier transform of the test function $f(\mathbf{r})$, and V is the volume of the unit cell. In order for this averaging to be valid, it is necessary to require that the fields are in the long wavelength limit, $\lambda \gg a$, where a is the length of one side of the cubic unit cell. By using the relation $|\mathbf{k}| = \frac{2\pi}{\lambda}$, it can be seen that this requirement is fulfilled when $(|\mathbf{k}| \cdot a) \ll 2\pi$. For the sake of simplicity, only $\mathbf{k}$-values contained in the first Brillouin zone will be considered, and the test function $f(\mathbf{r})$ is chosen such that $f(\mathbf{k}) \simeq 1$ in this analysis [6]. By employing the averaging procedure described by equation (39) and (40) on the microscopic fields in (4), along with the fact that they are periodic Floquet waves, gives

$$i\mathbf{k} \times \mathbf{E} = i\omega\mathbf{B}, \tag{41a}$$

$$i\mathbf{k} \times \frac{\mathbf{B}}{\mu_0} = -i\omega\epsilon_0\mathbf{E} - i\omega\langle\mathbf{p}\rangle + \mathbf{J}_{\text{ext}}, \tag{41b}$$

where the macroscopic fields $\mathbf{E} = \langle\mathbf{e}\rangle$ and $\mathbf{B} = \langle\mathbf{b}\rangle$ are defined, and the relation $\mathbf{j} = i\omega\mathbf{p}$ obtained from charge conservation has been used [3, 23]. The nabla operator has been expressed in terms of $i\mathbf{k}$. The effective electromagnetic response of the system is contained in $-i\omega\langle\mathbf{p}\rangle$, which now will undergo the same averaging procedure. Inserting $\mathbf{p}$ into equation (40) gives

$$\langle \mathbf{p}(\mathbf{r}) \rangle = \frac{\exp(i\mathbf{k}\cdot\mathbf{r})}{V} \int_V \mathbf{p} \exp(-i\mathbf{k}\cdot\mathbf{r}) d^3\mathbf{r}, \tag{42}$$

and by Taylor-expanding the exponential term as $\exp(-i\mathbf{k}\cdot\mathbf{r}) \simeq 1 - i\mathbf{k}\cdot\mathbf{r} - (\mathbf{k}\cdot\mathbf{r}^2)/2$ [1], it is found that

$$\begin{aligned} \frac{\exp(i\mathbf{k}\cdot\mathbf{r})}{V} \cdot \left(\int_V \mathbf{p} d^3\mathbf{r} - i\mathbf{k}\cdot \int_V \mathbf{r}\mathbf{p} d^3\mathbf{r} - \frac{1}{2}\int_V (\mathbf{k}\cdot\mathbf{r})^2 \mathbf{p} d^3\mathbf{r} \right) \\ \equiv \mathbf{P} - \frac{\mathbf{k}\times\mathbf{M}}{\omega} - i\mathbf{k}\cdot\mathbf{Q} + \mathbf{R}, \end{aligned} \tag{43}$$

where the tensor $\mathbf{rp}$ has been decomposed into its antisymmetric and symmetric parts,

$$\begin{aligned} \mathbf{k}\cdot\mathbf{r}\mathbf{p} &= \mathbf{k}\cdot\frac{(\mathbf{r}\mathbf{p} - \mathbf{p}\mathbf{r})}{2} + \mathbf{k}\cdot\frac{(\mathbf{r}\mathbf{p} + \mathbf{p}\mathbf{r})}{2} \\ &= -\frac{\mathbf{k}\times\mathbf{r}\times\mathbf{p}}{2} + \mathbf{k}\cdot\frac{(\mathbf{r}\mathbf{p} + \mathbf{p}\mathbf{r})}{2}, \end{aligned} \tag{44}$$

and where the following properties can be identified:

$$\mathbf{P} = \frac{\exp(i\mathbf{k}\cdot\mathbf{r})}{V}\int_V \mathbf{p} d^3\mathbf{r} \qquad \text{Electric Dipole,} \tag{45a}$$

$$\mathbf{M} = -i\omega\frac{\exp(i\mathbf{k}\cdot\mathbf{r})}{2V}\int_V \mathbf{r}\times\mathbf{p} d^3\mathbf{r} \qquad \text{Magnetic Dipole} \tag{45b}$$

$$\mathbf{Q} = \frac{\exp(i\mathbf{k}\cdot\mathbf{r})}{2V}\int_V (\mathbf{r}\mathbf{p} + \mathbf{p}\mathbf{r}) d^3\mathbf{r} \qquad \text{Electric Quadropole,} \tag{45c}$$

$$\mathbf{R} = -\frac{\exp(i\mathbf{k}\cdot\mathbf{r})}{2V}\int_V (\mathbf{k}\cdot\mathbf{r})^2 \mathbf{p} d^3\mathbf{r} \qquad \text{Higher order terms.} \tag{45d}$$

The electric dipole, magnetic dipole and electric quadropole are commonly included in the expansion of $\langle \mathbf{p} \rangle$, while it is uncommon to include the higher order terms $\mathbf{R}$. It is convenient to define the combined quantity

$$i\mathbf{k}\cdot\mathbf{Q}^{\text{tot}} \equiv \frac{\mathbf{k}\times\mathbf{M}}{\omega} + i\mathbf{k}\cdot\mathbf{Q}, \tag{46}$$

which includes both the magnetic dipole and electric quadropole into one tensor $\mathbf{Q}^{\text{tot}}$ [23], which can be expressed as

$$\mathbf{Q}^{\text{tot}} = \frac{\exp(i\mathbf{k}\cdot\mathbf{r})}{V}\int_V \mathbf{r}\mathbf{p} d^3\mathbf{r}, \tag{47}$$

in its integral form. It is convenient to express equation (43) in component form,

$$\langle p_i \rangle = P_i - \frac{\varepsilon_{ijk} k_j M_k}{\omega} - ik_j Q_{ij} + R_i, \tag{48}$$

where ε_{ijk} is the Levi-Civita symbol and summation over repeated indices is implied [23]. The quantities P_i, Q_{ij}^{tot} and R_i can also be expressed using their constitutive relations

$$P_i = \epsilon_0 \chi_{ij} E_j + \zeta_{ikj} k_k E_j + \eta_{iklj} k_k k_l E_j, \tag{49a}$$

$$Q_{ij}^{tot} = \alpha_{ijk} E_k + i\gamma_{ijlm} k_l E_m, \tag{49b}$$

$$R_i = \psi_{iklj} k_k k_l E_j, \tag{49c}$$

where it is assumed that the medium is linear [23], and where

$$Q_{ij}^{\text{tot}} = Q_{ij} - \frac{i\varepsilon_{ijk}M_k}{\omega}. \tag{50}$$

The tensor elements ζ_{ikj} and α_{ijk} describe magneto-electric coupling between the fields [23]. Equation (49) shows that the contributions of $\mathbf{P}$, $\mathbf{Q}^{\text{tot}}$ and $\mathbf{R}$ to the averaged microscopic polarization $\langle \mathbf{p} \rangle$, can be divided into $\mathcal{O}(k^0)$, $\mathcal{O}(k^1)$ and $\mathcal{O}(k^2)$ contributions. The assumption of having an electromagnetic wave in the long wavelength limit, immidiately restricts the wavevector $\mathbf{k}$ from being large. This suggests that the $\mathcal{O}(k^2)$ terms in (49) must be considerably smaller than the remaining terms included in $\langle \mathbf{p} \rangle$, effectively making entire $\mathbf{R}$ and the $\mathcal{O}(k^2)$ term in $\mathbf{P}$ negligible. This is however not necessarily true under all circumstances, as will be demonstrated in the following section.

4.2 Significance of higher order terms

For this demonstration it is convenient to consider a one-dimensional periodic metamaterial, consisting of slabs of different permittivities ϵ_1 and ϵ_2 as depicted below:

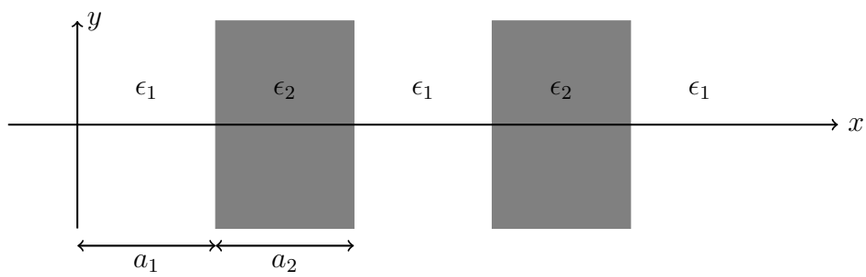

Figure 4: One-dimensional metamaterial, comprising slabs of thickness a_1 and a_2 with permittivities ϵ_1 and ϵ_2 which extends infinitely to the left and right.

If the wavevector $\mathbf{k} = k_x\hat{\mathbf{x}}$ such that it is assumed to be in the direction of periodicity, and the fields are assumed to be tangential to the unit cell boundaries such that $\mathbf{k} \perp \mathbf{p}$ [23], it is possible to rewrite equation (46) into

$$\frac{\mathbf{k} \times \mathbf{M}}{\omega} + i\mathbf{k} \cdot \mathbf{Q} = \frac{\mathbf{k} \times 2\mathbf{M}}{\omega}. \tag{51}$$

The interpretation of this rewriting is that the contribution to $i\mathbf{k} \cdot \mathbf{Q}^{\text{tot}}$ from the magnetic dipole $\mathbf{M}$ and the electric quadropole $\mathbf{Q}$ is identical. Inserting these contributions into equation (43) gives

$$\langle p \rangle = P + \frac{2k_x M}{\omega} + R, \tag{52}$$

where the integrals of the expansion terms given in equation (45) simplify to [23]

$$P = \frac{\exp(ik_x x)}{a} \int p(x)dx, \tag{53a}$$

$$M = -i\omega \frac{\exp(ik_x x)}{a} \int \frac{xp(x)}{2} dx, \tag{53b}$$

$$R = -\frac{k_x^2 \exp(ik_x x)}{2a} \int x^2 p(x)dx. \tag{53c}$$

when the axis of periodicity is taken to be the x-axis. It is also possible to express P, M and R by using the constitutive relations in equation (49),

$$P = \epsilon_0 \chi E + \zeta k E + \eta k_x^2 E, \tag{54a}$$

$$2M = -i\omega\alpha E + \gamma k_x \omega E, \tag{54b}$$

$$R = \psi k_x^2 E, \tag{54c}$$

where (51) and (49b) have been used to find equation (54b). Under very special circumstances, it is reasonable to assume that the microscopic electric field is of the form $e = \bar{E}\exp(ik_x x) = E$ where $\bar{E}$ is a constant value. This assumption corresponds to an electric field of the same form as in equation (38), except that in this case the periodic modulation $V(\mathbf{r})$ is constant. It is therefore clear that this problem is simplified by assuming the microscopic electric field to be simple a plane wave. By inserting $e = \bar{E}\exp(ik_x x) = E$ into (53) it is found that

$$\frac{\partial^2}{\partial k_x^2}\left[\frac{P}{E}\right] = -\frac{\partial}{\partial k_x}\left[\frac{2M}{\omega E}\right] = \frac{2R}{k_x^2 E}, \tag{55}$$

leading to

$$\eta = -\frac{\gamma}{2} = \psi. \tag{56}$$

Although this example is indeed a special case, and the analytical expression in equation (56) is not generally valid, it still provides an interesting result. Equation (56) clearly show that neglecting the $\mathbf{R}$ is not meaningful for the one-dimensional metamaterial, since it's $\mathcal{O}(k^2)$ term is equal in magnitude to the $\mathcal{O}(k^2)$ in $\mathbf{P}$ and $\mathcal{O}(k^1)$ term in $\mathbf{Q}^{\text{tot}}$. With this result in mind it is reasonable to suspect that a similar relation

$$\eta \simeq -\frac{\gamma}{2} \simeq \psi, \tag{57}$$

might be valid for other more complex metamaterial unit cells.

5 Effective parameters

The objective of this section is to derive effective parameters a set of effective tensors ϵ and μ, that describe the electromagnetic response of a metamaterial. From Maxwell's macroscopic equations in (41), it is possible to define the effective permittivity by

$$\epsilon_0\epsilon(\omega,\mathbf{k})\mathbf{E} = \epsilon_0\mathbf{E} + \langle\mathbf{p}\rangle, \tag{58}$$

which is the definition employed by Landau-Lifshitz [9]. This definition includes the entire electromagnetic response of the medium into the nonlocal effective parameter $\epsilon(\omega,\mathbf{k})$. By substituting $\langle\mathbf{p}\rangle$ with the expansion terms given in equation (49) and expressing the permittivity in component form it is possible to obtain [23]:

$$\epsilon_{ij}(\omega,\mathbf{k}) - \delta_{ij} = \chi_{ij} + \frac{1}{\epsilon_0}(\zeta_{ikj} - i\alpha_{ikj})k_k + \frac{1}{\epsilon_0}(\psi_{iklj} + \gamma_{iklj} + \eta_{iklj})k_k k_l. \tag{59}$$

Since the quantities in equation (41) and (58) are macroscopic, it can be argued that even though each parameter may contribute independently to the microscopic fields, only the sums $(\zeta - i\alpha)$ and $(\psi + \gamma + \eta)$ appearing in equation (59) will contribute to the macroscopic fields [23]. For non-gyrotropic media, $\epsilon(\omega,-\mathbf{k}) = \epsilon(\omega,\mathbf{k})$ [5, 9] such that the odd order terms in (59) must vanish, which implies that

$$\zeta_{ikj} = i\alpha_{ijk}. \tag{60}$$

since only their sum is of importance. Furthermore, it can also be argued that ψ, γ and η contribute equally to the $\mathcal{O}(k^2)$ term in equation (59). The contributions of $\langle\mathbf{p}\rangle$ can be divided into two parts by transforming

$$-i\omega\langle\mathbf{p}\rangle \to -i\omega\mathbf{P} + i\mathbf{k}\times\mathbf{M}, \tag{61}$$

where $\mathbf{P}$ and $\mathbf{M}$ are arbitrarily chosen [23]. Inserting this transformation into (41b) gives

$$i\mathbf{k}\times\frac{\mathbf{B}}{\mu_0} = -i\omega\epsilon_0\mathbf{E} - i\omega\mathbf{P} + i\mathbf{k}\times\mathbf{M} + \mathbf{J}_{\text{ext}}, \tag{62}$$

and by moving the $i\mathbf{k}\times\mathbf{M}$ over to the left side, it is possible to find

$$i\mathbf{k}\times\left[\frac{\mathbf{B}}{\mu_0} - \mathbf{M}\right] = -i\omega\epsilon_0\mathbf{E} - i\omega\mathbf{P} + \mathbf{J}_{\text{ext}}. \tag{63}$$

In accordance with the combinations of the fields that appear in equation (63), it is now convenient to define $\mathbf{H} = \mathbf{B}/\mu\mu_0 = \mathbf{B}/\mu_0 - \mathbf{M}$ and $\mathbf{D} = \epsilon\epsilon_0\mathbf{E} = \epsilon_0\mathbf{E} + \mathbf{P}$. These definitions hold the effective parameters ϵ and μ, and can therefore be used to express $\epsilon(\omega,\mathbf{k})$. Equation (58) and (61) can both be solved for the averaged microscopic polarization density $\langle\mathbf{p}\rangle$,

$$\langle\mathbf{p}\rangle = \epsilon_0\mathbf{E}(\epsilon(\omega,\mathbf{k}) - 1), \tag{64a}$$

$$\langle\mathbf{p}\rangle = \mathbf{P} - \frac{\mathbf{k}\times\mathbf{M}}{\omega}, \tag{64b}$$

and setting these two equations equal to each other gives

$$\epsilon_0\mathbf{E}(\epsilon(\omega,\mathbf{k}) - 1) = \mathbf{P} - \frac{\mathbf{k}\times\mathbf{M}}{\omega}. \tag{65}$$

The definitions of $\mathbf{D}$ and $\mathbf{H}$ can be rearranged such that

$$\mathbf{P} = \epsilon_0(\epsilon - 1)\mathbf{E}, \tag{66a}$$

$$\mathbf{M} = \frac{1}{\mu_0}(1 - \frac{1}{\mu})\mathbf{B}, \tag{66b}$$

and inserted into equation (65),

$$\epsilon_0\mathbf{E}(\epsilon(\omega, \mathbf{k}) - 1) = \epsilon_0\mathbf{E}(\epsilon - 1) - \frac{\mathbf{k} \times (1 - \mu^{-1})\mathbf{k} \times \mathbf{E}}{\mu_0\omega^2}. \tag{67}$$

where (41a) have been used to substitute for $\mathbf{B}$ in (66b) [23]. Since $\mathbf{E}$ appears in each term of this equation, it can be argued that the left and the right sides of this equation operate on $\mathbf{E}$, and that these operators are equal [23]

$$\epsilon(\omega, \mathbf{k}) = \epsilon - \frac{c^2}{\omega^2}\mathbf{k} \times (1 - \mu^{-1})\mathbf{k} \times . \tag{68}$$

Equation (67) provides an expression that shows the relation between the unlocal effective parameter $\epsilon(\omega, \mathbf{k})$ and the local effective parameters ϵ and μ, where $\epsilon \equiv \lim_{\mathbf{k}\to 0}\epsilon(\omega, \mathbf{k})$. This definition can be employed in order to express the resulting tensor $(1 - \mu^{-1})$, by assuming $\mathbf{k} = k_x\hat{\mathbf{x}}$ where $(k_x a) \ll 1$ and renaming $(1 - \mu^{-1}) = \overline{\overline{U}}_{ij}$. Inserting into equation (67) gives

$$\epsilon(\omega, \mathbf{k})\mathbf{E} = \epsilon_0\mathbf{E} - \frac{c^2}{\omega^2}\mathbf{k} \times \overline{\overline{U}}_{ij} \cdot \mathbf{k} \times \mathbf{E}, \tag{69}$$

where the tensor $\overline{\overline{U}}_{ij}$ can be expressed [23]

$$\overline{\overline{U}}_{ij} = \begin{bmatrix} u_{11} & u_{12} & u_{13} \\ u_{21} & u_{22} & u_{23} \\ u_{31} & u_{32} & u_{33} \end{bmatrix}. \tag{70}$$

Inserting $\mathbf{k} = k_x\hat{\mathbf{x}}$, $\mathbf{E} = E_x\hat{\mathbf{x}} + E_y\hat{\mathbf{y}} + E_z\hat{\mathbf{z}}$ and $\overline{\overline{U}}_{ij}$ into the right side of equation (69) gives

$$\mathbf{k} \times \overline{\overline{U}}_{ij} \cdot \mathbf{k} \times \mathbf{E} = \mathbf{k} \times \overline{\overline{U}}_{ij} \cdot k_x(-E_z\hat{\mathbf{y}} + E_y\hat{\mathbf{z}}), \tag{71}$$

and by changing to matrix notation it is found that

$$\begin{aligned} k_x\mathbf{k} \times \begin{bmatrix} u_{11} & u_{12} & u_{13} \\ u_{21} & u_{22} & u_{23} \\ u_{31} & u_{32} & u_{33} \end{bmatrix} \begin{bmatrix} 0 \\ -E_z \\ E_y \end{bmatrix} \\ = k_x\mathbf{k} \times \begin{bmatrix} -u_{12}E_z + u_{13}E_y \\ -u_{22}E_z + u_{23}E_y \\ -u_{32}E_z + u_{33}E_y \end{bmatrix} \end{aligned} \tag{72}$$

on the right side. Completing the last cross product in equation (72) reveals that

$$\mathbf{k} \times \overline{\overline{U}}_{ij} \cdot \mathbf{k} \times \mathbf{E} = k_x^2 \begin{bmatrix} 0 & 0 & 0 \\ 0 & -u_{33} & u_{32} \\ 0 & u_{23} & -u_{22} \end{bmatrix} \begin{bmatrix} E_x \\ E_y \\ E_z \end{bmatrix}. \tag{73}$$

The choice of $\mathbf{k}$ limits the values in the tensor $\overline{\overline{U}}_{ij}$. Comparison with the expression for $\epsilon(\omega, \mathbf{k})$ in equation (59) makes it possible to express $(1 - \mu^{-1})$ by ψ, γ and η, such that [23]

$$\overline{\overline{U}}_{ij} = (1-\mu^{-1}) = \omega^2\mu_0 \begin{bmatrix} 0 & 0 & 0 \\ 0 & (\psi_{3113}+\gamma_{3113}+\eta_{3113}) & -(\psi_{3112}+\gamma_{3112}+\eta_{3112}) \\ 0 & -(\psi_{2113}+\gamma_{2113}+\eta_{2113}) & (\psi_{2112}+\gamma_{2112}+\eta_{2112}) \end{bmatrix}, \tag{74}$$

where the indices $i = j = 1$ due to the choice of $\mathbf{k} = k_x\hat{\mathbf{x}}$. Not only does equation (74) implicitly reveal a part of the tensor describing μ, but it also provides an important connection to the $\mathcal{O}(k^2)$ terms of P_i, Q_{ij}^{tot} and R_i in the multipole expansion of the averaged microscopic polarization density $\langle p_i \rangle$ in equation (49).

5.1 Casimir parameters

The Russakoff-Jackson formalism only includes the contribution from the magnetization $\mathbf{M}$ in the definition of the permittivity in equation (59). This means that the $\mathcal{O}(k^2)$ terms of P_i and R_i are excluded and gives

$$\epsilon_{ij}(\omega, \mathbf{k}) - \delta_{ij} = \chi_{ij} + \frac{1}{\epsilon_0}\gamma'_{iklj}k_k k_l, \tag{75}$$

where γ'_{iklj} exludes the part of γ_{iklj} that comes from $\mathbf{Q}$ [1, 23]. This definition of $\epsilon_{ij}(\omega, \mathbf{k})$ is known as the Casimir parameter. The Casimir parameter will be used for comparison in a later section of this thesis.

5.2 Landau-Lifshitz parameters

In opposite to the Casimir parameter, the Landau-Liftshitz definition of the permittivity in equation (59) includes all of the $\mathcal{O}(k^2)$ terms in $\langle p_i \rangle$ [6, 9, 23], resulting in

$$\epsilon_{ij}(\omega, \mathbf{k}) - \delta_{ij} = \chi_{ij} + \frac{1}{\epsilon_0}(\psi_{iklj} + \gamma_{iklj} + \eta_{iklj})k_k k_l. \tag{76}$$

It is clear that this definition of $\epsilon_{ij}(\omega, \mathbf{k})$ is identical with the definition in equation (75) under the assumption that η_{iklj} and ψ_{iklj} are neglible. On the other hand, if η_{iklj} and ψ_{iklj} are of the same size as γ_{iklj} it is clear that the Landau-Lifshitz parameter in equation (76) may differ significantly from the Casimir parameter in equation (75), and thus improve the accuracy of the effective parameters considerably.

6 Floquet solution of the inhomogeneous wave-equation

The wave-equation in a periodic, nonmagnetic structure with a relative permittivity $\varepsilon(\mathbf{r})$ containing a source $\mathbf{J}_{\text{ext}} = \mathbf{u}(\mathbf{r}) \exp(i\mathbf{k} \cdot \mathbf{r})[\text{A m}^{-2}]$, where $\mathbf{u}(\mathbf{r})$ is periodic, will according to equation (18) become [15]

$$\nabla \times \nabla \times \mathbf{e} - \frac{\omega^2}{c^2} \varepsilon(\mathbf{r}) \mathbf{e} = i\omega\mu_0 \mathbf{u}(\mathbf{r}) \exp(i\mathbf{k} \cdot \mathbf{r}). \tag{77}$$

According to Floquet theory, a solution to this equation is an electric field

$$\mathbf{e}(\mathbf{r}) = \mathbf{V}(\mathbf{r}) \exp(i\mathbf{k} \cdot \mathbf{r}) \tag{78}$$

where the function $\mathbf{V}(\mathbf{r})$ is periodic and can be expanded as a Fourier series

$$\mathbf{V}(\mathbf{r}) = \sum_{\mathbf{w}} \mathbf{V}_{\mathbf{w}} \exp(i\mathbf{w} \cdot \mathbf{r}). \tag{79}$$

Inserting the Fourier expansion of $\mathbf{V}(\mathbf{r})$ into equation (78) gives the electric field [15]

$$\mathbf{e}(\mathbf{r}) = \sum_{\mathbf{w}} \mathbf{V}_{\mathbf{w}} \exp(i(\mathbf{w} + \mathbf{k}) \cdot \mathbf{r}), \tag{80}$$

It is assumed that both $\varepsilon(\mathbf{r})$ and $\mathbf{u}(\mathbf{r})$ are periodic with the same period, such that they also can be expanded into the wavenumber domain [15]. These expansions are given below as [15]

$$\mathbf{u}(\mathbf{r}) = \sum_{\mathbf{\Theta}} \mathbf{u}_{\mathbf{\Theta}} \exp(i\mathbf{\Theta} \cdot \mathbf{r}) \tag{81}$$

and

$$\varepsilon(\mathbf{r}) = \sum_{\mathbf{\Theta}} \epsilon_{\mathbf{\Theta}} \exp(i\mathbf{\Theta} \cdot \mathbf{r}). \tag{82}$$

The vector $\mathbf{\Theta}$ denotes all possible reciprocal lattice vectors [15]. Furthermore, it is also determined that the two reciprocal summation-vectors $\mathbf{w}$ and $\mathbf{\Theta}$ consist of n numbers, such that there are n $\mathbf{w}$'s and $\mathbf{\Theta}$'s in each sum. Inserting equations (80), (81) and (82) into equation (77) and transforming the vector products into $\mathbf{k}$ space yield

$$\sum_{\mathbf{w}} \left[-(\mathbf{w} + \mathbf{k}) \times (\mathbf{w} + \mathbf{k}) \times -\frac{\omega^2}{c^2} \sum_{\mathbf{\Theta}} \epsilon_{\mathbf{\Theta}} \exp(i\mathbf{\Theta} \cdot \mathbf{r}) \right] \mathbf{V}_{\mathbf{w}} \exp(i(\mathbf{w} + \mathbf{k}) \cdot \mathbf{r}) = i\omega\mu_0 \sum_{\mathbf{\Theta}} \mathbf{u}_{\mathbf{\Theta}} \exp(i(\mathbf{\Theta} + \mathbf{k}) \cdot \mathbf{r}). \tag{83}$$

The $\exp(i\mathbf{k} \cdot \mathbf{r})$ term can be cancelled on both sides, such that

$$\sum_{\mathbf{w}} \left[-(\mathbf{w} + \mathbf{k}) \times (\mathbf{w} + \mathbf{k}) \times -\frac{\omega^2}{c^2} \sum_{\mathbf{\Theta}} \epsilon_{\mathbf{\Theta}} \exp(i\mathbf{\Theta} \cdot \mathbf{r}) \right] \mathbf{V}_{\mathbf{w}} \exp(i\mathbf{w} \cdot \mathbf{r}) = i\omega\mu_0 \sum_{\mathbf{\Theta}} \mathbf{u}_{\mathbf{\Theta}} \exp(i\mathbf{\Theta} \cdot \mathbf{r}). \tag{84}$$

The summation variable $\mathbf{w}$ is now renamed $\mathbf{w} \rightarrow \mathbf{q}$, and the coefficients of $\exp(i\mathbf{w} \cdot \mathbf{r})$ are equated on each side. Calculating the vector products in the first term yields

$$\Big[(\mathbf{w}+\mathbf{k})^2 - [(\mathbf{w}+\mathbf{k})(\mathbf{w}+\mathbf{k})]\Big]\mathbf{V}_{\mathbf{w}} - \frac{\omega^2}{c^2}\sum_{\mathbf{\Theta}} \epsilon_{\mathbf{\Theta}}\mathbf{V}_{\mathbf{q}} = i\omega\mu_0\mathbf{u}_{\mathbf{w}}, \tag{85}$$

where $(\mathbf{w}+\mathbf{k})(\mathbf{w}+\mathbf{k})$ is the outer product of $\mathbf{w}+\mathbf{k}$. Keeping in mind that $\mathbf{\Theta}+\mathbf{q}=\mathbf{w}$ on the left side, and substituting for $\mathbf{w}$ into the coefficient $\mathbf{V}_{\mathbf{q}}$ in order to reobtain the sum over $\mathbf{w}$, gives the expression in equation (86). Here it is assumed that the source is a constant that only excites the zero order harmonic, such that $\mathbf{u}(\mathbf{r})=\mathbf{u}_0$ and

$$\Big[(\mathbf{w}+\mathbf{k})^2 - [(\mathbf{w}+\mathbf{k})(\mathbf{w}+\mathbf{k})]\Big]\mathbf{V}_{\mathbf{w}} - \frac{\omega^2}{c^2}\sum_{\mathbf{\Theta}} \epsilon_{\mathbf{\Theta}}\mathbf{V}_{\mathbf{w}-\mathbf{\Theta}} = i\omega\mu_0\mathbf{u}_0\delta_{\mathbf{w}0}, \tag{86}$$

where $\delta_{\mathbf{w}0}$ is the Kronecker-delta function. By renaming $\mathbf{w}-\mathbf{\Theta}=\mathbf{\Theta}'$, and inserting for $\mathbf{\Theta}$ in $\epsilon_{\mathbf{\Theta}}$, the following equation is finally obtained,

$$\Big[(\mathbf{w}+\mathbf{k})^2 - [(\mathbf{w}+\mathbf{k})(\mathbf{w}+\mathbf{k})]\Big]\mathbf{V}_{\mathbf{w}} - \frac{\omega^2}{c^2}\sum_{\mathbf{\Theta}'} \epsilon_{\mathbf{w}-\mathbf{\Theta}'}\mathbf{V}_{\mathbf{\Theta}'} = i\omega\mu_0\mathbf{u}_0\delta_{\mathbf{w}0}. \tag{87}$$

The solution of this equation forms the theoretical basis for the implementations of the plane wave expansion method in the following chapters.

7 One-dimensional plane wave expansion method

This chapter suggests an algorithm for solving the microscopic electric field inside a one-dimensional unit cell using the Floquet theory derived earlier. The process of implementing the algorithm in MATLAB will also be described in detail.

The following theory will employ vectors located in two different vector spaces. In order to easily distinguish between quantities in these two vector spaces, the following nomenclature is defined:

- Unit vectors in the physical space are written as $\hat{\mathbf{x}}$, $\hat{\mathbf{y}}$, $\hat{\mathbf{z}}$.
- Vectors in the physical space defined by components along the x, y and z axes, are written with bold-face characters, $\mathbf{A}$.
- Vectors in the n-dimensional vector space are written with bold-face characters and an overline, $\overline{\mathbf{A}}$.
- Matrices in the n-dimensional vector space are written with bold-face characters and two overlines, $\overline{\overline{\mathbf{A}}}$.

7.1 Matrix equation for one-dimensional unit cell

The objective of this section is to develop an algorithm for calculating the microscopic electric field $\mathbf{e}(\mathbf{r})$ given in equation (80) inside a given one-dimensional metamaterial unit cell using MATLAB. The unit cell is represented by a vector with a discrete number of microscopic permittivity-values that may vary over the length of the vector.

It is assumed that $\mathbf{e}(\mathbf{r})$ is a transversal wave propagating in the $\hat{\mathbf{x}}$-direction, such that $\mathbf{e}(\mathbf{r}) = e\hat{\mathbf{y}}$ and $\mathbf{k} = k\hat{\mathbf{x}}$. Consequently, it follows that the coefficients in the plane wave expansion of $\mathbf{e}(\mathbf{r})$ in equation (80) become $\mathbf{V}_\mathbf{w} = V_\mathbf{w}\hat{\mathbf{y}}$. Furthermore, it is assumed that the one-dimensional unit cell is infinitely periodic along the x-axis, and that the unit cell under consideration is positioned with one end located in origo. Subsequently, the reciprocal lattice vectors $\mathbf{w}$ and $\mathbf{\Theta}$ will also be scalar components pointing in the $\hat{\mathbf{x}}$-direction such that $\mathbf{w} = w\hat{\mathbf{x}}$ and $\mathbf{\Theta} = \Theta\hat{\mathbf{x}}$. Since the choice of source $\mathbf{u}_0$ is arbitrary, it is chosen to be constant and pointing along the y-axis such that $\mathbf{u}_0 = u_0\hat{\mathbf{y}}$. During this chapter, it will be argued that equation (87) can be written in matrix form as

$$\left(\begin{bmatrix} (w_{-\lfloor \frac{n}{2} \rfloor} + k_{-\lfloor \frac{n}{2} \rfloor})^2 & & 0 \\ & \ddots & \\ 0 & & (w_{+\lfloor \frac{n}{2} \rfloor} + k_{+\lfloor \frac{n}{2} \rfloor})^2 \end{bmatrix} - \frac{\omega^2}{c^2} \begin{bmatrix} \epsilon_0 & \ddots & \epsilon_{-(n-1)} \\ \ddots & \epsilon_0 & \ddots \\ \epsilon_{+(n-1)} & \ddots & \epsilon_0 \end{bmatrix} \right) \cdot \overline{\mathbf{V}}_\mathbf{w} = i\omega\mu_0 \begin{bmatrix} 0 \\ \vdots \\ u_0 \\ \vdots \\ 0 \end{bmatrix}, \tag{88}$$

from which the coefficients of the $\hat{\mathbf{y}}$-component of the unknown, $\overline{\mathbf{V}}_\mathbf{w}$, can be obtained. There are a total of n reciprocal lattice vectors in both $\overline{\mathbf{w}}$ and $\overline{\mathbf{\Theta}}$, which requires n coefficients in $\overline{\mathbf{V}}_\mathbf{w}$, arranged as

$$\overline{\mathbf{V}}_{\mathbf{w}} = \begin{bmatrix} V_{-\frac{n}{2}} \\ \vdots \\ V_0 \\ \vdots \\ V_{+\frac{n}{2}} \end{bmatrix}, \tag{89}$$

where it is convenient to define the integer $P = \lfloor \frac{n}{2} \rfloor$. The motivation for expressing equation (87) as in equation (88), is because it can be solved quite efficiently for high n using MATLAB's matrix functionalities. The process of obtaining equation (88) will be described in detail in the subsequent sections, before the solution of the matrix equation will be presented.

7.1.1 Matrix representation of curl operator

The objective in this subsection is to find a matrix representation of the curl operator that makes the two first terms in equation (87),

$$\Big[(\mathbf{w}+\mathbf{k})^2 - [(\mathbf{w}+\mathbf{k})(\mathbf{w}+\mathbf{k})]\Big]\mathbf{V}_{\mathbf{w}}. \tag{90}$$

- **Determine matrix for $(\mathbf{w}+\mathbf{k})^2$**

  The term $(\mathbf{w}+\mathbf{k})^2 \cdot \mathbf{V}_{\mathbf{w}}$, is a scalar multiplied by the plane wave coefficient $\mathbf{V}_{\mathbf{w}} = V_{\mathbf{w}}\hat{\mathbf{y}}$. The scalar is the length of $\mathbf{w}+\mathbf{k}$ squared, and defined as

  $$(\mathbf{w}+\mathbf{k})^2 = (w_x+k_x)^2 + (w_y+k_y)^2 + (w_z+k_z)^2. \tag{91}$$

  However, the unit cell under consideration is located along the x-axis, which means that $w_y = w_z = k_y = k_z = 0$. Inserting into equation (91) gives $(\mathbf{w}+\mathbf{k})^2 \cdot \mathbf{V}_{\mathbf{w}} = (w_x+k_x)^2\mathbf{V}_{\mathbf{w}}$. Having established the scalar in the first term, it must now be inserted into a matrix. Since there are n components of $\overline{\mathbf{w}}$, the different scalars are arranged along the diagonal of the matrix $\overline{\overline{(\mathbf{w}+\mathbf{k})}}^2$ given by

  $$\overline{\overline{(\mathbf{w}+\mathbf{k})}}^2 = \begin{bmatrix} (w_1+k)^2 & & 0 \\ & \ddots & \\ 0 & & (w_n+k)^2 \end{bmatrix}, \tag{92}$$

  such that the resulting matrix elements will be $(w_m+k)^2 \cdot V_m$ in row m when the matrix is multiplied with the solution column vector $\overline{\mathbf{V}}_{\mathbf{w}}$ given in equation (89).

- **Determine matrix for $(\mathbf{w}+\mathbf{k})(\mathbf{w}+\mathbf{k})$**

  The outer product $(\mathbf{w}+\mathbf{k})(\mathbf{w}+\mathbf{k})$ in the second term, is a $3x3$ matrix containing various combinations of the x, y and z components of $\mathbf{w}+\mathbf{k}$. Setting the $\hat{\mathbf{y}}$ and $\hat{\mathbf{z}}$-components of $(\mathbf{w}+\mathbf{k})$ equal to zero, and calculating the resulting outer product matrix gives

  $$(\mathbf{w}+\mathbf{k})(\mathbf{w}+\mathbf{k}) = \begin{bmatrix} (w_x+k_x)^2 & 0 & 0 \\ 0 & 0 & 0 \\ 0 & 0 & 0 \end{bmatrix}. \tag{93}$$

  The matrix in (93) is then multiplied by the unkown plane wave coefficient $\mathbf{V}_{\mathbf{w}} = V_{\mathbf{w}}\hat{\mathbf{y}}$,

$$\begin{bmatrix} (w_x+k_x)^2 & 0 & 0 \\ 0 & 0 & 0 \\ 0 & 0 & 0 \end{bmatrix} \cdot \begin{bmatrix} 0 \\ V_{\mathbf{w}} \\ 0 \end{bmatrix} = \begin{bmatrix} 0 & 0 & 0 \\ 0 & 0 & 0 \\ 0 & 0 & 0 \end{bmatrix}. \tag{94}$$

Since the outerproduct equals zero for the given unit cell when $\mathbf{e}(\mathbf{r}) = e\hat{\mathbf{y}}$, the corresponding matrix representation will be the zero-matrix and it can be cancelled from equation (87).

After evaluating the two terms in equation (90) independently, the complete matrix representation of the curl operator is given by

$$\overline{\overline{(\mathbf{w}+\mathbf{k})}}^2 \cdot \overline{\mathbf{V}}_{\mathbf{w}} = \begin{bmatrix} (w_1+k)^2 & & 0 \\ & \ddots & \\ 0 & & (w_n+k)^2 \end{bmatrix} \cdot \begin{bmatrix} V_1 \\ \vdots \\ V_n \end{bmatrix}. \tag{95}$$

7.1.2 Vector representations in the matrix equation

Before the rest of the matrix equation can be developed, it is necessary to define the vector quantities $\mathbf{w}$ and $\mathbf{\Theta}$ more accurately. These vectors are reciprocal lattice vectors spanning the length of the unit cell in k-space. Since the algorithm requires two sets containing n $\mathbf{w}$'s and $\mathbf{\Theta}$'s, there is a need for arranging these vectors correctly before they can be used in the matrix equation (87).

Since the solution $\overline{\mathbf{V}}_{\mathbf{w}}$ already is arranged in a column vector, it is practical to do the same thing with $\mathbf{w}$ and $\mathbf{\Theta}$. The two sets of reciprocal lattice vectors, $\overline{\mathbf{w}}$ and $\overline{\mathbf{\Theta}}$ are defined as

$$\overline{\mathbf{w}} = \begin{bmatrix} w_{-P} \\ \vdots \\ w_0 \\ \vdots \\ w_{+P} \end{bmatrix}, \tag{96}$$

$$\overline{\mathbf{\Theta}} = \begin{bmatrix} \Theta_{-P} \\ \vdots \\ \Theta_0 \\ \vdots \\ \Theta_{+P} \end{bmatrix}, \tag{97}$$

Both $\overline{\mathbf{w}}$ and $\overline{\mathbf{\Theta}}$ has been shifted such that the shortest vectors in the sets are located in the middle of the column vector. As a consequence, $n = 2P+1$, will always be an odd number and the reason for this vector shift will become evident in the next section. The vectors $\mathbf{k}$ and $\mathbf{u}_0$ are constants determined by the source, and therefore independent of position within the column vectors. The difference between these two vectors is that $\mathbf{k}$ is a constant for all harmonics, while $\mathbf{u} = \mathbf{u}_0$ is constant for only the zero order harmonic. The vector representations of $\mathbf{k}$ and $\mathbf{u}_0$ in the matrix equation are given by

$$\overline{\mathbf{k}} = \begin{bmatrix} k \\ \vdots \\ k \\ \vdots \\ k \end{bmatrix}, \tag{98}$$

$$\overline{\mathbf{u}} = \begin{bmatrix} 0 \\ \vdots \\ u_0 \\ \vdots \\ 0 \end{bmatrix}. \tag{99}$$

The shift in $\overline{\mathbf{w}}$ and $\overline{\mathbf{\Theta}}$ also results in a shift in the curl operator,

$$\overline{\overline{(\mathbf{w}+\mathbf{k})}}^2 = \begin{bmatrix} (w_{-P}+k)^2 & & 0 \\ & \ddots & \\ 0 & & (w_{+P}+k)^2 \end{bmatrix}, \tag{100}$$

and a shift in the solution column vector

$$\overline{\mathbf{V}}_{\mathbf{w}} = \begin{bmatrix} V_{-P} \\ \vdots \\ V_0 \\ \vdots \\ V_{+P} \end{bmatrix}, \tag{101}$$

so that they coincide with equation (89).

7.1.3 Constructing the convolution matrix

The object of this section is to find a nxn matrix representation of the factor $\sum_{\mathbf{\Theta}} \epsilon_{\mathbf{w}-\mathbf{\Theta}'} V_{\mathbf{\Theta}'}$ in equation (87). It will be shown that this can be done by creating a convolution matrix, $\overline{\overline{\mathbf{\Gamma}}}$, and multiplying it with the column vector $\overline{\mathbf{V}}_{\mathbf{w}}$ given in equation (89).

The convolution matrix $\overline{\overline{\mathbf{\Gamma}}}$ is the representaion of $\varepsilon(x)$ in k-space on matrix form, and contains the Fourier coefficients obtained from the 1D discrete-fourier-transform (DFT) given by (82). The process of creating the convolution matrix is described by the following 3 steps.

- **Step 1: Determine Fourier coefficients**

  The discrete Fourier transform of $\varepsilon(x)$ given in equation (82), can be calculated using MATLABs fast Fourier transform function `fft(..)`. This function takes a discrete input vector $x(m)$ of length M as input and calculates the Fast Fourier transform (FFT) [19] $X(k)$ as,

  $$X(k) = \sum_{m=0}^{M-1} x(m) \exp\left(-i\frac{2\pi \cdot km}{M}\right), \tag{102}$$

  where the index m has been shifted to start at $m = 0$. $X(k)$ will be a vector of the same length as $x(m)$. Similarly, the original vector $x(m)$ can be obtained by the Inverse Fourier transform (IFFT) function `ifft(..)` [19] given by

  $$x(m) = \frac{1}{M} \sum_{k=0}^{M-1} X(k) \exp\left(i\frac{2\pi \cdot km}{M}\right). \tag{103}$$

  In order to apply the FFT and IFFT capabilities in MATLAB, the correspondence between equation (103) and equation (82) must be confirmed. They both express the inverse transforms and must therefore be identical in order to be used correctly. By comparing the arguments in the exponential functions in equation (103) and equation (82), it is found that the expressions for the discrete Fourier transforms will be identical if the set of reciprocal lattice vectors Θ_m are given by

  $$\Theta_m = \frac{2\pi}{M} \cdot m, \quad m = 0, 1, 2, ..., M-1. \tag{104}$$

  The set of w_m also share the same expansions as the set of Θ_m in equation (104). Now there is only one remaining difference between equation (103) and (82), namely the scaling factor $\frac{1}{M}$. This factor is omitted by dividing the FFT by M, and multiplying the IFFT by M. This confirms the correspondance between equation (82) and the IFFT in MATLAB. The FFT and IFFT can now be used to calculate the Fourier coefficients $\epsilon_{\mathbf{\Theta}}$ in equation (82), and the original microscopic permittivity $\varepsilon(x)$ can be calculated from the Inverse Fourier transform in equation (103) [19]. Using the FFT function to calculate the Fourier coefficients in equation (82), results in the column vector ϵ_{Θ_m} given by

$$\epsilon_{\Theta_m} = \begin{bmatrix} \epsilon_{\Theta_0} \\ \epsilon_{\Theta_1} \\ \vdots \\ \epsilon_{\Theta_{M-2}} \\ \epsilon_{\Theta_{M-1}} \end{bmatrix}. \tag{105}$$

It is worth mentioning that the use of the `fft(..)` and `ifft(..)` functions are interchangeable. The effect of `fft(..)` will be reversed by `ifft(..)`, and vice versa with only a difference in the $\frac{1}{M}$ factor in the `ifft(..)` function.

- **Step 2: Shifting the fourier coefficients**

  In the previous step, the Fourier coefficients ϵ_{Θ_m} of the microscopic permitivitty $\varepsilon(x)$ was found on the form given in equation (105). In order to obtain ϵ_{Θ_m} on the same form as w_p and Θ_p equation (96) and (97), ϵ_{Θ_m} must be shifted such that the zero order harmonic is located at the center of the vector. This can be accomplished by using MATLABs `fftshift(..)` and `ifftshift(..)` functions, which swaps the left and right halves of the vector given as input [21]. Applying `fftshift(..)` to the vector ϵ_{Θ_m} in (105) gives the following vector

$$\epsilon_{\Theta_m} = \begin{bmatrix} \epsilon_{\Theta_{\frac{M}{2}}} \\ \epsilon_{\Theta_{\frac{M}{2}+1}} \\ \vdots \\ \epsilon_{\Theta_0} \\ \vdots \\ \epsilon_{\Theta_{\frac{M}{2}-2}} \\ \epsilon_{\Theta_{\frac{M}{2}-1}} \end{bmatrix}, \tag{106}$$

  where the original vector can be reobtained by calling `ifftshift(..)`. At this point it is worth noting that very little of the information in the original microscopic permittivity function $\varepsilon(x)$ has been lost. However, the number of spatial harmonics must now be reduced in order to calculate the matrix equation in (88) effectively.

  From the set of M coefficients in equation (106), the $2P_f + 1$ coefficients at the center are selected to form a new subset

$$\epsilon_{\Theta_p} = \begin{bmatrix} \epsilon_{\Theta_{-P_f}} \\ \vdots \\ \epsilon_{\Theta_0} \\ \vdots \\ \epsilon_{\Theta_{+P_f}} \end{bmatrix}, \tag{107}$$

  the number $P_f = n-1 = 2P$ is an even number, and indicates the highest spatial harmonic that is not filtered out. This process is essentially the same as applying a low-pass filter on the Fourier coefficients. It is here assumed that M is odd, and that $P_f \ll M$, so that the selected coefficients provides a good representation of $\varepsilon(x)$. In order to obtain good accuracy, it is desirable to have P_f as large at possible. It has been argued that $P_f \geq 100$ spatial harmonics along each dimension gives sufficient accuracy [17, 18].

- **Step 3: Insert coefficients into convolution matrix**

  Having obtained the set of the $2P_f + 1$ lowest order harmonics given in ϵ_{Θ_p}, it only remains to insert the coefficients properly into the convolution matrix. This is done in a way that makes ϵ_{Θ_p} into a Toeplitz matrix [17], which involves inserting the zero order harmonic along the diagonal of the matrix and distributing the higher order harmonics symmetrically around the diagonal. The resulting convolution matrix $\overline{\overline{\mathbf{\Gamma}}}$ equals

$$\overline{\overline{\mathbf{\Gamma}}} = \begin{bmatrix} \epsilon_0 & \epsilon_{-1} & \ddots & \epsilon_{-P_f} \\ \epsilon_{+1} & \epsilon_0 & \epsilon_{-1} & \ddots \\ \ddots & \epsilon_{+1} & \epsilon_0 & \epsilon_{-1} \\ \epsilon_{+P_f} & \ddots & \epsilon_{+1} & \epsilon_0 \end{bmatrix}. \tag{108}$$

  The dimension of the convolution matrix $\overline{\overline{\mathbf{\Gamma}}}$ is now $n^2 = (2P + 1)^2 = (P_f + 1)^2$, and can be inserted for $\sum_{\mathbf{\Theta}'} \epsilon_{\mathbf{w}-\mathbf{\Theta}'}$ in the matrix equation (87).

7.1.4 Calculating the matrix equation

After establishing all of the matrices in equation (87), the solution $\overline{\mathbf{V}}_{\mathbf{w}}$ can now be calculated by performing simple matrix operations in MATLAB. The matrix on the left side of equation (87) is inverted and multiplied by the matrix on the right side such that

$$\begin{bmatrix} V_{y,-P} \\ \vdots \\ V_{y,0} \\ \vdots \\ V_{y,+P} \end{bmatrix} = i\omega\mu_0 \cdot \left[\overline{\overline{(\mathbf{w} + \mathbf{k})}}^2 - (\frac{\omega}{c})^2 \cdot \overline{\overline{\mathbf{\Gamma}}} \right]^{-1} \cdot \begin{bmatrix} 0 \\ \vdots \\ u_0 \\ \vdots \\ 0 \end{bmatrix}. \tag{109}$$

The solution is found as the product of the nxn matrix and the $nx1$ row vector in equation (109). The periodic function $\mathbf{V}(\mathbf{r})$ inside the unit cell, can now be found by shifting the solution vector back to

$$\begin{bmatrix} V_{y,0} \\ \vdots \\ V_{y,n} \end{bmatrix}, \tag{110}$$

and taking the IFFT as in equation (103). The microscopic electric field $\mathbf{e}(\mathbf{r})$ is subsequently found by $\mathbf{V}(\mathbf{r}) \cdot \exp(i\mathbf{k} \cdot \mathbf{r})$ as in equation (80) [15].

8 Two-dimensional plane wave expansion method

This chapter suggests two algorithms for solving the microscopic electric field inside a two-dimensional unit cell by employing Floquet theory. Two different types of solutions to this problem will be presented here. The first solution is for electric fields that are transversal to the direction of propagation, and the second solution is for electric fields that are located in the plane of the direction of propagation. The process of implementing both algorithms in MATLAB will be described in the subsequent sections. The permittivity $\varepsilon(x, y)$ is represented by a matrix, preferably of a large size, where each element contains the permittivity at the given point (x, y) inside the matrix.

In what follows, there will be two adjustments to the nomenclature defined in the previous chapter:

- Vectors in the n^2-dimensional vector space are written with bold-face characters and an overline, $\overline{\mathbf{A}}$.
- Matrices in the n^2-dimensional vector space are written with bold-face characters and two overlines, $\overline{\overline{\mathbf{A}}}$.

8.1 Master equation

In the Floquet theory that was presented earlier, it was found that the wave equation in an inhomogeneous medium is given by

$$\Big[(\mathbf{w}+\mathbf{k})^2 - [(\mathbf{w}+\mathbf{k})(\mathbf{w}+\mathbf{k})]\Big]\mathbf{V}_{\mathbf{w}} - \frac{\omega^2}{c^2}\sum_{\mathbf{\Theta}'}\epsilon_{\mathbf{w}-\mathbf{\Theta}'}\mathbf{V}_{\mathbf{\Theta}'} = i\omega\mu_0\mathbf{u}_0, \qquad (111)$$

when the electric field $\mathbf{e}$ is expanded as a sum of plane waves given by equation (80), and the source $\mathbf{u}_0$ and microscopic permittivity $\varepsilon(\mathbf{r})$ are given by the plane wave expansions in equation (81) and equation (82) [15]. The subject of this chapter is to develop two algorithms for calculating the electric field $\mathbf{e}(\mathbf{r})$ inside a two-dimensional unit cell, by solving equation (111).

The two-dimensional plane wave expansion method (PWEM) assumes a unit cell situated in the x-y plane, which implies that the reciprocal lattice vectors are given by $\mathbf{w} = w_x\hat{\mathbf{x}} + w_y\hat{\mathbf{y}}$ and $\mathbf{\Theta} = \Theta_x\hat{\mathbf{x}} + \Theta_y\hat{\mathbf{y}}$.

The first algorithm assumes that the electric field is polarized transversal to the unit cell, such that $\mathbf{e}(\mathbf{r}) = e_z\hat{\mathbf{z}}$. This algorithm will be referred to as the transversal field algorithm.

The second algorithm assumes that the electric field is polarized in the plane of the unit cell, such that $\mathbf{e}(\mathbf{r}) = e_x\hat{\mathbf{x}} + e_y\hat{\mathbf{y}}$. This algorithm will be referred to as the parallel field algorithm.

8.1.1 Common terms

Before developing the two different algorithms, it is convenient to define some of the terms in equation (111) that are shared among both of them.

The solution vector $\overline{\mathbf{V}}_{\mathbf{w}}$ for the two-dimensional algorithms, are shifted such that the zero order harmonic is located at the center of the column vector, and is expressed as

$$\overline{\mathbf{V}}_{\mathbf{w}} = \begin{bmatrix} V_{-P,-S} \\ V_{-P,-S+1} \\ \vdots \\ V_{0,0} \\ \vdots \\ V_{+P,+S-1} \\ V_{+P,+S} \end{bmatrix}, \tag{112}$$

where the integers $P = \lfloor \frac{n}{2} \rfloor$ and $S = \lfloor \frac{n}{2} \rfloor$. It is emphasized that the ordering of the coefficients in equation (112) is analogous to the ordering of the one-dimensional solution column vector in equation (89). In order to simplify the notation in the matrices in the subsequent chapters, it is practical to define the sum-vector $\mathbf{T} = \mathbf{w} + \mathbf{k}$ such that

$$T_x = w_x + k_x, \tag{113a}$$
$$T_y = w_y + k_y, \tag{113b}$$
$$T_z = w_z + k_z, \tag{113c}$$

where it is assumed that $T_z = 0$ in the both of the following algorithms.

The first term on the left side of equation (111) is the sum of $(\mathbf{w} + \mathbf{k})^2$, and will be identical for both algorithms since they both employ the same set of reciprocal lattice vectors in the x-y plane. The matrix representation of $(\mathbf{w} + \mathbf{k})^2$ is given as

$$\overline{\overline{\mathbf{w} + \mathbf{k}}}^2 = \begin{bmatrix} (T_x^2 + T_y^2)_{-P,-S} & & & & 0 \\ & \ddots & & & \\ & & (T_x^2 + T_y^2)_{0,0} & & \\ & & & \ddots & \\ 0 & & & & (T_x^2 + T_y^2)_{+P,+S} \end{bmatrix}, \tag{114}$$

which is in accordance with the coefficients in equation (112) and is analogous with the matrix representation of the same term in the one-dimensional matrix equation (88).

8.1.2 The two-dimensional convolution matrix

In order to express equation (111) as a matrix equation, it is necessary to find the matrix representation of the term $\sum_{\mathbf{\Theta}'} \epsilon_{\mathbf{w}-\mathbf{\Theta}'}$. As in the one-dimensional PWEM, this term becomes a convolution matrix $\overline{\overline{\mathbf{\Gamma}}}$.

The two-dimensional convolution matrix $\overline{\overline{\mathbf{\Gamma}}}$, contains the Fourier coefficients obtained by performing a two-dimensional Fourier transform of the permittivity $\varepsilon(x, y)$ in the unit cell. Since the reciprocal lattice vectors $\mathbf{w}$ and $\mathbf{\Theta}$ are located in the x-y plane, it follows that the summation

$$\sum_{\mathbf{\Theta}'} \epsilon_{\mathbf{w}-\mathbf{\Theta}'} = \sum_{\Theta_x'} \sum_{\Theta_y'} \epsilon_{w_x-\Theta_x', w_y-\Theta_y'}, \tag{115}$$

becomes a two-dimensional convolution between $\mathbf{w}$ and $\mathbf{\Theta}$. From equation (115) it is seen that the coefficient of the lowest order, $\epsilon_{0,0}$, will be the coefficient where $\mathbf{w} = \mathbf{\Theta}'$, and that it therefore will be placed along the diagonal

of the convolution matrix. Furthermore, it is also seen that other coefficients of low order will be placed close to the diagonal of the convolution matrix, since the lattice vector components will be close to identical along the diagonal. Higher order coeffecients are correspondingly distributed towards the bottom left and top right corners of the convolution matrix, far away from the diagonal. The coefficients that are largest in magnitude are generally found along and close to the diagonal, since spatial harmonics tends to couple the most energy into modes that have similar indices [17].

The Fourier coefficients of $\varepsilon(x, y)$ are calculated using the MATLAB's `fft2` function. The `fft2` function utilizes the exact same algorithm as the one-dimensional `fft` function to calculate the Fourier coefficients of $\varepsilon(x, y)$ [20]. It follows that the correspondance between equation (82) and the `fft` algorithm in MATLAB, has already been verified and that it is therefore unnecessary to repeat this process for the two-dimensional unit cell.

After the Fourier coefficients of $\varepsilon(x, y)$ are obtained using the `fft2` function, they are shifted such that the zero order harmonic is located at the center of the matrix. Ideally it is desirable to use all of the coefficients in the convolution matrix, but this is infeasible due to the number of spatial harmonics in the resulting matrix. The $2P_f + 1 = 2S_f + 1$ lowest order coefficients centered around the DC value along each dimension is therefore extracted, such that the set of Fourier coefficients essentially are low-pass filtered into a matrix

$$\begin{bmatrix} \epsilon_{-P_f,+S_f} & & \epsilon_{0,+S_f} & & \epsilon_{+P_f,+S_f} \\ & & \vdots & & \\ \epsilon_{-P_f,0} & \cdots & \epsilon_{0,0} & \cdots & \epsilon_{+P_f,0} \\ & & \vdots & & \\ \epsilon_{-P_f,-S_f} & & \epsilon_{0,-S_f} & & \epsilon_{+P_f,-P_f} \end{bmatrix}, \tag{116}$$

leaving only the lowest order spatial harmonics, and where the indices $P_f = 2P$ and $S_f = 2S$. In order to describe the insertion of the various spatial harmonics in equation (116) into the convolution matrix, it is beneficial to consider the convolution matrix $\overline{\overline{\mathbf{\Gamma}}}$ as one large matrix containing n^2 matrices $\overline{\overline{\mathbf{G}}}$ that contains n^2 Fourier coefficients. This allows for expressing the convolution matrix $\overline{\overline{\mathbf{\Gamma}}}$ as

$$\overline{\overline{\mathbf{\Gamma}}} = \begin{bmatrix} \overline{\overline{\mathbf{G}}}_0 & \overline{\overline{\mathbf{G}}}_{-1} & \ddots & \overline{\overline{\mathbf{G}}}_{-S_f} \\ \overline{\overline{\mathbf{G}}}_{+1} & \overline{\overline{\mathbf{G}}}_0 & \overline{\overline{\mathbf{G}}}_{-1} & \ddots \\ \ddots & \overline{\overline{\mathbf{G}}}_{+1} & \overline{\overline{\mathbf{G}}}_0 & \overline{\overline{\mathbf{G}}}_{-1} \\ \overline{\overline{\mathbf{G}}}_{+S_f} & \ddots & \overline{\overline{\mathbf{G}}}_{+1} & \overline{\overline{\mathbf{G}}}_0 \end{bmatrix}, \tag{117}$$

where the matrices $\overline{\overline{\mathbf{G}}}$ are given by

$$\overline{\overline{\mathbf{G}}} = \begin{bmatrix} \epsilon_0 & \epsilon_{-1} & \ddots & \epsilon_{-P_f} \\ \epsilon_{+1} & \epsilon_0 & \epsilon_{-1} & \ddots \\ \ddots & \epsilon_{+1} & \epsilon_0 & \epsilon_{-1} \\ \epsilon_{+P_f} & \ddots & \epsilon_{+1} & \epsilon_0 \end{bmatrix}, \tag{118}$$

and have the same Toeplitz symmetry as the one-dimensional convolution matrix in equation (108) [17]. Note that the coefficients are inserted into the convolution matrix according to the summation in equation (115). The resulting convolution matrix $\overline{\overline{\mathbf{\Gamma}}}$ will generally not have Toeplitz symmetry,

but will have a coefficient distribution that resembles the Toeplitz symmetry in the sense that higher order coefficients are located far off the matrix diagonal. The two-dimensional convolution matrix contains a total of $n^4 = (P_f + 1)^4 = (S_f + 1)^4$ coefficients. A visualization of the coefficient distribution in the two-dimensional convolution matrix for $n = 3$ is given in equation (161) in Appendix A.

Since the unit cell is two-dimensional, it is possible to rotate the unit cell by 90°,180° or 270°. In order to obtain the correct convolution matrix for a rotated unit cell, it is important to keep the axes employed by MATLAB in mind. The indexing used in MATLAB places origo in the top left corner of the matrix containing the unit cell, which is different from most coordinate systems that have origo located in the bottom left corner. The coordinate system of the unit cell (x-y) and MATLAB's coordinate system (x'-y') are depicted below.

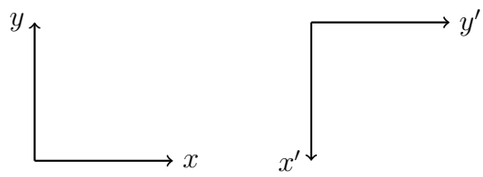

Figure 5: Orientation of coordinate system (x-y) compared orientation of transformed coordinate system (x'-y').

By mirroring the MATLAB-coordinate system about the y' axis it is seen that

$$x' = y, \tag{119a}$$
$$y' = x, \tag{119b}$$

implying that a 90° rotation from x to y corresponds to a 90° rotation from y' to x'. By mirroring the the MATLAB-coordinate system back again it is seen that the rotation is in fact in the opposite direction as depicted below:

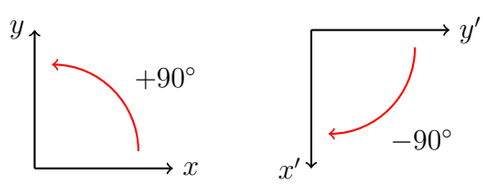

Figure 6: Rotation in regular coordinate system (x-y) compared rotation in transformed coordinate system (x'-y').

Given this relation between the two different coordinate systems that are employed in the PWEM, it is necessary to rotate the unit cell in the *opposite direction* of the intentional direction before the Fourier transform in order to obtain the correct two-dimensional convolution matrix. If the unit cell is rotated ±180°, no rotation is necessary.

8.2 Transversal field algorithm

This algorithm assumes a transversal microscopic electric field propagating in the x-y plane, such that $\mathbf{e}(\mathbf{r}) = e\hat{\mathbf{z}}$ and $\mathbf{k} = k_x\hat{\mathbf{x}} + k_y\hat{\mathbf{y}}$. According to equation (80), $\mathbf{V_w} = V_\mathbf{w}\hat{\mathbf{z}}$, which also implies that the source $\mathbf{u}_0 = u_0\hat{\mathbf{z}}$. It will in the following be shown that equation (111) can be written in matrix form as

$$\left(\begin{bmatrix} T^2_{x,-P,-S} + T^2_{y,-P,-S} & & 0 \\ & \ddots & \\ 0 & & T^2_{x,+P,+S} + T^2_{y,+P,+S} \end{bmatrix} - \frac{\omega^2}{c^2}\overline{\overline{\mathbf{\Gamma}}} \right) \overline{\mathbf{V}}_\mathbf{w} = i\omega\mu_0 \begin{bmatrix} 0 \\ \vdots \\ u_0 \\ \vdots \\ 0 \end{bmatrix}, \tag{120}$$

where the solution vector $\overline{\mathbf{V}}_\mathbf{w}$ given by equation (112) will contain n^2 elements.

8.2.1 Matrix equation for transversal fields

In order to determine the matrix equation for transversal microscopic electric fields, it is necessary to analyze the left side equation (111) in vector form.

The second term on the left side of equation (111) is the outerproduct $(\mathbf{T})(\mathbf{T})$. Since the electric field is polarized transversely to the plane of propagation, $\mathbf{V_w} = V_\mathbf{w}\hat{\mathbf{z}}$, this term is found as

$$(\mathbf{T})(\mathbf{T}) \cdot V_\mathbf{w}\hat{\mathbf{z}} = \begin{bmatrix} T_x^2 & T_xT_y & 0 \\ T_yT_x & T_y^2 & 0 \\ 0 & 0 & 0 \end{bmatrix} \cdot \begin{bmatrix} 0 \\ 0 \\ V_\mathbf{w} \end{bmatrix}, \tag{121}$$

which equals the zero matrix. The contribution from the outerproduct term is therefore zero, and can be omitted from the matrix equation. The source $\mathbf{u}_0 = u_0\hat{\mathbf{z}}$ is represented as the column vector

$$\overline{\mathbf{u}}_0 = \begin{bmatrix} 0 \\ \vdots \\ u_0 \\ \vdots \\ 0 \end{bmatrix}, \tag{122}$$

which is identical to the source representation in the one-dimensional plane wave expansion method. Having represented all of the terms in equation (111) as matrices, it is now possible to calculate the solution column vector in equation (112) by solving equation (120).

8.3 Parallel field algorithm

This algorithm assumes that the electric field $\mathbf{e}(\mathbf{r})$ is propagating in a direction parallel to the x-y plane, and that the polarization of $\mathbf{e}(\mathbf{r})$ also lies in the unit cell plane, such that $\mathbf{e} = e_x\hat{\mathbf{x}} + e_y\hat{\mathbf{y}}$. The solution of the electric field will therefore differ from the previous two algorithms, since it now consists of two components, e_x and e_y.

The expansion of the electric field given in equation (80) requires the coefficients $\mathbf{V}_\mathbf{w} = V_{\mathbf{w},x}\hat{\mathbf{x}} + V_{\mathbf{w},y}\hat{\mathbf{y}}$, and equation (111) will now become two coupled matrix equations that yields the two column vectors $\overline{\mathbf{V}}_{\mathbf{w},x}$ and $\overline{\mathbf{V}}_{\mathbf{w},y}$. The system of matrix equations can be written as

$$\begin{bmatrix} \overline{\overline{\mathbf{A}}} & \overline{\overline{\mathbf{B}}} \\ \overline{\overline{\mathbf{C}}} & \overline{\overline{\mathbf{D}}} \end{bmatrix} \begin{bmatrix} \overline{\mathbf{V}}_{\mathbf{w},x} \\ \overline{\mathbf{V}}_{\mathbf{w},y} \end{bmatrix} = i\omega\mu_0 \begin{bmatrix} \overline{\mathbf{u}}_x \\ \overline{\mathbf{u}}_y \end{bmatrix}, \tag{123}$$

where $\overline{\mathbf{u}}_x$ and $\overline{\mathbf{u}}_y$ are the components of the source $\mathbf{u}_0$ in the x and y directions, and the matrices $\overline{\overline{\mathbf{A}}}$, $\overline{\overline{\mathbf{B}}}$, $\overline{\overline{\mathbf{C}}}$ and $\overline{\overline{\mathbf{D}}}$ are composite matrices given by the three terms on the left side of equation (111). The solution vectors $\overline{\mathbf{V}}_{\mathbf{w},x}$ and $\overline{\mathbf{V}}_{\mathbf{w},y}$, are given in the same form as in equation (112). The following section will describe the process of obtaining equation (123).

8.3.1 Matrix equation for parallel fields

In order to determine the matrices $\overline{\overline{\mathbf{A}}}$, $\overline{\overline{\mathbf{B}}}$, $\overline{\overline{\mathbf{C}}}$ and $\overline{\overline{\mathbf{D}}}$, it is necessary to first evaluate equation (111) in vector form. Since the coefficients of $\mathbf{e}(\mathbf{r})$ has two components, $\overline{\mathbf{V}}_{\mathbf{w},x}$ and $\overline{\mathbf{V}}_{\mathbf{w},y}$, the outerproduct in equation (111) for two-dimensional structures will differ from the outerproduct that was obtained for one-dimensional structures in equation (93). Adding $\mathbf{w}$ and $\mathbf{k}$ yields the vector $\mathbf{T} = T_x\hat{\mathbf{x}} + T_y\hat{\mathbf{y}}$, and calculating the outerproduct gives

$$(\mathbf{T})(\mathbf{T}) = \begin{bmatrix} T_x^2 & T_xT_y & 0 \\ T_yT_x & T_y^2 & 0 \\ 0 & 0 & 0 \end{bmatrix}. \tag{124}$$

When the outerproduct is multiplied by the solution vector $\mathbf{V}_\mathbf{w} = V_{\mathbf{w},x}\hat{\mathbf{x}} + V_{\mathbf{w},y}\hat{\mathbf{y}}$, the resulting matrix equals

$$(\mathbf{T})(\mathbf{T}) \cdot \mathbf{V}_\mathbf{w} = \begin{bmatrix} T_x^2V_{\mathbf{w},x} + T_xT_yV_{\mathbf{w},y} \\ T_y^2V_{\mathbf{w},y} + T_yT_xV_{\mathbf{w},x} \end{bmatrix}. \tag{125}$$

This outerproduct now has two significant features that differs the one that was calculated for one-dimensional unit cells. Firstly, the resulting matrix is nonzero. Secondly, equation (125) shows that $V_{\mathbf{w},x}$ and $V_{\mathbf{w},y}$ are coupled to each other. This coupling structure motivatates the matrix notation used in equation (123), which can be solved efficiently in MATLAB. In order to determine $\overline{\overline{\mathbf{A}}}$, $\overline{\overline{\mathbf{B}}}$, $\overline{\overline{\mathbf{C}}}$ and $\overline{\overline{\mathbf{D}}}$, it requires matrix representations of the scalars in the outerproduct and the first term on the left side of equation (111).

The scalars T_x^2, T_y^2 and T_xT_y are expressed in matrix form as

$$\overline{\overline{\mathbf{T}}}_x^2 = \begin{bmatrix} T_{x,-P,-S}^2 & & 0 \\ & \ddots & \\ 0 & & T_{x,+P,+S}^2 \end{bmatrix}, \tag{126a}$$

$$\overline{\overline{\mathbf{T}}}_y^2 = \begin{bmatrix} T_{y,-P,-S}^2 & & 0 \\ & \ddots & \\ 0 & & T_{y,+P,+S}^2 \end{bmatrix}, \tag{126b}$$

$$\overline{\overline{\mathbf{T}_x \mathbf{T}_y}} = \begin{bmatrix} (T_x T_y)_{-P,-S} & & 0 \\ & \ddots & \\ 0 & & (T_x T_y)_{+P,+S} \end{bmatrix}, \tag{126c}$$

which are diagonal matrices that is consistent with the ordering of coefficients in equation (112). The remaining term on the left side of equation (111), $(\mathbf{w}+\mathbf{k})^2$, is already found in equation (114). Having determined the matrix representations of all the matrices on the left side of equation (111), $\overline{\overline{\mathbf{A}}}$, $\overline{\overline{\mathbf{B}}}$, $\overline{\overline{\mathbf{C}}}$ and $\overline{\overline{\mathbf{D}}}$ can now be found as

$$\overline{\overline{\mathbf{A}}} = \overline{\overline{\mathbf{w}+\mathbf{k}}}^2 - \overline{\overline{\mathbf{T}}}_x^2 - (\frac{\omega}{c})^2 \overline{\overline{\mathbf{\Gamma}}}, \tag{127a}$$

$$\overline{\overline{\mathbf{C}}} = \overline{\overline{\mathbf{B}}} = -\overline{\overline{\mathbf{T}_x \mathbf{T}}}_y, \tag{127b}$$

$$\overline{\overline{\mathbf{D}}} = \overline{\overline{\mathbf{w}+\mathbf{k}}}^2 - \overline{\overline{\mathbf{T}}}_y^2 - (\frac{\omega}{c})^2 \overline{\overline{\mathbf{\Gamma}}}, \tag{127c}$$

containing a total of n^4 elements each. The source $\mathbf{u}_0$ in equation (111), contains two components, $\overline{\mathbf{u}}_x$ and $\overline{\mathbf{u}}_y$, which are represented by

$$\overline{\mathbf{u}}_{x,y} = \begin{bmatrix} 0 \\ \vdots \\ u_0 \\ \vdots \\ 0 \end{bmatrix}, \tag{128}$$

and where the constants u_0 are user defined. By stacking $\overline{\mathbf{V}}_{\mathbf{w},x}$ on top of $\overline{\mathbf{V}}_{\mathbf{w},y}$, and $\overline{\mathbf{u}}_x$ on top of $\overline{\mathbf{u}}_y$, forming two column vectors of length $2n^2$, the coupled matrix equation set in equation (123) is finally obtained.

The equation set can now be solved by using MATLAB's `linsolve(..)` function [22], which will return the column vector containing $\overline{\mathbf{V}}_{\mathbf{w},x}$ and $\overline{\mathbf{V}}_{\mathbf{w},y}$.

8.4 Creating the electric field matrix

After solving equation (120) or (123), there are only a few more steps before it is finally possible to obtain the solution $\mathbf{e}(x, y)$.

Both matrix equations provides column vectors $\overline{\mathbf{V}}_{\mathbf{w}}$ given by equation (112), containing the Fourier coefficients of the periodic function $\mathbf{V}(\mathbf{r})$. Since the unit cell is two-dimensional, it is necessary to insert the solution coefficients into a matrix, which can be transformed back to the real domain. The coefficients are first rearranged as

$$\overline{\overline{\mathbf{V}}}_{\mathbf{w}} = \begin{bmatrix} V_{-P,+S} & & V_{0,+S} & & V_{+P,+S} \\ & & \vdots & & \\ V_{-P,0} & \cdots & V_{0,0} & \cdots & V_{+P,0} \\ & & \vdots & & \\ V_{-P,-S} & & V_{0,-S} & & V_{+P,-S} \end{bmatrix}, \tag{129}$$

then shifted, and finally transformed back to the $\mathbf{r}$ domain using MATLAB's `ifft2(..)` function. The transversal field algorithm will produce the solution $V_z(x, y)$, while the parallel field algorithm will produce the two solutions $V_x(x, y)$ amd $V_y(x, y)$.

The solution of the microscopic electric field $\mathbf{e}(\mathbf{r})$ is generally found as

$$\mathbf{e}(\mathbf{r}) = \left(V_x \hat{\mathbf{x}} + V_y \hat{\mathbf{y}} + V_z \hat{\mathbf{z}} \right) \cdot \exp\left(i\mathbf{k} \cdot \mathbf{r} \right), \tag{130}$$

according to equation (80).

9 Determining η_{iklj}, γ_{ijlm} and ψ_{iklj}

Previously it was argued that the higher order terms of the multipole expansion in (43) was not negligible for the special one-dimensional situation depicted in figure 4, where the electric field was assumed to be of the form $e = \bar{E}\exp(ik_x x)$ and where $\bar{E}$ was a constant value. Although this was a special occurrence, it does motivate a more general investigation of the higher order terms, in order to properly understand their significance in common metamaterials. The aim of this section is to describe an algorithm for determining the parameters η, γ and ψ describing the relative size of the $\mathcal{O}(k^2)$ terms in (49) inside an arbitrary two-dimensional metamaterial unit cell in the x-y plane, by employing the two-dimensional PWEM for parallel fields.

The simple method for calculating η, γ and ψ employed in the one-dimensional example, does unfortunately not translate well into a two-dimensional situation. A major difference is that the electric field $\mathbf{E}$ and the wavevector $\mathbf{k}$ may in general have several components which will subsequently also result in different components of $\mathbf{P}$, $\mathbf{Q}^{\text{tot}}$ and $\mathbf{R}$. As a direct consequence, it can be seen that it is not possible to solve for any of the parameters directly, because the two-dimensional unit cell generally contains two components of the electric field. This can be exemplified by considering P_i in (49) in the case where an arbitrary unit cell is excited by a source $\mathbf{J}_{\text{ext}} = J_{\text{ext}}\hat{\mathbf{y}}$ with $\mathbf{k} = k_x\hat{\mathbf{x}}$. Inserting into equation (49a) and differentiating two times with respect to k_x gives

$$\frac{\partial^2 P_x}{\partial k_x^2} = 2\bigg(\eta_{xxxx}E_x + \eta_{xxxy}E_y\bigg). \tag{131}$$

Here it can be seen that there are two components, E_x and E_y, that contribute to P_x, and it can be deduced that a similar expression also exist for P_y. Since generally $E_x \neq 0$ and $E_y \neq 0$ for an arbitrary unit cell, and equation (131) contains two unkowns, η_{xxxx} and η_{xxxy}, it is not possible to solve this equation on its own. In order to obtain the solutions η_{xxxx} and η_{xxxy} it is necessary to develop another linearly independent equation containing η_{xxxx} and η_{xxxy} [11], and solve the equations as a linear system.

Another major difference from the one-dimensional example is that the parameters for a two-dimensional unit cell are tensors, η_{iklj}, γ_{ijlm} and ψ_{iklj}, that are dependent on the polarization of the electric field and the geometry of the unit cell. The values of η, γ and ψ that was found in the one-dimensional example are in fact also tensor elements, but could be solved separately due to the fact that $E_x = 0$. Since each tensor η, γ and ψ contains several elements, it is inefficient to solve for every single tensor value. It is therefore necessary to consider which tensor elements that are of interest.

If the wavevector $\mathbf{k}$ is kept constant in one direction, e.g. such that $\mathbf{k} = k_x\hat{\mathbf{x}}$, it was previously found that it was possible to express the local permeability-tensor as in equation (74), and it is therefore convenient to determine the parameters η_{iklj}, γ_{ijlm} and ψ_{iklj} appearing in this equation.

Since the microscopic electric field induces by the PWEM only contains components in the x-y plane such that $E_x \neq 0$, $E_y \neq 0$, $E_z = 0$, it is convenient to determine the parameters η_{2112}, γ_{2112} and ψ_{2112}. This section will therefore focus on determining the parameters η_{2112}, γ_{2112} and ψ_{2112}.

9.1 Simulating magnitudes of multipole expansion terms

The aim of this chapter is to develop an algorithm for determining the relative size of Q_{ij}^{tot}, R_i and P_i, by using the electric field solutions provided by the Parallel field PWEM algorithm. In order to determine the numerical values of η_{2112}, γ_{2112} and ψ_{2112}, it is necessary to analyze equations (48) and (49). Here it is seen that there are two obstacles that must be dealt with in order to solve a desired index variation of each parameter.

Firstly, since each constitutive relation in (49) carries two different parameters η, γ and ψ for E_x and E_y, it is not possible to solve for only one parameter at a time. This requires a linear system of equations which solves for both parameters for a given constitutive relation.

Secondly, the excitation of the source must be carefully selected because this will in turn determine the indices of $\mathbf{k}$ and $\mathbf{E}$. Only a certain combination of k and E can reveal the $_{2112}$-parameters.

Keeping these two obstacles in mind, the following two polarization configurations are proposed:

$$\text{Configuration 1:} \quad \mathbf{k} = k_x\hat{\mathbf{x}}, \quad \mathbf{J}_{\text{ext}} = J_{\text{ext}}\hat{\mathbf{y}}, \tag{132a}$$

$$\text{Configuration 2:} \quad \mathbf{k} = k_x\hat{\mathbf{x}}, \quad \mathbf{J}_{\text{ext}} = J_{\text{ext}}\hat{\mathbf{x}}. \tag{132b}$$

The expressions for P_i, Q_{ij}^{tot} and R_i in (49) are sums including several terms, and it will now be argued that they are simplified by selecting the two configurations in equation (132). Due to the uniformity of the unit cell in the z-direction, the source $\mathbf{J}_{\text{ext}}$ will generally produce an electric field $\mathbf{E} = E_x\hat{\mathbf{x}}+E_y\hat{\mathbf{y}}$, which means that all the terms that include E_z, k_y and k_z in (49) must be zero. Taking these simplifications into consideration leaves the following P_x and P_y components of the parameters in (49) for configuration 1:

$$P_x = \epsilon_0\chi_{xx}E_x + \epsilon_0\chi_{xy}E_y + \zeta_{xxx}k_xE_x + \zeta_{xxy}k_xE_y + \eta_{xxxx}k_x^2E_x + \eta_{xxxy}k_x^2E_y, \tag{133a}$$

$$P_y = \epsilon_0\chi_{yx}E_x + \epsilon_0\chi_{yy}E_y + \zeta_{yxx}k_xE_x + \zeta_{yxy}k_xE_y + \eta_{yxxx}k_x^2E_x + \eta_{yxxy}k_x^2E_y. \tag{133b}$$

And similarly for configuration 2:

$$P_x^\dagger = \epsilon_0\chi_{xx}E_x^\dagger + \epsilon_0\chi_{xy}E_y^\dagger + \zeta_{xxx}k_xE_x^\dagger + \zeta_{xxy}k_xE_y^\dagger + \eta_{xxxx}k_x^2E_x^\dagger + \eta_{xxxy}k_x^2E_y^\dagger, \tag{134a}$$

$$P_y^\dagger = \epsilon_0\chi_{yx}E_x^\dagger + \epsilon_0\chi_{yy}E_y^\dagger + \zeta_{yxx}k_xE_x^\dagger + \zeta_{yxy}k_xE_y^\dagger + \eta_{yxxx}k_x^2E_x^\dagger + \eta_{yxxy}k_x^2E_y^\dagger. \tag{134b}$$

The tensor parameters in equations (133) and (134) describe the electromagnetic response of the unit cell, and are therefore independent of the selection of source. This means that the parameters χ, ζ and η do not change despite the different fields (indicated by the $\dagger$ superscript) originating from the changed direction of the source $\mathbf{J}_{\text{ext}}$. It is therefore convenient to define:

$$\kappa_P \equiv \epsilon_0\chi_{xx} + \zeta_{xxx}k_x + \eta_{xxxx}k_x^2, \tag{135a}$$

$$\tau_P \equiv \epsilon_0\chi_{xy} + \zeta_{xxy}k_x + \eta_{xxxy}k_x^2, \tag{135b}$$

$$\phi_P \equiv \epsilon_0\chi_{yx} + \zeta_{yxx}k_x + \eta_{yxxx}k_x^2, \tag{135c}$$

$$\theta_P \equiv \epsilon_0\chi_{yy} + \zeta_{yxy}k_x + \eta_{yxxy}k_x^2. \tag{135d}$$

These four constants are practical because they hold four tensor values of η that will emerge when they are differentiated two times with respect to k_x. By using these constants it is now possible to rearrange equation (133) and (134) in matrix form

$$\begin{bmatrix} P_x \\ P_x^\dagger \end{bmatrix} = \begin{bmatrix} E_x & E_y \\ E_x^\dagger & E_y^\dagger \end{bmatrix} \cdot \begin{bmatrix} \kappa_P \\ \tau_P \end{bmatrix}, \tag{136a}$$

$$\begin{bmatrix} P_y \\ P_y^\dagger \end{bmatrix} = \begin{bmatrix} E_x & E_y \\ E_x^\dagger & E_y^\dagger \end{bmatrix} \cdot \begin{bmatrix} \phi_P \\ \theta_P \end{bmatrix}, \tag{136b}$$

which allows for solving the constants κ, τ, ϕ and θ by employing matrix algebra, and subsequently the following parameters: η_{xxxx}, η_{xxxy}, η_{yxxx} and η_{yxxy}. The exact same approach can be used to determine γ and ψ for the same four indices. Inserting for $\mathbf{E} = E_x\hat{\mathbf{x}} + E_y\hat{\mathbf{y}}$ and $\mathbf{k} = k_x\hat{\mathbf{x}}$ into the expressions for Q_{ij}^{tot} and R_i, configuration 1 gives:

$$Q_{xx}^{tot} = \alpha_{xxx}E_x + \alpha_{xxy}E_y + i\gamma_{xxxx}k_xE_x + i\gamma_{xxxy}k_xE_y, \tag{137a}$$

$$Q_{yx}^{tot} = \alpha_{yxx}E_x + \alpha_{yxy}E_y + i\gamma_{yxxx}k_xE_x + i\gamma_{yxxy}k_xE_y, \tag{137b}$$

$$R_x = \psi_{xxxx}k_x^2E_x + \psi_{xxxy}k_x^2E_y, \tag{138a}$$

$$R_y = \psi_{yxxx}k_x^2E_x + \psi_{yxxy}k_x^2E_y. \tag{138b}$$

And configuration 2 subsequently becomes:

$$Q_{xx}^{tot\dagger} = \alpha_{xxx}E_x^\dagger + \alpha_{xxy}E_y^\dagger + i\gamma_{xxxx}k_xE_x^\dagger + i\gamma_{xxxy}k_xE_y^\dagger, \tag{139a}$$

$$Q_{yx}^{tot\dagger} = \alpha_{yxx}E_x^\dagger + \alpha_{yxy}E_y^\dagger + i\gamma_{yxxx}k_xE_x^\dagger + i\gamma_{yxxy}k_xE_y^\dagger, \tag{139b}$$

$$R_x^\dagger = \psi_{xxxx}k_x^2E_x^\dagger + \psi_{xxxy}k_x^2E_y^\dagger, \tag{140a}$$

$$R_y^\dagger = \psi_{yxxx}k_x^2E_x^\dagger + \psi_{yxxy}k_x^2E_y^\dagger. \tag{140b}$$

The similarity between the expressions for Q_{ij}^{tot} and R_i in (137) - (140) and the expressions for P_i in (133) and (134) suggests the following definitions:

$$\kappa_Q \equiv \alpha_{xxx} + i\gamma_{xxxx}k_x, \tag{141a}$$

$$\tau_Q \equiv \alpha_{xxy} + i\gamma_{xxxy}k_x, \tag{141b}$$

$$\phi_Q \equiv \alpha_{yxx} + i\gamma_{yxxx}k_x, \tag{141c}$$

$$\theta_Q \equiv \alpha_{yxy} + i\gamma_{yxxy}k_x. \tag{141d}$$

$$\kappa_R \equiv \psi_{xxxx}k_x^2, \tag{142a}$$

$$\tau_R \equiv \psi_{xxxy}k_x^2, \tag{142b}$$

$$\phi_R \equiv \psi_{yxxx}k_x^2, \tag{142c}$$

$$\theta_R \equiv \psi_{yxxy}k_x^2. \tag{142d}$$

The constants defined in (141) and (142) can be solved by matrix algebra on the following expressions:

$$\begin{bmatrix} Q_{yx} \\ Q_{yx}^{\dagger} \end{bmatrix} = \begin{bmatrix} E_x & E_y \\ E_x^{\dagger} & E_y^{\dagger} \end{bmatrix} \cdot \begin{bmatrix} \kappa_Q \\ \tau_Q \end{bmatrix}, \tag{143a}$$

$$\begin{bmatrix} Q_{xx} \\ Q_{xx}^{\dagger} \end{bmatrix} = \begin{bmatrix} E_x & E_y \\ E_x^{\dagger} & E_y^{\dagger} \end{bmatrix} \cdot \begin{bmatrix} \phi_Q \\ \theta_Q \end{bmatrix}, \tag{143b}$$

$$\begin{bmatrix} R_x \\ R_x^{\dagger} \end{bmatrix} = \begin{bmatrix} E_x & E_y \\ E_x^{\dagger} & E_y^{\dagger} \end{bmatrix} \cdot \begin{bmatrix} \kappa_R \\ \tau_R \end{bmatrix}, \tag{143c}$$

$$\begin{bmatrix} R_y \\ R_y^{\dagger} \end{bmatrix} = \begin{bmatrix} E_x & E_y \\ E_x^{\dagger} & E_y^{\dagger} \end{bmatrix} \cdot \begin{bmatrix} \phi_R \\ \theta_R \end{bmatrix}. \tag{143d}$$

It is emphasized that these matrix equations are analogous to the two matrix equations in (136), and that they can be used further to solve for γ_{xxxx}, γ_{xxxy}, γ_{yxxx},γ_{yxxy} and ψ_{xxxx}, ψ_{xxxy}, ψ_{yxxx}, ψ_{yxxy} by differentiating and dividing by k_x. The parameters appearing in equation (74) can be identified as: $\eta_{yxxy} = \eta_{2112}$, $\gamma_{yxxy} = \gamma_{2112}$ and $\psi_{yxxy} = \psi_{2112}$.

Having obtained equations that can provide solutions for the desired index variations of η, γ and ψ, the attention of this section will now shift towards determining the numerical values of the expansion terms in equation (48) and equation (50).

9.2 Evaluating terms of the multipole expansion

In order to use the set of matrix equations that was derived in the previous section, it is necessary to determine the numerical values of the expansion terms defined in equation (45) and (47) under the restricting conditions of test-configuration 1 and 2.

Common to all of the expansion term integrals in equation (45) and (47), is the presence of the microscopic polarization density $\mathbf{p}$, which can be expressed [6, 23]

$$\mathbf{p} = \mathbf{e} \cdot \epsilon_0 \big(\varepsilon - 1\big), \tag{144}$$

The multipole expansion terms are vector quantities which may contain components in all directions, and it is necessary to determine their components before they can be evaluated.

Given that the specific source $\mathbf{J}_{\text{ext}}$ that is employed in the two configurations is polarized in the x-y plane, it follows that only p_x and p_y components are induced in the unit cell. It is seen from equation (48) that having only x and y components of the polarization, immidiately restricts the possible components of the multipole expansion terms. By inserting $\mathbf{p} = p_x\mathbf{x} + \hat{} p_y\hat{\mathbf{y}}$ along with $\mathbf{k} = k_x\hat{\mathbf{x}}$ into equation (45a), P_x and P_y is found as

$$P_x = \frac{\exp\left(ik_x x\right)}{V} \int_V p_x(x,y) dxdydz, \tag{145a}$$

$$P_y = \frac{\exp\left(ik_x x\right)}{V} \int_V p_y(x,y) dxdydz, \tag{145b}$$

and similarly R_x and R_y is found as

$$R_x = -\frac{\exp(ik_x x)}{2V}\int_V (k_x x)^2 p_x(x,y)dxdydz, \tag{146a}$$

$$R_y = -\frac{\exp(ik_x x)}{2V}\int_V (k_x x)^2 p_y(x,y)dxdydz. \tag{146b}$$

The integrand in equation (47) contains a tensor product, **rp**, which can be written as

$$\begin{bmatrix} x \\ y \\ z \end{bmatrix} \begin{bmatrix} p_x & p_y & 0 \end{bmatrix} = \begin{bmatrix} xp_x & xp_y & 0 \\ yp_x & yp_y & 0 \\ zp_x & zp_y & 0 \end{bmatrix}, \tag{147}$$

in the special case when $p_z = 0$. The two components Q_{xx}^{tot} and Q_{yx}^{tot} can now be obtained as

$$Q_{xx}^{\text{tot}} = \frac{\exp(ik_x x)}{V}\int_V xp_x(x,y)dxdydz, \tag{148a}$$

$$Q_{yx}^{\text{tot}} = \frac{\exp(ik_x x)}{V}\int_V xp_y(x,y)dxdydz. \tag{148b}$$

As explained in the derivation of the macroscopic electromagnetic fields, the integrals in (145), (146) and (148) are generally triple integrals over the volume V of the metamaterial unit cell. In this case however, it is assumed that the unit cell is two-dimensional and that the z-axis is infinitely extruded. The unit cell can therefore be regarded as a column of length l with a square cross-section. If the unit cell in question is located at the middle of the column, the integral of P_x becomes

$$\begin{aligned} P_x &= \frac{\exp(ik_x x)}{V}\int_{-\frac{l}{2}}^{\frac{l}{2}}\int_0^a\int_0^a p_x(x,y)dxdydz \\ &= \frac{\exp(ik_x x)}{A}\int_0^a\int_0^a p_x(x,y)dxdy, \end{aligned} \tag{149}$$

upon insertion of the integration limits for the z variable, where $A = a^2$ is the area of the square cross-section. Since **p** does not have any z-dependence, it follows that the integral with respect to z becomes unity. The same argument is also valid for the remaining integrals in (145), (148) and (146), such that they can be written:

$$P_x = \frac{\exp(ik_x x)}{A}\int_A p_x(x,y)dxdy, \tag{150a}$$

$$P_y = \frac{\exp(ik_x x)}{A}\int_A p_y(x,y)dxdy, \tag{150b}$$

$$Q_{xx}^{\text{tot}} = \frac{\exp(ik_x x)}{A}\int_A xp_x(x,y)dxdy, \tag{150c}$$

$$Q_{yx}^{\text{tot}} = \frac{\exp(ik_x x)}{A}\int_A xp_y(x,y)dxdy, \tag{150d}$$

$$R_x = -\frac{\exp(ik_x x)}{2A}\int_A (k_x x)^2 p_x(x,y)dxdy, \tag{150e}$$

$$R_y = -\frac{\exp(ik_x x)}{2A}\int_A (k_x x)^2 p_y(x,y)dxdy. \tag{150f}$$

The integrals are now in their component form, which facilitates the use of a computer for determining them as discrete sums. MATLAB offers a built in function, `sum(...)`, which is ideal for this purpose.

9.3 Rotated scheme

It is convenient to create a set of auxiliary test configurations in order to verify that the parameters calculated using configuration 1 and 2 in (132) are correct. One easy way of doing this is by rotating configuration 1 and 2 90° counterclockwise. This scheme is beneficial mainly because of three reasons:

- The numerical values for corresponding index variations in η, γ and ψ can be reproduced if the unit cell is rotated along with configuration 1 and 2, exploiting the fact that the rotation does not alter the physical situation at all.
- Any structure that is symmetric about the x and y axes should provide the same values for corresponding index variations in η, γ and ψ, upon rotation of the test configurations. Alternatively, the same holds true also when the configuration is fixed and the unit cell itself is rotated.
- Rotating the test configurations by 90 degrees counterclockwise will reveal a different set of index variations in η, γ and ψ.

It is therefore advantageous to introduce the following two test configurations:

$$\text{Configuration 3:} \quad \mathbf{k} = k_y\hat{\mathbf{y}}, \quad \mathbf{J}_{\text{ext}} = -J_{\text{ext}}\hat{\mathbf{x}}, \tag{151a}$$

$$\text{Configuration 4:} \quad \mathbf{k} = k_y\hat{\mathbf{y}}, \quad \mathbf{J}_{\text{ext}} = J_{\text{ext}}\hat{\mathbf{y}}. \tag{151b}$$

From now on, configurations 1 and 2 will be reffered to as scheme 1, and configurations 3 and 4 will be referred to as scheme 2. Scheme 1 and 2 differs only by the 90 degree rotation, which results in $\mathbf{k} = k_y\hat{\mathbf{y}}$. Inserting k_y together with $\mathbf{E} = E_x\hat{\mathbf{x}} + E_y\hat{\mathbf{y}}$ into (49) yields the following expressions for P_x, P_y, Q_{xy}^{tot}, Q_{yy}^{tot}, R_x and R_y in configuration 3:

$$P_x = \epsilon_0\chi_{xx}E_x + \epsilon_0\chi_{xy}E_y + \zeta_{xyx}k_yE_x + \zeta_{xyy}k_yE_y + \eta_{xyyx}k_y^2E_x + \eta_{xyyy}k_y^2E_y, \tag{152a}$$

$$P_y = \epsilon_0\chi_{yx}E_x + \epsilon_0\chi_{yy}E_y + \zeta_{yyx}k_yE_x + \zeta_{yyy}k_yE_y + \eta_{yyyx}k_y^2E_x + \eta_{yyyy}k_y^2E_y. \tag{152b}$$

$$Q_{xy}^{tot} = \alpha_{xyx}E_x + \alpha_{xyy}E_y + i\gamma_{xyyx}k_yE_x + i\gamma_{xyyy}k_yE_y, \tag{152c}$$

$$Q_{yy}^{tot} = \alpha_{yyx}E_x + \alpha_{yyy}E_y + i\gamma_{yyyx}k_yE_x + i\gamma_{yyyy}k_yE_y, \tag{152d}$$

$$R_x = \psi_{xyyx}k_y^2E_x + \psi_{xyyy}k_y^2E_y, \tag{152e}$$

$$R_y = \psi_{yyyx}k_y^2E_x + \psi_{yyyy}k_y^2E_y. \tag{152f}$$

And similarly for configuration 4:

$$P_x^\dagger = \epsilon_0\chi_{xx}E_x^\dagger + \epsilon_0\chi_{xy}E_y^\dagger + \zeta_{xyx}k_yE_x^\dagger + \zeta_{xyy}k_yE_y^\dagger + \eta_{xyyx}k_y^2E_x^\dagger + \eta_{xyyy}k_y^2E_y^\dagger, \tag{153a}$$

$$P_y^\dagger = \epsilon_0\chi_{yx}E_x^\dagger + \epsilon_0\chi_{yy}E_y^\dagger + \zeta_{yyx}k_yE_x^\dagger + \zeta_{yyy}k_yE_y^\dagger + \eta_{yyyx}k_y^2E_x^\dagger + \eta_{yyyy}k_y^2E_y^\dagger. \tag{153b}$$

$$Q_{xy}^{tot\dagger} = \alpha_{xyx}E_x^\dagger + \alpha_{xyy}E_y^\dagger + i\gamma_{xyyx}k_yE_x^\dagger + i\gamma_{xyyy}k_yE_y^\dagger, \tag{153c}$$

$$Q_{yy}^{tot\dagger} = \alpha_{yyx}E_x^\dagger + \alpha_{yyy}E_y^\dagger + i\gamma_{yyyx}k_yE_x^\dagger + i\gamma_{yyyy}k_yE_y^\dagger, \tag{153d}$$

$$R_x^\dagger = \psi_{xyyx}k_y^2E_x^\dagger + \psi_{xyyy}k_y^2E_y^\dagger, \tag{153e}$$

$$R_y^\dagger = \psi_{yyyx}k_y^2E_x^\dagger + \psi_{yyyy}k_y^2E_y^\dagger. \tag{153f}$$

It is important to note that the tensor parameters ζ_{ikj}, η_{iklj}, α_{ijk}, γ_{ijlm} and ψ_{iklj} revealed by scheme 2, contain completely different indices from the tensor parameters revealed by scheme 1. A direct comparison between the parameters of these two schemes for an arbitrary unit cell is therefore generally not meaningful. Such comparisons are however meaningful in the special case where the unit cell is symmetric about the x and y axes.

It is desirable to define sets of linear equations, similarly to the ones that was found for scheme 1. Since the expressions for P_x, P_y, R_x and R_y are identical, it is possible to employ equations (136a) (136b), (143c) and (143d) directly, by multiplying by k_y^2 instead of k_x^2 in the expressions for R_x and R_y. By inserting for k_y in equation (48) it is seen that the change of component in $\mathbf{k}$, requires a change of the components in $\mathbf{Q}^{\text{tot}}$. The two sets of linear equations for the new components of $\mathbf{Q}^{\text{tot}}$, namely Q_{xy} and Q_{yy}, are found as

$$\begin{bmatrix} Q_{xy} \\ Q_{xy}^\dagger \end{bmatrix} = \begin{bmatrix} E_x & E_y \\ E_x^\dagger & E_y^\dagger \end{bmatrix} \cdot \begin{bmatrix} \kappa_Q \\ \tau_Q \end{bmatrix}, \tag{154a}$$

$$\begin{bmatrix} Q_{yy} \\ Q_{yy}^\dagger \end{bmatrix} = \begin{bmatrix} E_x & E_y \\ E_x^\dagger & E_y^\dagger \end{bmatrix} \cdot \begin{bmatrix} \phi_Q \\ \theta_Q \end{bmatrix}. \tag{154b}$$

Analogous to scheme 1, the following constants are also defined:

$$\kappa_P \equiv \epsilon_0\chi_{xx} + \zeta_{xyx}k_y + \eta_{xyyx}k_y^2, \tag{155a}$$

$$\tau_P \equiv \epsilon_0\chi_{xy} + \zeta_{xyy}k_y + \eta_{xyyy}k_y^2, \tag{155b}$$

$$\phi_P \equiv \epsilon_0\chi_{yx} + \zeta_{yyx}k_y + \eta_{yyyx}k_y^2, \tag{155c}$$

$$\theta_P \equiv \epsilon_0\chi_{yy} + \zeta_{yyy}k_y + \eta_{yyyy}k_y^2. \tag{155d}$$

$$\kappa_Q \equiv \alpha_{xyx} + i\gamma_{xyyx}k_y, \tag{156a}$$

$$\tau_Q \equiv \alpha_{xyy} + i\gamma_{xyyy}k_y, \tag{156b}$$

$$\phi_Q \equiv \alpha_{yyx} + i\gamma_{yyyx}k_y, \tag{156c}$$

$$\theta_Q \equiv \alpha_{yyy} + i\gamma_{yyyy}k_y. \tag{156d}$$

$$\kappa_R \equiv \psi_{xyyx} k_y^2, \tag{157a}$$
$$\tau_R \equiv \psi_{xyyy} k_y^2, \tag{157b}$$
$$\phi_R \equiv \psi_{yyyx} k_y^2, \tag{157c}$$
$$\theta_R \equiv \psi_{yyyy} k_y^2. \tag{157d}$$

By determining the integrals of P_x, P_y, Q_{xy}^{tot}, Q_{yy}^{tot}, R_x, and R_y solving the sets of linear equations, the constants in (155) through (157) are obtained. The parameters $\eta_{xyyx} = \eta_{1221}$, $\gamma_{xyyx} = \gamma_{1221}$ and $\psi_{xyyx} = \psi_{1221}$ can now be obtained from these constants by differentiating and dividing by k_y, and subsequently be compared to the parameters that is found from scheme 1 if the unit cell is symmetric about both the x- and y- axes.

10 Results and Discussion

The results presented in this chapter are obtained by employing the plane wave expansion method for parallel fields, and the simulated parameters will be determined by employing polarization scheme 1.

10.1 Determining an optimal test structure

In order to ensure that the the parameters η, γ and ψ and subsequently any effective material parameters $\epsilon(\omega, \mathbf{k})$, ϵ and μ are accurate, it is necessary to demand the following of the PWEM algorithm:

- The electric field must show good convergence when the number of data points in its representation is increased.
- The inverse Fourier transform of the computer represented structure must be a physically meaningful, and be sufficiently similar to the original structure.

It will be the focus of this chapter to elaborate on- and investigate whether these requirements are fulfilled or not, and it will be shown that satisfying all of them simultaneously can prove to be quite challenging. This testing process is included in the results chapter because finding an optimal test structure is a valuable result by itself, and it is clear that a good test structure will yield better results in the subsequent result-sections.

The copper split-ring cylinder (CSRC) is a geometry that commonly occurs in metamaterial publications [12, 16, 31], and consist of two thin copper rings of different size that have been split and placed such that the splits are on opposite side of each other. The CSRC is not only interesting because of comparative reasons, but also because it is well translated from a three-dimensional into a two-dimensional unit cell. The microscopic permittivity $\varepsilon(x, y)$ of a CSRC in a unit cell of normalized length $a = 1$ can be represented in MATLAB by an imaginary part given in figure 7,

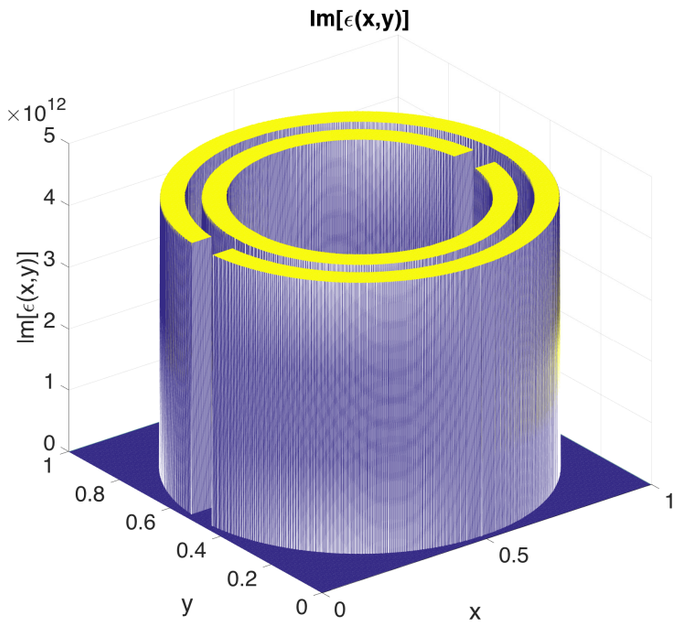

Figure 7: Copper split-ring cylinder in vacuum : $\mathrm{Im}[\varepsilon(x,y)]$. Note that the legend and axes in this plot utilizes ϵ rather than ε to denote the microscopic permittivity, since MATLAB does not support using the latter symbol by default.

where the imaginary part have been obtained from using the relation $\varepsilon = 1 - \frac{\sigma_{Cu}}{i\epsilon_0\omega}$ [23], and where the conductivity of copper $\sigma_{Cu} = 58.5 \times 10^6\,[\mathrm{S/m}]$ [27]. The plot of $\mathrm{Re}[\varepsilon(x,y)]$ has been omitted since it is unity throughout the entire unit cell. Figure 7 shows that the CSRC is a complex two-dimensional structure containing rapid spatial variations along the x and y- axes, but also a large relative difference between the values of the permittivity along the z-axis.

It is of great interest to determine the significance of $\mathbf{R}$ for this metamaterial unit cell. However, it is necessary to ensure the soundness of the representation of the CSRC in MATLAB before simulations of η, γ and ψ can be performed.

It is necessary to require that the microscopic electric field calculated by the PWEM has converged before it can be taken as correct, and be used to perform further calculations. By convergence, it is meant that a solution $\mathbf{e}(x,y)$ for a given number of spatial harmonics n does not change significantly when the solution matrix $\overline{\overline{\mathbf{V}}}_{\mathbf{w}}$ in equation (129) is padded with a given number of zeroes. Padding $\overline{\overline{\mathbf{V}}}_{\mathbf{w}}$ with zeroes should ideally only smoothen the solution $\mathbf{e}(x,y)$, and not alter it.

Allthough Fourier theory dictates that convergence can also be achieved by increasing the number n of spatial harmonics, the results in the subsequent sections will employ relatively low values of n, due to the fact that the PWEM run-time $t_{\mathrm{run}} > 45$ minutes when $n > 95$ spatial harmonics is employed.

The convergence of the CSRC in figure 7 can be determined by plotting the electric fields for $n = 31$ and padding the solution matrix $\overline{\overline{\mathbf{V}}}_{\mathbf{w}}$ in equation (129) with zeros to emulate $n = 41$, $n = 51$ and spatial harmonics. It is convenient to plot the components e_x and e_y along lines in the unit cell for comparitive

reasons. Figures 8, 9 and 10 show the plots of e_x and e_y along the x- and y axes for $n = 31$, $n = 41$ and $n = 51$ where the normalized parameters $\frac{\omega a}{c} = 0.2\pi$ and $\mathbf{k}a = 0.2\hat{\mathbf{x}}$ with the source $\mathbf{u}_0 = \exp(-ik_x\frac{a}{2})\hat{\mathbf{y}}$ have been employed. The source is multiplied by the factor $\exp(-ik_x\frac{a}{2})$ in order to shift the coordinate system such that origo is located at the center of the CSRC.

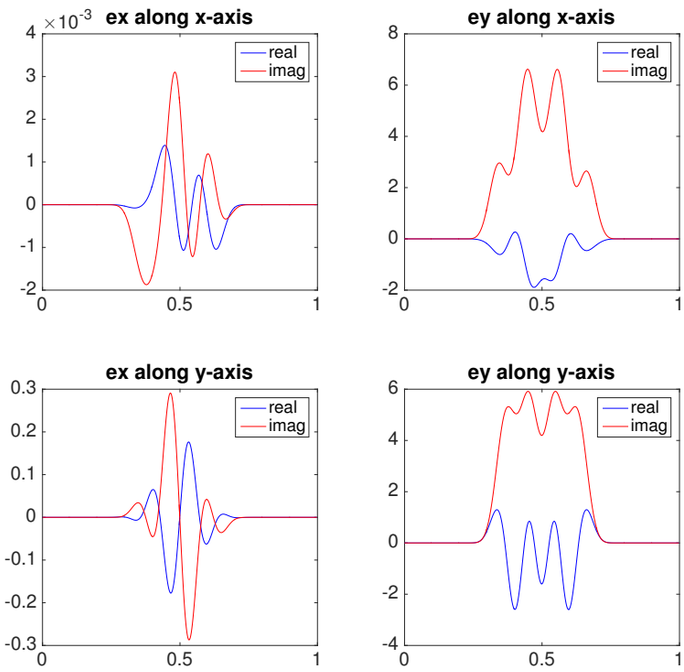

Figure 8: Microscopic electric field in copper split-ring for $n = 31$ ($t_{\text{run}} = 10.77\,[\text{sec}]$).

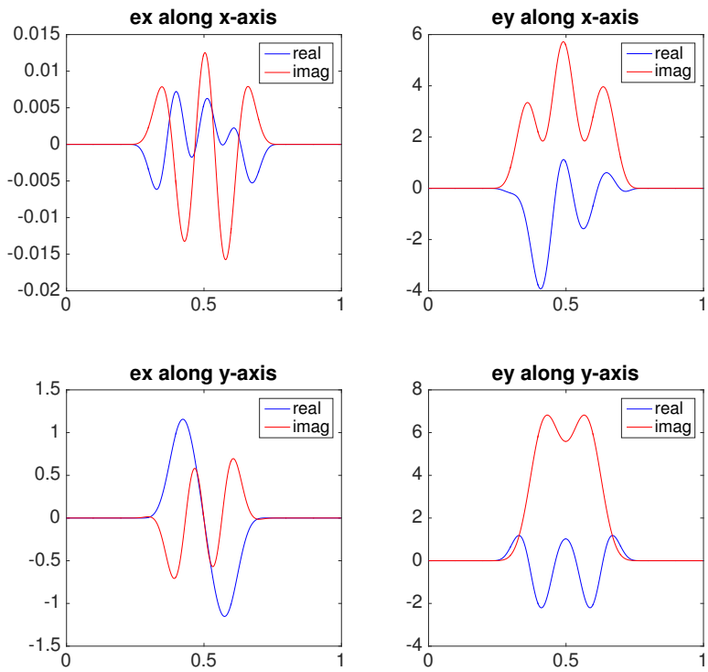

Figure 9: Microscopic electric field in copper split-ring for $n = 31$ padded with zeros to $n = 41$ ($t_{\text{run}} = 22.84\,[\text{sec}]$).

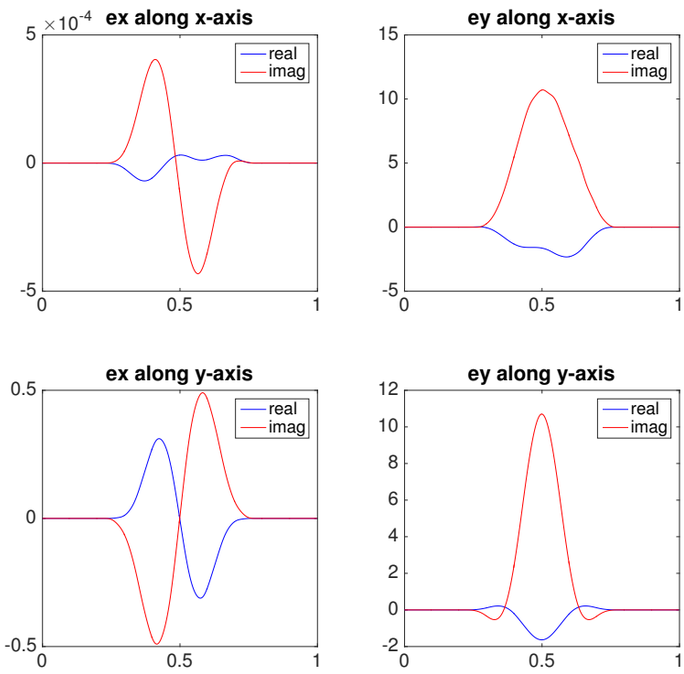

Figure 10: Microscopic electric field in copper split-ring for $n = 31$ padded with zeros to $n = 51$ ($t_{\text{run}} = 55.53\,[\text{sec}]$).

It can be seen from figures 8, 9 and 10 that the solution $\mathbf{e}(x, y)$ is not only varying significantly in amplitude, but also oscillates rapidly. These plots clearly indicate that $\mathbf{e}(x, y)$ has not converged for the selected resolution $n = 31$. It is possible to understand why by considering the solution of the microscopic electric field that is expected from a physical interpretation.

Since only $n = 31$ spatial harmonics have been used, it is reasonable to expect that any variations in the unit cell that occur within the distance $d_{\text{res}} = \frac{a}{31} \simeq 0.03$ will not be properly represented by the given amount of Fourier coefficients. Although equation (16) assumes that $\mathbf{e}(x, y)$ propagates through a planar interface, it can be used to approximate the skin depth such that $\delta \simeq 1.2 \times 10^{-5}\,\text{m}$.

It is expected that $\mathbf{e}(x, y)$ becomes an evanescent wave inside each ring, and it can therefore be assumed that it will decay as an exponential function, oscillating towards zero value until it reaches a length $\delta \simeq 1.2 \times 10^{-5}\,[\text{m}]$ inside the conducting rings. Since the skin depth δ is significantly smaller than the resolution length d_{res} restricted by the Fourier transform, the solution of $\mathbf{e}(x, y)$ is nowhere near beeing able to resolve the evanescent field inside each conducting layer. The length of the gap between the rings in figure 7 is approximately in the order of $d_{\text{gap}} = \frac{a}{25} = 0.04\,\text{m}$, and this distance is also to short to be properly resolved when only $n = 31$ spatial harmonics are employed.

When the solution vector $\overline{\overline{\mathbf{V}}}_{\mathbf{w}}$ is padded with a different number of zeros, these small variations of the unit cell are included and excluded from $\mathbf{e}(x, y)$ resulting in severly different plots depicted in 8, 9 and 10. The result is that $\mathbf{e}(x, y)$ changes drastically when the solution matrix $\overline{\overline{\mathbf{V}}}_{\mathbf{w}}$ is padded with additional zeros.

Another problem might be the discontinuities of the representation of the

CSRC in figure 7. The permittivity $\varepsilon(x, y)$ makes a sudden jump from 0 to 4.405×10^{12} in value, and it can be argued that the two-dimensional Fourier transform used in the PWEM is not capable to resolve this discontinuity properly. With the recent discussion in mind, there are three remedies that might improve the convergence of $\mathbf{e}(x, y)$ in the unit cell depicted in figure 7:

- Increase the spatial resolution n.
- Reduce the geometric complexity of the unit cell.
- Reduce the numerical value of $\mathrm{Im}[\varepsilon(x, y)]$ in the conducting material.

A quick calculation reveals that the first suggestion requires $n > 80000$ in order to resolve the skin depth δ, which would result in a very long run-time for the PWEM. The focus of the remainder of this section is therefore to further explore the two remaning remedies.

To better understand how the CSRC in figure 7 is treated within the PWEM, it is useful to consider the inverse fourier transform of the structure for a given number of spatial harmonics n. Figure 11 shows the inverse transformed permittivity of the unit cell containing the CSRC, where only the n lowest order Fourier coefficients of the permittivity have been used to reproduce the unit cell. Since $\mathrm{Re}[\varepsilon(x, y)] = 1$, only $\mathrm{Im}[\varepsilon(x, y)]$ is depicted in figure 11.

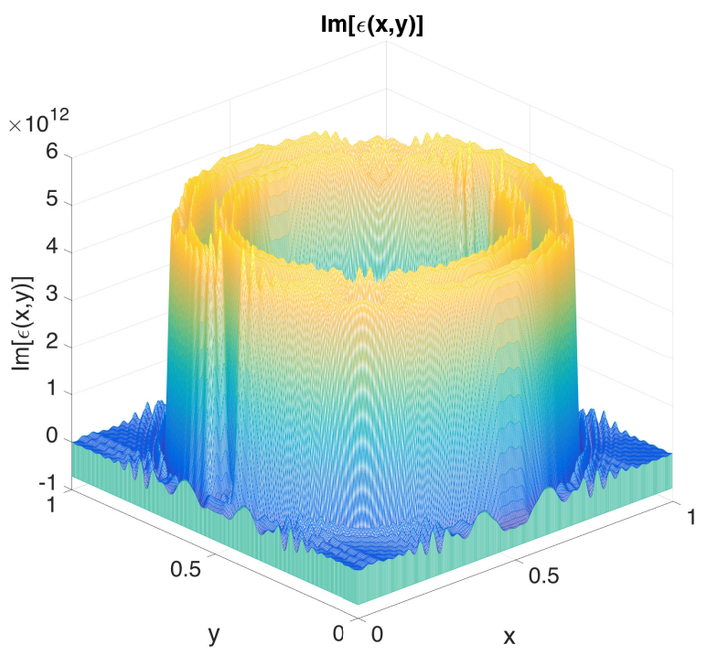

Figure 11: Inverse Fourier transformed unit cell containing CSRC using only $n = 31$ spatial harmonics.

As explained earlier, extracting only the lowest order coefficients from the Fourier transformed structure such that equation (116) is obtained, is essentially the same as low-pass filtering the original structure. This can be seen clearly in figure 11 since the edges of the rings appear to be less defined, which is consistent with having removed higher order spatial harmonics. Figure 11 also provide additional explanations as to why the plots in figure 8, 9 and 10 show no tendencies of convergence. Firstly, it is evident that the inverse transformed structure display rapid oscillations in value originating from the

abrupt interfaces in the unit cell. It can be seen that the function seems to overshoot the desired value of $\mathrm{Im}[\varepsilon(x, y)]$ inside both rings, which is characteristic to Gibb's phenomenon [11, p. 510]. These are all factors that depress the convergence of $\mathbf{e}(x, y)$.

It can also be observed that $\mathrm{Im}[\varepsilon(x, y)] \neq 0$ around and between the walls of the split-ring cylinders as intended, but does in fact oscillate in a range between $\pm 1 \times 10^{11}$. This is especially problematic that because this implies a significantly high conductivity in the region of the unit cell that is supposed to only contain vacuum. The unit cell depicted in figure 11 thus describes a copper split-ring resonator submerged in a slightly less conducting medium, rather than a copper split-ring resonator in vacuum.

Since increasing the amount of spatial harmonics n is futile, it is necessary to improve the extraction of coefficients from the Fourier transformed permittivity matrix. In order to obtain an inverse Fourier transform that closer resembles the original unit cell in figure 7, it is useful to employ windowing techniques such that the amplitudes of the higher order spatial harmonics included in the PWEM are reduced gradually to zero rather than having the abrupt cut-off that a traditional low-pass filter creates. Figure 12 depicts a two-dimensional generalization of a Blackman-Harris window function $W(p, s)$, where the variables $p \in [-P_f, +P_f]$ and $s \in [-S_f, +S_f]$ indicate the coordinate of the spatial harmonic $\epsilon_{p,s}$ in equation (116).

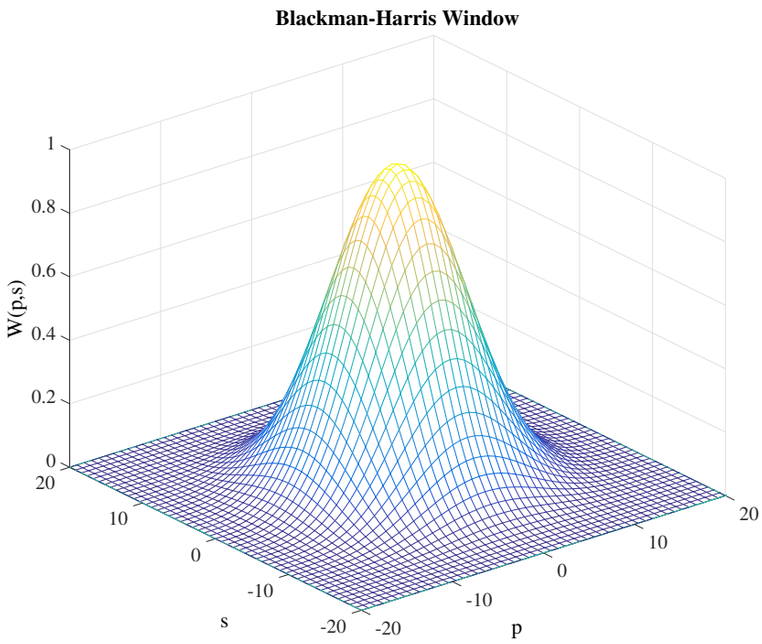

Figure 12: Two-dimensional Blackman-Harris filter $W(p, s)$, where $p \in [-20, +20]$ and $s \in [-20, +20]$.

The depiction of the Blackman-Harris window in figure 12 contains $51x51$ points, but will in general consist of $(2P_f + 1)(2S_f + 1)$ points in order to match the number of coefficients contained in equation (116). The effect of the Blackman-Harris window is clearly seen by comparing the inverse transform

of the CSRC for $n = 31$ without windowing in figure 11 with the inverse transform in figure 13.

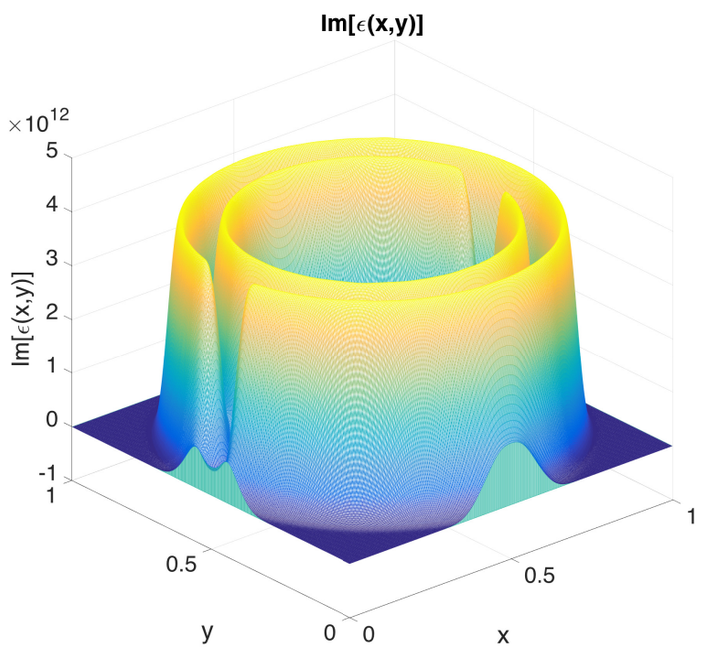

Figure 13: Inverse Fourier transformed unit cell containing CSRC using only $n = 31$ spatial harmonics and employing a Blackman-Harris window in the extraction of Fourier coefficients.

The application of the Blackman-Harris window removes the rapid oscillations in the IFT, thus making the transitions between low- and high-index media less abrupt and the structure smoother. Allthough this arguably will improve the convergence of $\mathbf{e}(x, y)$, it is still problematic that $\mathrm{Im}[\varepsilon(x, y)] \neq 0$ in the areas of the unit cell that contains vacuum. Because the physical significance of the inverse transformed structure in figure 13 is still not representative of the original CSRC in figure 7, it is necessary to make further adjustments to the unit cell.

The Fourier transform employed by the PWEM appears to struggle with the high numerical value of the permittivity in the unit cell containing the CSRC in figure 7, so the next remedy for improving the convergence of $\mathbf{e}(x, y)$ is therefore to lower the permittivity. By lowering the permittivity and reducing the geometric complexity within the unit cell, it was found that the structure depicted in figure 14 did show adequate convergence for $n = 31$ spatial harmonics.

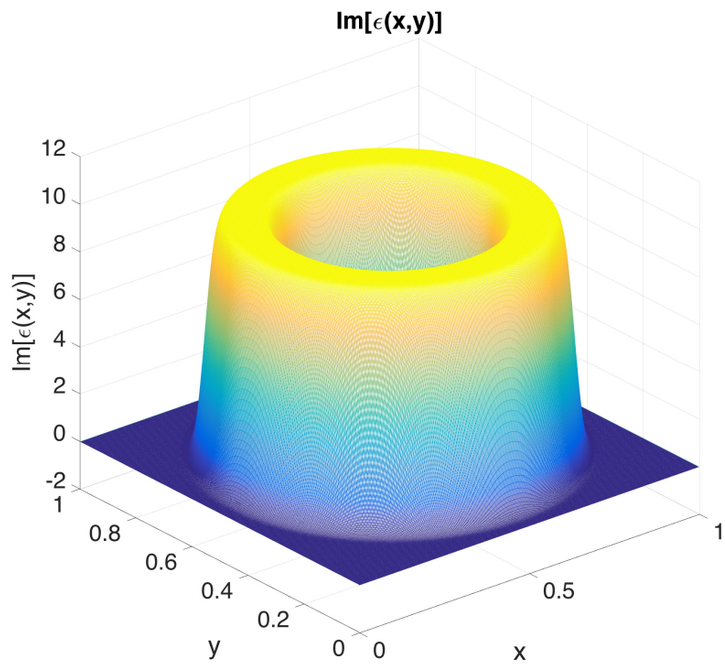

Figure 14: Inverse Fourier transformed unit cell containing vacuum and a weakly conducting annulus with $\varepsilon = 1 + 10i$, using only $n = 31$ spatial harmonics and employing a Blackman-Harris window in the extraction of Fourier coefficients.

The weakly conducting annulus with $\varepsilon = 1 + 10i$ in figure 14 is in many ways a simplification of the CSRC, since both the complexity of the geometry and the conductivity has been reduced. The microscopic electric field is calculated using input parameters $\frac{\omega a}{c} = 0.2\pi$, $\mathbf{k} = 0.2\hat{\mathbf{x}}$, $\mathbf{u}_0 = \exp(-ik_x\frac{a}{2})\hat{\mathbf{y}}$ and $n = 41$ spatial harmonics. Figures 15 and 16 show $\mathbf{e}(x, y)$ plotted along the x and y axes, for $n = 41$ and for $n = 41$ where equation (116) has been padded with zeros to emulate $n = 61$ spatial harmonics.

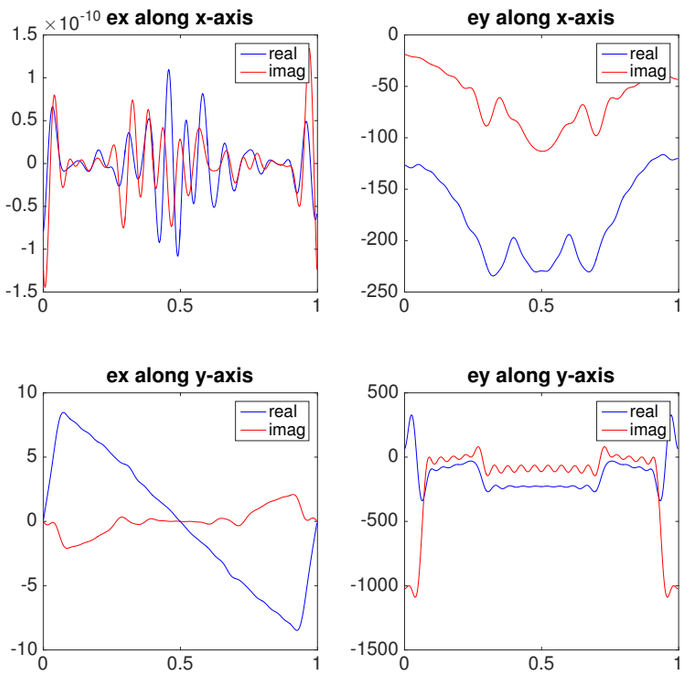

Figure 15: Microscopic electric field in conducting annulus for $n = 41$ ($t_{\text{run}} = 22.79\,[\text{sec}]$).

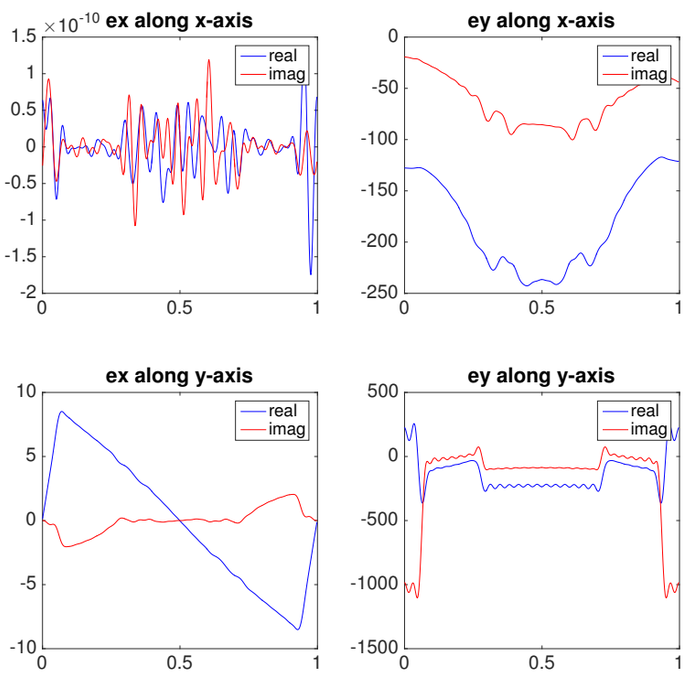

Figure 16: Microscopic electric field in copper split-ring for $n = 41$ padded with zeros to $n = 61$ ($t_{\text{run}} = 130.92\,[\text{sec}]$).

From the plots in figures 15 and 16 it can be seen that $\mathbf{e}(x, y)$ seems to converge for $n = 41$, and that the curves in figure 16 appear slightly smoother than the corresponding curves in figure 15 which is expected from the windowing procedure. Although the unit cell in figure 14 is indeed a greatly simplified version of the CSRC in figure 7, it is has been shown in this section that the PWEM is unable to produce a converged solution $\mathbf{e}(x, y)$ for moderate numbers of spatial harmonics n if the unit cell does not fulfill the following two requirements:

- The variations within the unit cell must occur on distances that are longer than the resolution length $d_{\text{res}} = \frac{a}{n}$.
- The numerical value of the permittivity must be in the order of 10.

These requirements will be of paramount priority when selecting the unit cells that are tested in the subsequent chapters, in order to ensure convergence of the calculated microscopic electric field.

10.2 Calculations of effective parameters

10.2.1 Dielectric annulus in vacuum

This section will present and discuss the microscopic electric field $\mathbf{e}(x, y)$ in a dielectric annulus simulated by the PWEM, and the parameters η, γ and ψ that is obtained by using $\mathbf{e}(x, y)$ to calculate the various terms in the multipole expansion of $\langle \mathbf{p}(x, y) \rangle$ given in equation (45).

First it is convenient to consider the qualitative solution of

$$-\mathbf{k} \times \mathbf{k} \times \mathbf{e}(\mathbf{r}) - \frac{\omega^2}{c^2} \varepsilon(\mathbf{r}) \mathbf{e}(\mathbf{r}) = i\omega\mu_0 \mathbf{u}_0 \exp(i\mathbf{k} \cdot \mathbf{r}), \tag{158}$$

which is the inhomogeneous wave-equation for a unit cell containing a dielectric annulus. If $(\mathbf{k} \cdot \mathbf{r}) \ll 1$ and the permittivity $\varepsilon(\mathbf{r})$ and source $\mathbf{u}(\mathbf{r})$ are real valued, it can be argued that the solution $\mathbf{e}(x, y)$ should be imaginary because of the factor i on the right side of equation (158). It should therefore be possible to obtain a purely imaginary microscopic electric field $\mathbf{e}(\mathbf{r})$ by exciting the given unit cell with real valued source, and it is this theoretical solution that will be pursued in the following. The unit cell containing the dielectric annulus is depicted in the figure below, and is represented by a matrix containing 499×499 point values of $\varepsilon(x, y)$ in MATLAB.

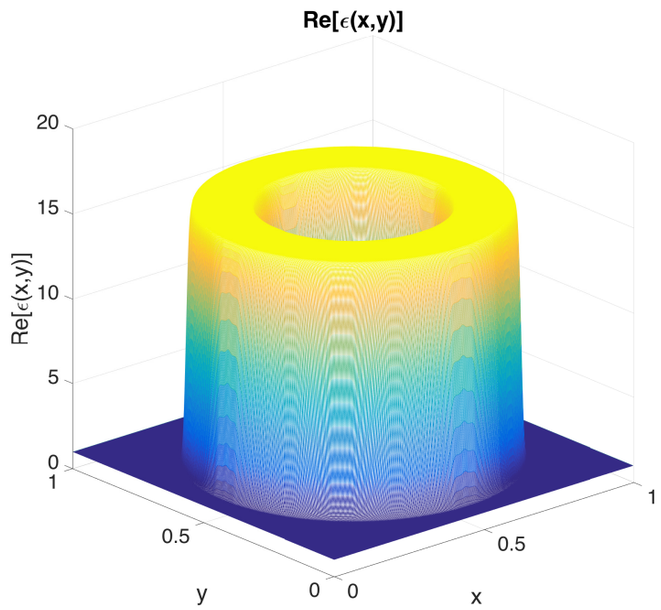

Figure 17: Dielectric annulus in vacuum with microscopic permittivity $\varepsilon = 16$. Inverse Fourier transform represented by $n^2 = 91^2$ coefficients.

The unit cell is excited with normalized input parameters $\frac{\omega a}{c} = 0.2\pi$, $\mathbf{k}a = 0.2\hat{\mathbf{x}}$ and source $\mathbf{u}_0 = \exp(-ik_x \frac{a}{2})\hat{\mathbf{y}}$. The phase factor $(-ik_x \frac{a}{2})$ in the source shifts the coordinate system such that origo is located at the center of the annulus. In order to ensure field convergence, it is necessary to compare the calculated electric fields for a given value of n with the calculated electric field for the same n but where the latter has been padded such that it comprises a greater number of Fourier coefficients. Convergence is achieved if the two fields are identical. A practical way to visualize the different electric fields, is by plotting the components of $\mathbf{e}$ and $\mathbf{p}$ along the x and y axes. Figures 18 and 19 show the plots of $\mathbf{e}(x, y)$ and $\mathbf{p}(x, y)$ along the x and y axes for $n = 41$ coefficients, but

where the Fourier transform of the electric field in figure 19 has been padded to include $n = 61$ coefficients in the PWEM.

Figure 18: $\mathbf{e}(x, y)$ and $\mathbf{p}(x, y)$ for $n = 41$

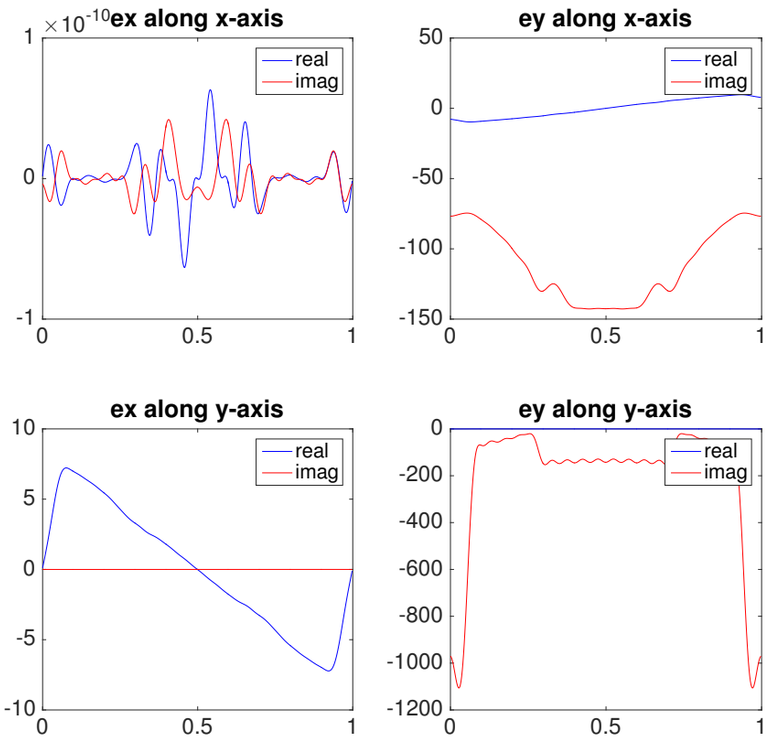

(a) Microscopic electric field $\mathbf{e}(x, y)$ in dielectric annulus for $n = 41$.

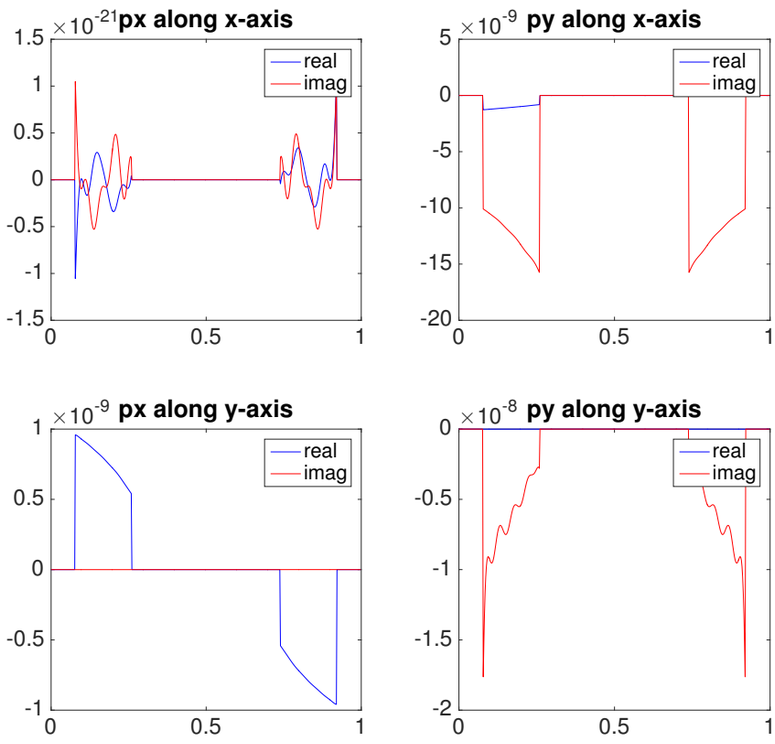

(b) Microscopic polarization density $\mathbf{p}(x, y)$ in dielectric annulus for $n = 41$.

Figure 19: $\mathbf{e}(x, y)$ and $\mathbf{p}(x, y)$ for $n = 41$ padded to $n = 61$.

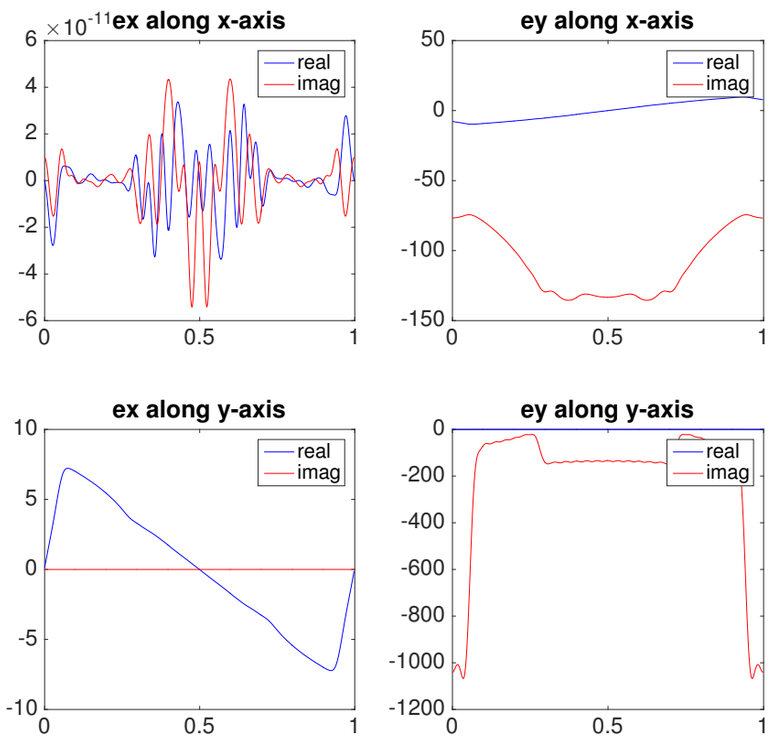

(a) Microscopic electric field $\mathbf{e}(x, y)$ in dielectric annulus for $n = 41$ with padding to $n = 61$.

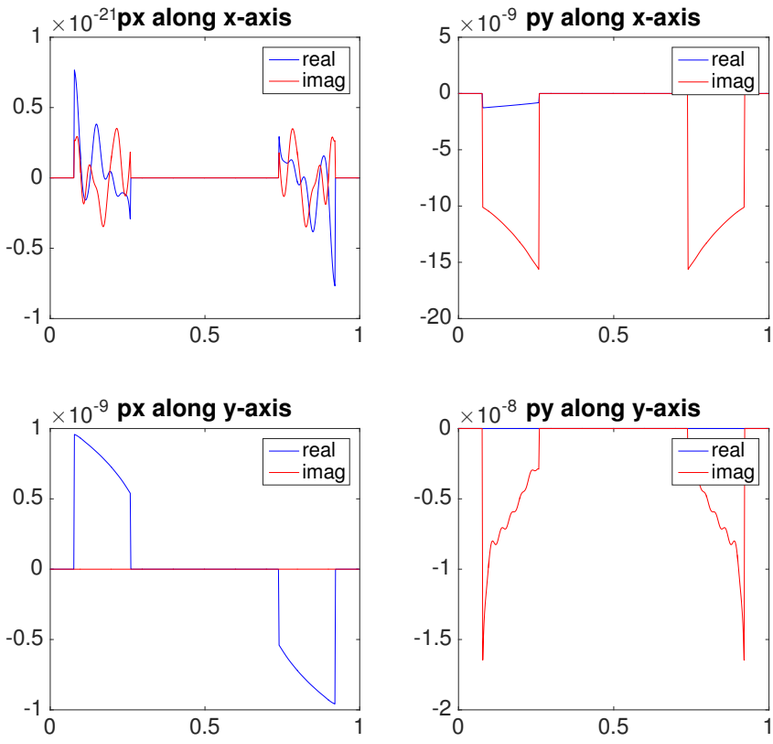

(b) Microscopic polarization density $\mathbf{p}(x, y)$ in dielectric annulus for $n = 41$ with padding to $n = 61$.

From these plots it is seen that the solution of the electric field generated by the PWEM is close to converging for $n = 41$. Although the plot of p_x along the x- axis in figure 19 is different from the plot of p_x along the x- axis in figure 18, this difference is neglibly small compared to the magnitude of the other plots. It can also be argued that e_x should approach zero in value since the excitation $\mathbf{u}_0$ primarily effects e_y, and that the oscillating behavior of p_x arises from the fact that e_x is converging towards zero.

It is also apparent that the solution of $\mathbf{e}(x, y)$ contains both a real and imaginary parts, in contradiction to the argument that was made previously by assuming the source to be purely real in equation (158). The observed real and imaginary parts of $\mathbf{e}(x, y)$ in figures 18 and 19 can be understood by assuming the source $\mathbf{J}_{\text{ext}} = \mathbf{u}_0 \exp(i\mathbf{k} \cdot \mathbf{r})$ to excite an electric field

$$\mathbf{e}_{\text{ext}}(x, y) = \mathbf{e}_0(x, y) + \mathbf{e}_0(x, y) \cdot (i\mathbf{k} \cdot \mathbf{r}), \tag{159}$$

where the exponential factor of the source has been expanded as a Taylor-series. Equation (159) show that the solution $\mathbf{e}_{\text{ext}}$ contains a large imaginary electrostatic part in $\mathbf{e}_0(x, y)$, but also allows the solution of $\mathbf{e}_{\text{ext}}(x, y)$ to have a small spatially varying real-valued part $\mathbf{e}_0(x, y) \cdot (i\mathbf{k} \cdot \mathbf{r}) = \mathbf{e}_0(x, y) \cdot (ik_x \cdot x)$. The plots in figure 18 and 19 seems to agree with this interpretation since $\text{Re}[e_y(x, y)] \ll \text{Im}[e_y(x, y)]$. The qualitative description of the microscopic field solution conveniently splits the solution $\mathbf{e}_{\text{ext}}(x, y)$ into real and imaginary parts, and it is therefore convenient to plot the normalized vector fields of $\text{Re}[\mathbf{e}(x, y)]$ and $\text{Im}[\mathbf{e}(x, y)]$:

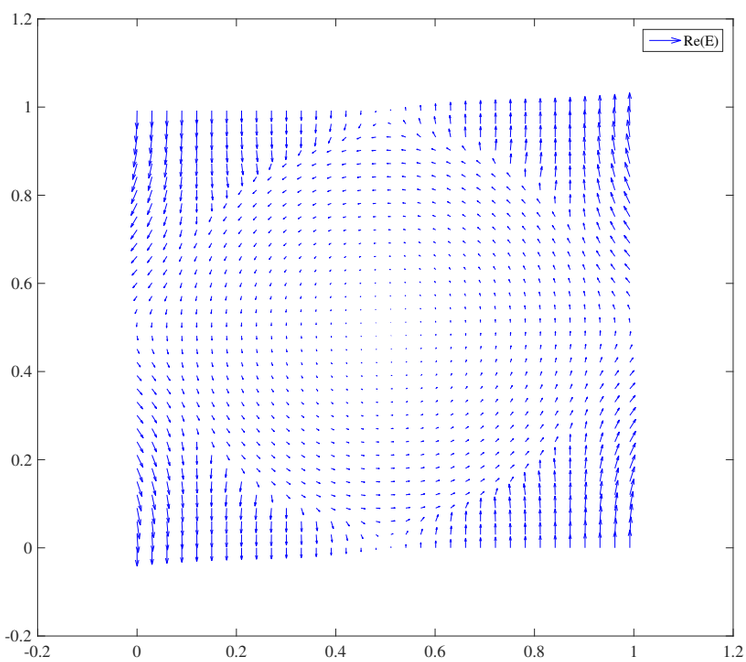

Figure 20: Normalized vector field $\text{Re}[\mathbf{e}(x, y)]$

From figure 20 it can be seen that $\text{Re}[\mathbf{e}(x, y)]$ appears to circulate in counter-clockwise direction within the region of high permittivity, while becoming

slightly smaller inside of it. The vector field almost vanishes in the center vacuum hole, but still displays circulating behaviour.

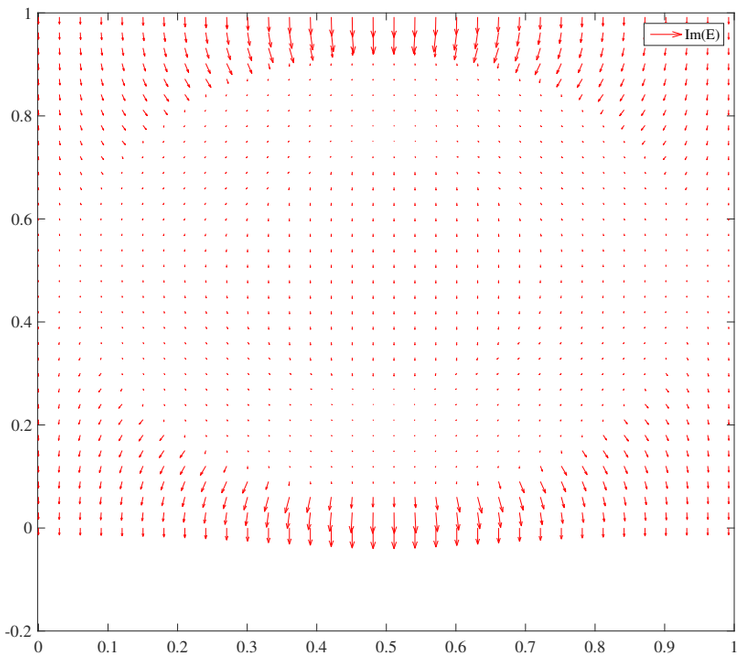

Figure 21: Normalized vector field $\mathrm{Im}[\mathbf{e}(x, y)]$

Figure 21 shows that $\mathrm{Im}[\mathbf{e}(x, y)]$ is drawn towards the annulus from the outside, and becomes noticeably smaller inside the region of high permittivity. It is interesting to plot the vector field of the microscopic polarization, $\mathrm{Re}[\mathbf{p}(x, y)]$ and $\mathrm{Im}[\mathbf{p}(x, y)]$, in order to resolve the vector field in the region of high permittivity with greater accuracy:

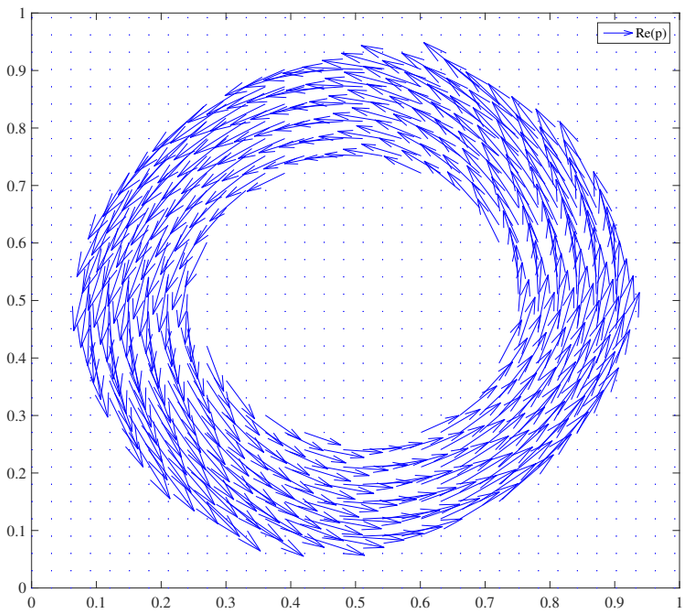

Figure 22: Normalized vector field $\mathrm{Re}[\mathbf{p}(x, y)]$

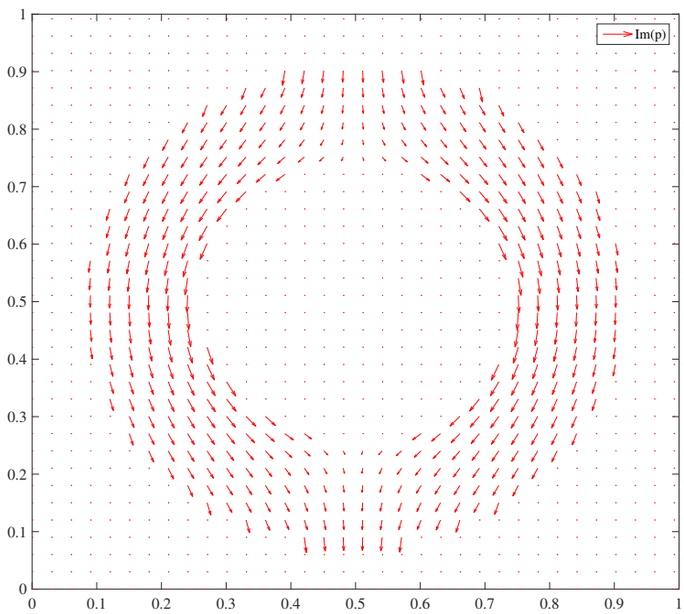

Figure 23: Normalized vector field $\mathrm{Im}[\mathbf{p}(x, y)]$

Figure 22 confirms the counter-clockwise circulation of $\mathrm{Re}[\mathbf{e}(x,y)]$ within the high permittivity region, and figure 23 shows that $\mathrm{Im}[\mathbf{e}(x,y)]$ enters the high index region and tends to follow the shape of the annulus before breaking out at the bottom. It is also worth noting that the vectors in figure 22 are scaled 50 times larger than the vectors in figure 23.

The vector fields that have been plotted in figures 20 to 23 seems to agree with the qualitative interpretation in equation (159). First of all, it is clear that $\mathbf{e}(x,y)$ comprises both real and imaginary parts, and that it is not purely imaginary as was first deduced from considering equation (158). Secondly, equation (159) explains why $\mathrm{Im}[\mathbf{e}(x,y)] > \mathrm{Re}[\mathbf{e}(x,y)]$ and why their vector fields are significantly differerent. The source $\mathbf{J}_{\text{ext}}$ excites the electric field $\mathbf{e}_{\text{ext}}$, which can be split into two contributions. The largest contribution, which is the part that corresponds to $\mathrm{Im}[\mathbf{e}(x,y)]$ in figure 21, is a uniform electric field that is pulled towards the regions of higher permittivity, as would be expected from electrostatic theory. The other part of of the qualitative solution, $\mathrm{Re}[\mathbf{e}_{\text{ext}}]$ in figure 20, is position dependent and therefore circulates within the high permittivity region.

Furthermore, it can also be argued that the circulation of $\mathrm{Re}[\mathbf{e}(x,y)]$ will give rise to a magnetic field $\mathbf{b} = b_0\hat{\mathbf{z}}$ by using Faraday's law in equation (4a), which in turn will generate a circulating displacement current $\mathbf{D}$ inside the annulus [3, 26]. This interpretation correlates to some degree with results obtained by Andryieuski et al. [25].

Having obtained a decent understanding of the electric field $\mathbf{e}(x,y)$ inside the unit cell depicted in figure 17, it is now time to investigate the significance of $\mathbf{R}$ in the multipole expansion in (45). The parameters η_{2112}, γ_{2112} and ψ_{2112} are calculated for $\frac{\omega a}{c} = 0.2\pi$ with sources $\mathbf{u}_0 = \exp(-ik_x\frac{a}{2})\hat{\mathbf{y}}$ and $\mathbf{u}_0 = \exp(-ik_x\frac{a}{2})\hat{\mathbf{x}}$, by iterating through $k_x a = 0.1, 0.2, 0.3$ and are given in table 1, where it can be seen that the relative size between the parameters seems to agree with what was predicted in equation (57).

Table 1: Normalized parameters for dielectric annulus in vacuum evaluated in $k_x a = 0.2$

$\eta_{2112}/\epsilon_0 a^2$	$-0.0481 + 0.0000i$
$\gamma_{2112}/\epsilon_0 a^2$	$0.1948 - 0.0001i$
$\psi_{2112}/\epsilon_0 a^2$	$-0.0595 + 0.0000i$

The dominant part of $\mathrm{Re}[\psi_{2112}] \simeq -0.32\mathrm{Re}[\gamma_{2112}] \simeq 1.27\mathrm{Re}[\eta_{2112}]$, which implies that R_y is indeed significant compared to the other terms in equation (48). This can be understood by looking at the integral that determines R_y in equation (150f). If $p_y(x,y)$ displays perfect odd symmetry about the x and y axes, it can be argued that the integral in equation (150f) should be zero, such that $R_y = 0$. It is however apparent that the plots of $p_y(x,y)$ along the x and y axis clearly display even symmetry about both axes, indicating that the integral in (150f) gives $R_y \neq 0$, and thus may give a significant ψ_{2112} compared with η_{2112} and γ_{2112}.

10.2.2 Conducting annulus in vacuum

This section will present and discuss the electric field $\mathbf{e}(x, y)$ in a unit cell containting a conducting annulus simulated by the PWEM, and the parameters η, γ and ψ that is obtained by using $\mathbf{e}(x, y)$ to calculate the various terms in the multipole expansion of $\langle \mathbf{p}(x, y) \rangle$ given in component form in equation (48).

The unit cell containing the conducting annulus is depicted in the figure below, and is represented by a matrix containing 499×499 point values of $\varepsilon(x, y)$ in MATLAB. As with the dielectric annulus, the convergence of the electric field in the unit cell containing the conducting annulus was achieved for $n = 41$ coefficients.

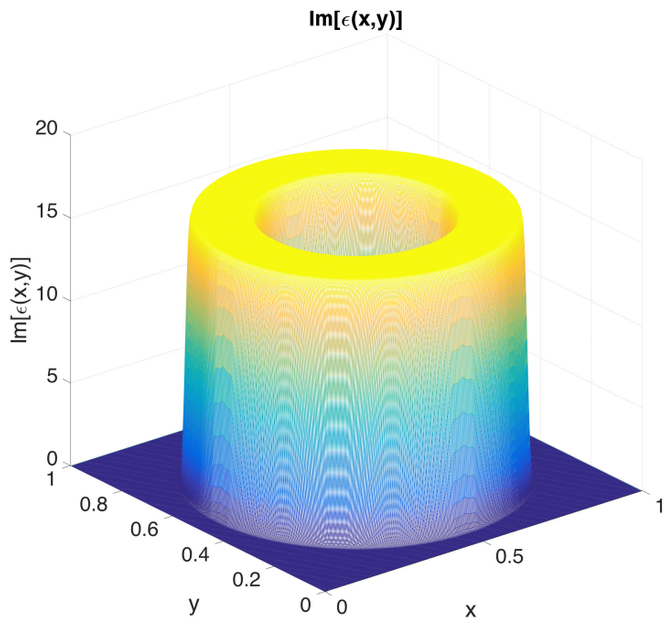

Figure 24: Conducting annulus in vacuum with microscopic permittivity $\varepsilon = 1 + 16i$. Inverse Fourier transform represented by $n^2 = 91^2$ coefficients.

Ideally, it would be beneficial to develop a qualitative solution similar to the one given in equation (159) for the dielectric annulus. This is unfortunately not as describing in the case where $\varepsilon = 1 + 16i$. The complex permittivity mixes the real and imaginary parts of the solution in equation (159), such that they no longer can be associated with a large electrostatic and a small spatially varying contribution. Although the entirety of the field is still meaningful, it is essentially split into two contributions that cannot easily be interpreted and related to an expected solution. Instead, this discussion will assess the simulated electric microscopic electric field $\mathbf{e}(x, y)$ and microscopic polarization $\mathbf{p}(x, y)$ by considering the conductive properties of the annulus. Suitable comparisons with the dielectric annulus will also be made.

Figure 25 depict the plots of $\mathbf{e}(x, y)$ and $\mathbf{p}(x, y)$ along the x- and y-axes, excited by a source $\mathbf{u}_0 = \exp(-ik_x \frac{a}{2})\hat{\mathbf{y}}$, and normalized input parameters $\frac{\omega a}{c} = 0.2\pi$ and $\mathbf{k} = 0.2\hat{\mathbf{x}}$. The simulation was performed with $n = 41$ padded to $n = 61$ spatial harmonics.

Figure 25: $\mathbf{e}(x, y)$ and $\mathbf{p}(x, y)$ for $n = 41$ padded to $n = 61$.

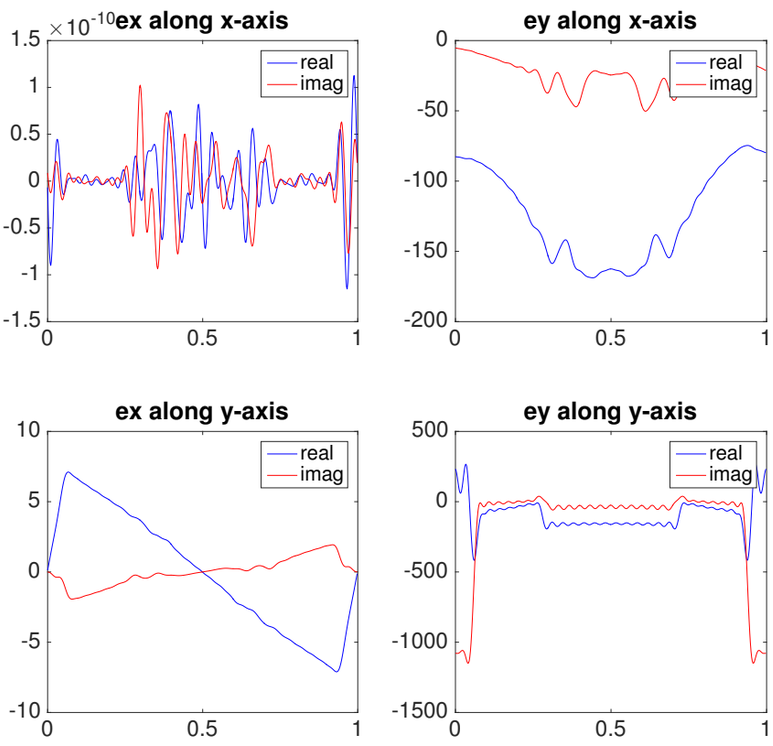

(a) Microscopic electric field $\mathbf{e}(x, y)$ in dielectric annulus for $n = 41$ with padding to $n = 61$.

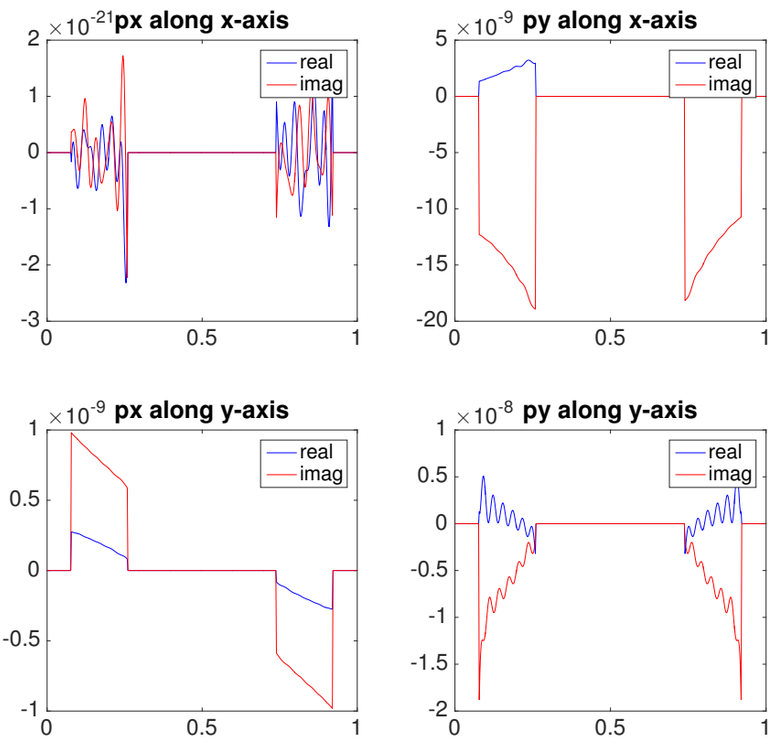

(b) Microscopic polarization density $\mathbf{p}(x, y)$ in dielectric annulus for $n = 41$ with padding.

The mixing of the real and imaginary parts of $\mathbf{e}(x, y)$ is evident since it can be seen that $\mathrm{Re}[\mathbf{e}(x, y)]$ and $\mathrm{Im}[\mathbf{e}(x, y)]$ are more similar in magnitude, as opposed to the plots of $\mathbf{e}(x, y)$ in the dielectric annulus given in figure 19. The most dominant component in figure 25a, e_y along the y-axis, is large outside of the annulus and drops quickly to a small value inside the annulus. The electric field is small but not nonzero in the vacuum hole at the center of the annulus.

The microscopic permittivity $\varepsilon = 1 + 16i$ corresponds to a conductivity $\sigma = 16\epsilon_0\omega = 2.6703 \times 10^{-2}\,[\mathrm{S/m}]$, which according to equation (16) gives $\delta = 0.56\,\mathrm{m}$. This theoretical skin depth suggests that the material is a very poor conductor since it predicts that $\delta \simeq 0.5\tilde{a}$, thus indicating that $\mathbf{e}(x, y)$ is nowhere close to vanishing inside the conducting material. It must however, be kept in mind that the derivation of the skin depth that was given earlier does not take any geometric precautions and may therefore be inaccurate. Figure 25a appears to confirm this inaccuracy since the magnitude of the electric field does drop significantly in value once it reaches the annulus. Apart from this inaccuracy, it is still reasonable to consider the annulus to be made of a very poorly conducting medium.

It is possible to argue that $\mathbf{e}(x, y)$ should be zero inside the vacuum hole at the center of the annulus if the material is indeed conducting because it would work as a Faraday cage. This is however not the case in these simulations because of the unlocalized distribution of the source that is employed.

The parameters η_{2112}, γ_{2112} and ψ_{2112} are calculated for normalized input parameters $\frac{\omega a}{c} = 0.2\pi$ with sources $\mathbf{u}_0 = \exp(-ik_x\frac{a}{2})\hat{\mathbf{y}}$ and $\mathbf{u}_0 = \exp(-ik_x\frac{a}{2})\hat{\mathbf{x}}$, by iterating through $k_x = 0.1, 0.2, 0.3$ and are given in the table below

Table 2: Normalized parameters for conducting annulus in vacuum evaluated in $k_x = 0.2$. The mixing of real and imaginary parts of the solution in equation (159) can also be observed here, since the real and imaginary part of the parameters are more similar in magnitude.

$\eta_{2112}/\epsilon_0 a^2$	$-0.0553 - 0.0226i$
$\gamma_{2112}/\epsilon_0 a^2$	$0.0112 + 0.1673i$
$\psi_{2112}/\epsilon_0 a^2$	$-0.0664 - 0.0483i$

It can be seen in table 2, that $\mathrm{Re}[\psi_{2112}] \simeq -0.38\mathrm{Im}[\gamma_{2112}] \simeq 1.12\mathrm{Re}[\eta_{2112}]$, implying that the R_y term is significant compared to the other expansion terms in equation (48). It is possible to employ the same line of argument as in the example with the dielectric annulus, in order to explain why η_{2112}, γ_{2112} and ψ_{2112} are of the same size. Figure 25 shows that the dominant part e_y of $\mathbf{e}(x, y)$ exhibit even symmetry, which may allow R_y to become large. A similarity between the dielectric and the conducting annulus, is that it is the electrostatic part of the solution, and not the spatially varying part that makes ψ_{2112} siginificant, because the former has a symmetric electric field.

This theory can be extended to predict the significance of ψ_{2112} in a unit cell containing an annulus made of a good conductor. From electrostatics, where it is assumed that $\sigma \to \infty$, it is possible to deduce that the electrostatic part of $\mathbf{e}(x, y)$ vanishes inside the conducting medium, thus leaving only the asymmetric part of $\mathbf{e}(x, y)$ which causes the circulation. When this circulating part is allowed to grow due to the high conductivity, $\mathbf{e}(x, y)$ becomes increasingly antisymmetric, resulting in that the integral in equation (150f) will give

$R_y = 0$ and subsequently $\psi_{2112} = 0$.

10.2.3 U-shaped split-ring resonator in vacuum

The examples that have been presented thus far in this thesis, are unit cells that are symmetric about both the x and y axes. It is therefore of great interest to explore the significance of $\mathbf{R}$ for a geometry that is antisymmetric. The aim of this section, is to perform simulations on a u-shaped split-ring resonator (USRR) geometrically similar to the ones used in [28], discuss the simulated electric fields and analyze the significance of $\mathbf{R}$.

The USRR that will be considered in the following, is submerged in vacuum and has a microscopic permittivity $\varepsilon = 10$. It has been shown in the previous examples that the PWEM converges for such low values of the permittivity, and it is therefore interesting to determine the parameters η_{2112}, γ_{2112} and ψ_{2112} for such a structure since it exemplifies a unit cell that is not symmetric about both axes. Figure 26 depicts a unit cell containing a u-shaped split-ring resonator, represented in MATLAB by 499×499 point values of $\varepsilon(x, y)$.

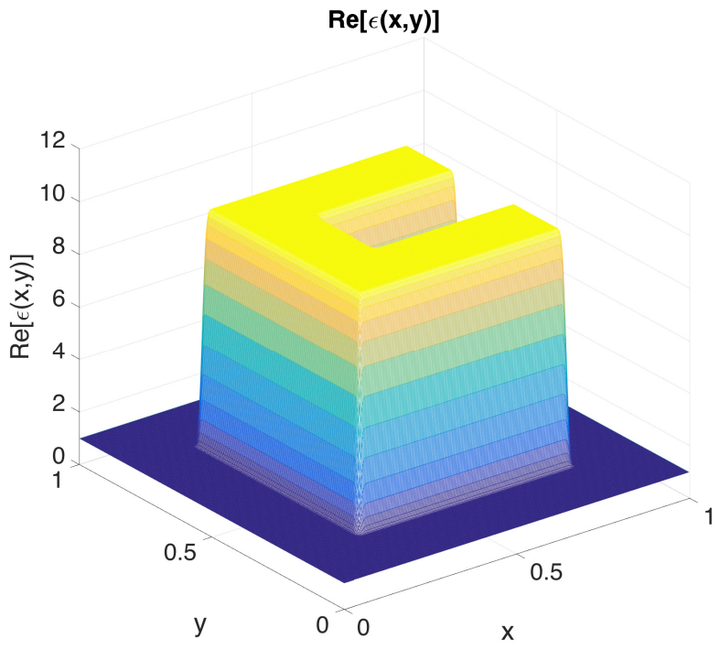

Figure 26: Conducting u-shaped split-ring cylinder with microscopic permittivity $\varepsilon = 10$. Inverse Fourier transform represented by $n^2 = 91^2$ coefficients.

By employing the PWEM with normalized input parameters $\frac{\omega a}{c} = 0.2\pi$, $\mathbf{k} = 0.2\hat{\mathbf{x}}$ with a source $\mathbf{u}_0 = \exp(-ik_x\frac{a}{2})\hat{\mathbf{y}}$, the microscopic electric field $\mathbf{e}(x, y)$ and microscopic polarization $\mathbf{p}(x, y)$ plotted along the x- and y axes in figure 27 are obtained.

Figure 27

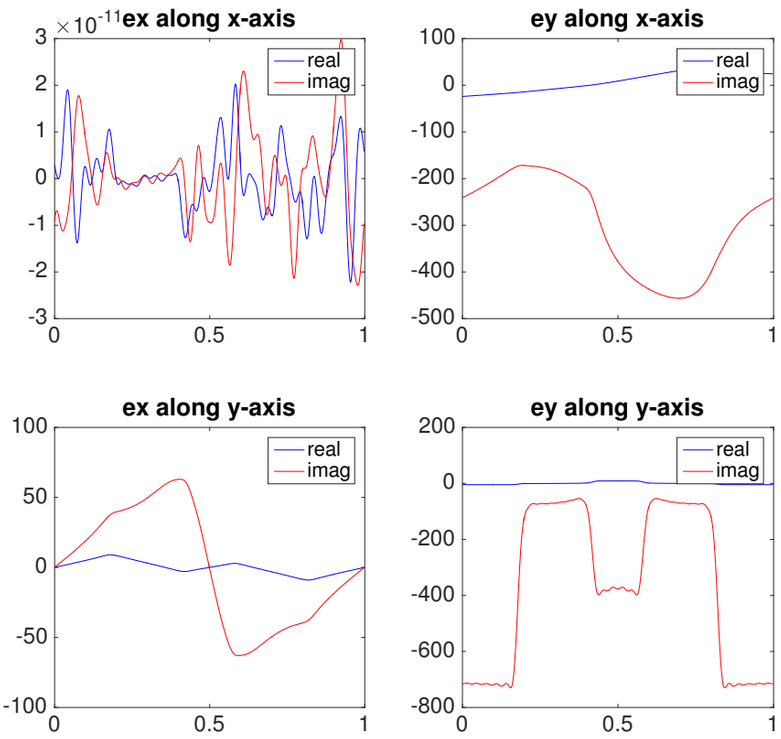

(a) Microscopic electric field $\mathbf{e}(x, y)$ in u-shaped split-ring for $n = 41$ with padding to $n = 61$.

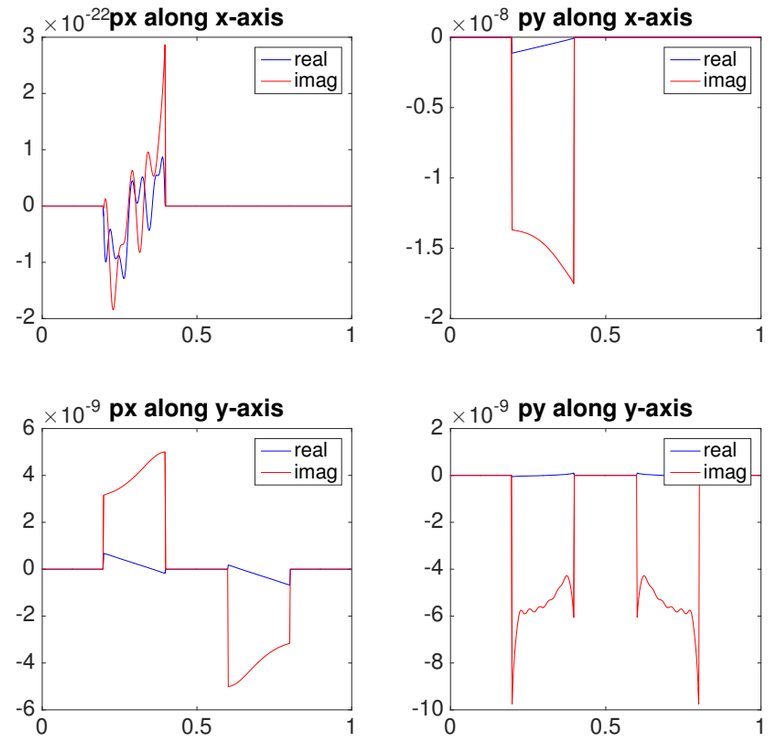

(b) Microscopic polarization density $\mathbf{p}(x, y)$ in u-shaped split-ring for $n = 41$ with padding to $n = 61$.

Since the USRR is only symmetric about the x-axis, it is not surprising that the field along the x-axis display no symmetric tendencies. The source is in the $\hat{\mathbf{y}}$ direction, and it can therefore be seen that the most dominant component of the electric field is e_y. Figure 27a show that e_y is relatively large outside of the USRR, and that it becomes significantly smaller within the dielectric layers it traverses on the y-axis. The e_y component is symmetric along the y-axis. The distribution of the least dominant component e_x, appears to be relatively antisymmetric along the y-axis random along the x-axis. The latter is likely due to numerical error in the PWEM. The simulated parameters η_{2112}, γ_{2112} and ψ_{2112} are calculated for normalized input parameters $\frac{\omega a}{c} = 0.2\pi$ with sources $\mathbf{u}_0 = \exp(-ik_x\frac{a}{2})\hat{\mathbf{y}}$ and $\mathbf{u}_0 = \exp(-ik_x\frac{a}{2})\hat{\mathbf{x}}$, by iterating through $k_x = 0.1, 0.2, 0.3$, and are given in table 3.

Table 3: Normalized parameters for u-shaped split-ring resonator evaluated in $k_x = 0.2$.

$\eta_{2112}/\epsilon_0 a^2$	$-0.0078 - 0.0002i$
$\gamma_{2112}/\epsilon_0 a^2$	$0.0337 - 0.0003i$
$\psi_{2112}/\epsilon_0 a^2$	$-0.0133 + 0.0002i$

Here it can be seen that $\mathrm{Re}[\psi_{2112}] \simeq -0.39\mathrm{Re}[\gamma_{2112}] \simeq 1.71\mathrm{Re}[\eta_{2112}]$, suggesting that $\mathbf{R}$ is significant in the expansion of $\langle\mathbf{p}\rangle$ in equation (43) for the USRR.

It must be mentioned that the USRR is in fact gyrotropic since the unit cell in figure 26 does not contain a center of symmetry that allows $\mathbf{r} \to -\mathbf{r}$ to be a symmetric operation [26]. This does however not affect the correctness of the parameters in table 3, since the algorithm for calculating η, γ and ψ does not assume non-gyrotropic media.

It has earlier been argued that it is the symmetric parts of the induced electric field in a given unit cell that leads to a significant $\mathbf{R}$. Since the USRR in figure 26 is purely dielectric, it is also possible to interpret the real and imaginary parts of the calculated microscopic electric field in figure 27 by using the qualitative solution provided in equation (159). As with the dielectric annulus, this qualitative solution divides $\mathbf{e}_{\mathrm{ext}}(x, y)$ into a large imaginary electrostatic part $\mathbf{e}_0(x, y)$ and a smaller spatially varying real-valued part $\mathbf{e}_0(x, y) \cdot (ik_x \cdot x)$ that can be recognized in figure 27.

The imaginary electrostatic part $\mathbf{e}_0(x, y)$ for the dielectric annulus in figure 17 provided a symmetric microscopic polarization p_y, which in turn explained why R_y became significant by considering the integral in equation (150f). This argumentation is also meaningful for the USRR in figure 26. Similarly it was also argued that an antisymmetric p_y would give $R_y \simeq 0$, and this argument was used to predict that $\psi_{2112} = 0$ for good conductors.

If this line of thought is extended further, it is possible to imagine that a USRR made from a conductor where $\sigma \to \infty$, equation (150f) gives $R_y \neq 0$ because p_y cannot become antisymmetric due to the fact that the structure itself is not symmetric about the y-axis. This arguably suggests that non-symmetric metamaterial unit cells containing conducting media are more likely to have a significant $\mathbf{R}$ in the multipole expansion in equation (43), than symmetric metamaterial unit cells containing conducting media.

10.3 Estimating Casimir and Landau-Lifshitz effective permeabilities μ_{33}

According to equation (74), it is possible to obtain the effective permeability μ_{33} by inserting the normalized parameters $(\eta_{2112} + \gamma_{2112} + \psi_{2112})/\epsilon_0 a^2$, such that

$$(1 - \mu_{33}^{-1}) = \left(\frac{\omega a}{c}\right)^2 \left(\frac{\eta_{2112}}{\epsilon_0 a^2} + \frac{\gamma_{2112}}{\epsilon_0 a^2} + \frac{\psi_{2112}}{\epsilon_0 a^2}\right). \tag{160}$$

This expression can now be employed to calculate effective permeabilities deduced from Casimir and Landau-Lifshitz formalisms in equations (75) and (76) by determining $(\eta_{2112} + \gamma_{2112} + \psi_{2112})/\epsilon_0 a^2$ as earlier, and the parameter γ'_{2112} by only including the contribution of the magnetization $\mathbf{M}$ in the calculation of γ_{2112}. The parameters are determined by using polarization scheme 1, and the representation of the unit cells in MATLAB that are employed for the simulations in this section consist of $199x199$ datapoints.

Only the effective permeabilities for the dielectric annulus and the conducting annulus in figures 17 and 24 are presented here, since the Casimir and Landau-Lifshitz formalisms in eqaution (75) and (76) assumes no magnetoelectric coupling, which is not correct for the USRR structure depicted in figure 26.

10.3.1 Effective μ_{33} for dielectric annulus

The Casimir and Landau-Lifshitz effective permeabilities for the dieletric annulus depicted in figure 17 are plotted for normalized angular frequencies in figures 28 and 29. The parameters η_{2112}, γ_{2112} and ψ_{2112} are evaluated for $k_x = 0.2$, $a = 1$ and with sources $\mathbf{u}_0 = \exp(-ik_x \frac{a}{2})\hat{\mathbf{y}}$ and $\mathbf{u}_0 = \exp(-ik_x \frac{a}{2})\hat{\mathbf{x}}$ for $n = 41$.

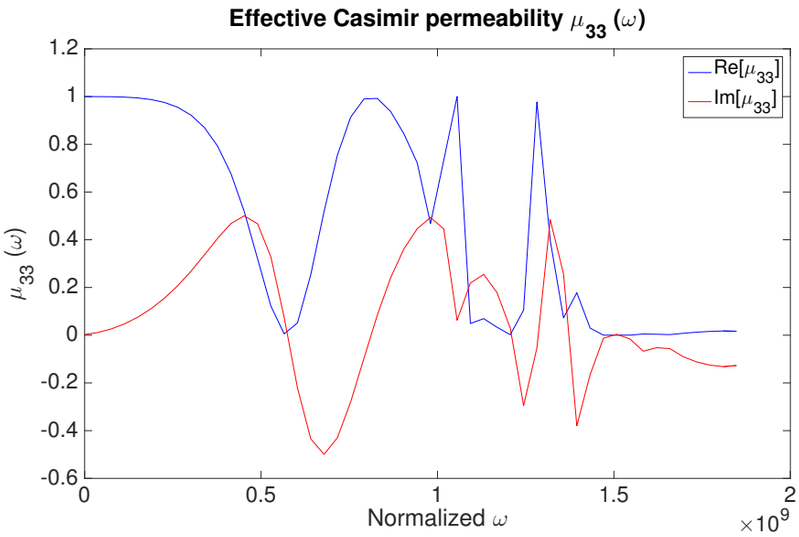

Figure 28: Effective Casimir permeability $\mu_{33}(\omega)$ in dielectric annulus, obtained from calculating the parameter γ'_{2112} for 50 values of ω and inserting into equation (74).

The main feature that can be seen in figures 28 and 29 is that they are indeed very different. This in accordance with the previous results since they conveyed that η_{2112}, γ_{2112} and ψ_{2112} were of similar magnitudes, suggesting that the $\mathcal{O}(k^2)$ terms in $\mathbf{P}$ and $\mathbf{R}$ contribute significantly to the effective parameters.

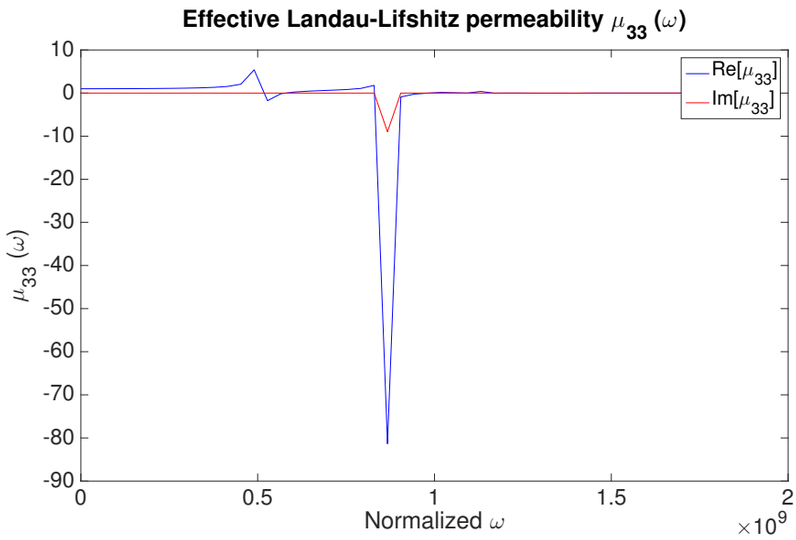

Figure 29: Effective Landau-Lifshitz permeability $\mu_{33}(\omega)$ in dielectric annulus, obtained from calculating the parameters η_{2112}, γ_{2112} and ψ_{2112} for 50 values of ω and inserting into equation (74).

The plot of the real and imaginary parts of the Casimir μ_{33} in figure 28 is oscillating around a small positive value and zero. This oscillation almost appears to be random. The Landau-Lifshitz μ_{33} in figure 29 has a normalized resonance at $\omega \simeq 0.8 \times 10^9$, and both the real and imaginary parts become negative at this resonance. It is surprising that the imaginary part of μ_{33} derived by the Landau-Lifshitz formalism is negative, since it is expected to only take positive values [23]. These features may indicate that the simulated electric field may have not converged properly, due to the fact that the number of datapoints in the unit cell has been reduced from $499x499$ to $199x199$ in this simulation.

10.3.2 Effective μ_{33} for conducting annulus

The Casimir and Landau-Lifshitz effective permeabilities for the conducting annulus depicted in figure 24 are plotted for normalized angular frequencies in figures 30 and 31. The parameters η_{2112}, γ_{2112} and ψ_{2112} are evaluated for $k_x = 0.2$, $a = 1$ and with sources $\mathbf{u}_0 = \exp(-ik_x\frac{a}{2})\hat{\mathbf{y}}$ and $\mathbf{u}_0 = \exp(-ik_x\frac{a}{2})\hat{\mathbf{x}}$ for $n = 41$.

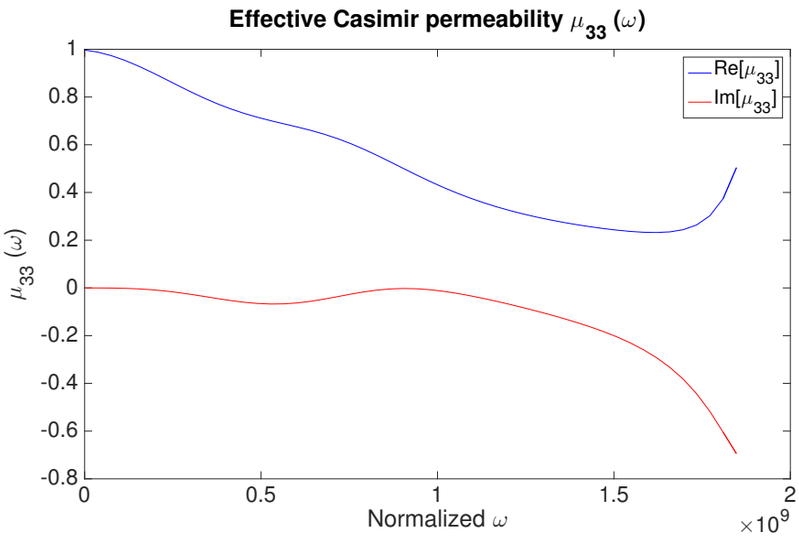

Figure 30: Effective Casimir permeability $\mu_{33}(\omega)$ in dielectric annulus, obtained from calculating the parameter γ'_{2112} for 50 values of ω and inserting into equation (74).

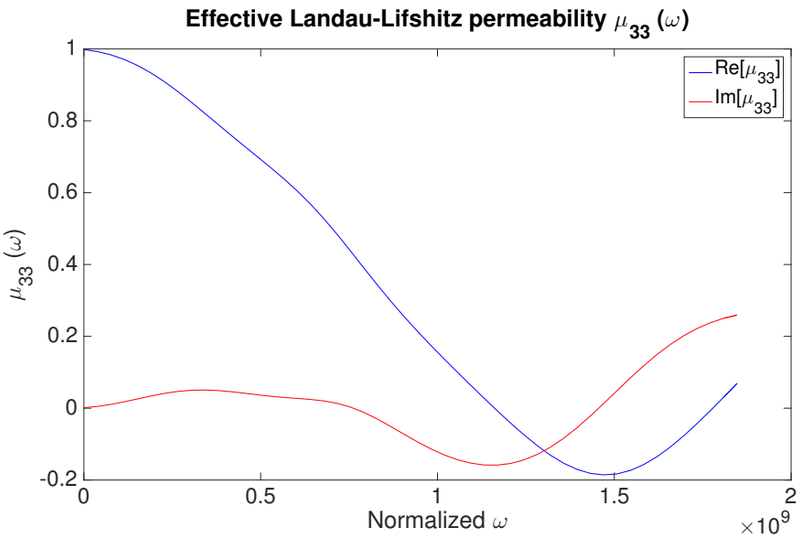

Figure 31: Effective Landau-Lifshitz permeability $\mu_{33}(\omega)$ in conducting annulus, obtained from calculating the parameters η_{2112}, γ_{2112} and ψ_{2112} for 50 values of ω and inserting into equation (74).

Allthough the plots of μ_{33} for the conducting annulus in figure 30 and 31 are more reminiscent of each other than the plots of the dielectric annulus, they clearly display different tendencies. These plots also support the significance of the higher order terms. The real part of the Casimir μ_{33} drops slightly down in value with increasing frequency but remains positive, while the imaginary part of the Casimir μ_{33} oscillates slightly around zero until it starts to drop below zero at around $\omega \simeq 1 \times 10^9$. The real part of the Landau-Lifshitz μ_{33}

drops with increasing frequency in a similar fashion to the real part of the Casimir μ_{33}, but to a value below zero. The imaginary part of the Landau-Lifshitz μ_{33} oscillates slightly around zero before it starts to increase at around $\omega \simeq 1 \times 10^9$.

It is still peculiar that the imaginary part of the Landau-Lifshitz μ_{33} takes negative values, but there are also other features in these plots that seems odd. It was argued that the significance of $\mathbf{R}$ in the conducting annulus would become smaller as the conductivity of the material increased. By using the relation $\varepsilon = 1 - \frac{\sigma}{i\epsilon_0\omega}$, and keeping $\mathrm{Im}[\varepsilon]$ at a fixed value, it can be seen that the conductivity increases linearly with the angular frequency ω. It would therefore arguably be possible to expect that the plots in figure 30 and 31 to become increasingly similar with increasing frequency, which is clearly not the case. This may also indicate poor convergence of the PWEM.

11 Concluding Remarks

11.1 The Process

This project sprawled from the interest in creating a computational tool that could aid the research of spatial dispersion in metamaterials. At first the idea was to attempt at implementing a numerical method described by Mário G. Silveirinha [6, 7]. This method was later replaced by a different approach inspired by Floquet theory somewhat influenced by Silveirinha's method [15], because it was preferable to develop a method that was self-contained. This method was based on expanding the microscopic electric field $\mathbf{e}$ as a sum of plane waves, and solving Maxwell's equations in an inhomogeneous medium. The Floquet based method led to an implementation in MATLAB of the plane-wave expansion method employing a distributed plane-wave source, capable of determining the microscopic electric field inside arbitrary one- and two-dimensional periodic metamaterial unit cells.

This application of the plane wave expansion method was further used to determine the siginificance of higher order terms in the expansion of $\langle \mathbf{p} \rangle$. A scheme for solving $\mathbf{P}$, $\mathbf{Q}^{\text{tot}}$ and $\mathbf{R}$ was implemented in MATLAB by employing the solution of $\mathbf{e}$ for two different source polarizations. By combining these two different polarizations it was then possible to determine the tensor values of the $\mathcal{O}(k^2)$ terms in $\langle \mathbf{p} \rangle$. During the process of successfully implementing this method, the implementation of the PWEM was thoroughly tested and limitations related to the magnitude of the microscopic permittivity in the unit cell, geometric complexity and computational accuracy was discovered. The numerical methods that were implemented during the course of this project, were eventually employed to provide the main results for this master thesis, as well as numerical simulations used for a scientific article submitted to American Physical Society: Physical Review B in January 2017 (Appendix B).

11.2 Conclusion

The plane wave expansion method for periodic metamaterials containing a plane wave source was used to determine the microscopic electric field in a unit cell containing a dielectric annulus, a unit cell containing a conducting annulus and a unit cell containing a dielectric u-shaped split ring resonator. These systems have been chosen in order to explore the influence of geometry on the effective parameters according to various schemes of homogenization.

A qualitative solution $\mathbf{e}_{\text{ext}}$ given by equation (159) was deduced for the dielectric annulus, suggesting that the microscopic electric field is split into a large electrostatic contribution given by $\text{Im}[\mathbf{e}_{\text{ext}}]$ and a smaller spatially varying contribution $\text{Re}[\mathbf{e}_{\text{ext}}]$. This interpretation agrees with plots of the components of $\mathbf{e}(x, y)$ and $\mathbf{p}(x, y)$, showing that $\text{Im}[\mathbf{e}] \gg \text{Re}[\mathbf{e}]$. Plotting the vector fields of $\mathbf{e}$ and $\mathbf{p}$ revealed that the spatially dependent part of the electric field circulated in counter-clockwise direction inside the dielectric annulus.

By assuming that the microscopic permittivity is complex, it was no longer meaningful to relate the plots of $\mathbf{e}(x, y)$ and $\mathbf{p}(x, y)$ in the unit cell containing the conducting annulus to the qualitative solution in equation (159). Instead, the plot of $\mathbf{e}(x, y)$ was interpreted using the conductive properties of the annulus, by comparing the skin depth obtained from equation (16) and the exponential decay observed in figure 25. The dielectric u-shaped split ring resonator was also interpreted by using the qualitative solution in equation (159).

The parameters η_{2112}, γ_{2112} and ψ_{2112} has been shown to be of the same order of magnitude in all three unit cells considered in this thesis. This indicates that the higher order multipoles $\mathbf{R}$ in $\langle \mathbf{p} \rangle$ should generally not be neglected, since their contribution to the effective parameter given in equation (59) is approximately equal.

By analyzing the simulated microscopic electric field together with the expression describing the expansion terms of $\langle \mathbf{p} \rangle$ in (45) and (47), it was argued that the electrostatic part of $\mathbf{e}$ was the main contribution to a significant $\mathbf{R}$. This is due to the fact that this electrostatic part was shown to be symmetrically distributed within the unit cell, suggesting that the integral that gives $\mathbf{R}$ could have a significant value. Based on this claim and the fact that the electrostatic contribution vanishes when $\sigma \to \infty$, it was also suggested that $\mathbf{R}$ would become insignificant in the unit cell containing the conductive annulus, because only the anti-symmetric part of $\mathbf{e}$ will in this case remain and subsequently give $\mathbf{R} = 0$. Similarly, this line of argument also suggest that $\mathbf{R}$ can remain significant in non-symmetric unit cells containing conductive media like the USRR, because the spatially varying part of $\mathbf{e}$ cannot be anti-symmetric due to the geometry of the unit cell.

The normalized parameters $(\eta_{2112} + \gamma_{2112} + \psi_{2112})/\epsilon_0 a^2$ were used to plot the effective permeability μ_{33} derived from the Landau-Lifshitz formalism in equation (76). The effective permability μ_{33} derived from the Casimir formalism in equation (75) was also plotted. Upon comparison, it was seen that the two formalisms result in different plots of μ_{33}, also suggesting that the higher order multipoles $\mathbf{R}$ in $\langle \mathbf{p} \rangle$ are significant. There were however, indications of the PWEM not converging as well as negative values of $\mathrm{Im}[\mu_{33}]$, suggesting that these plots may not be accurate.

11.3 Future Work

It would be interesting to implement a new version of the PWEM that calculates $\mathbf{D}$ directly, in order to analyze the field inside dielectric and conducting structures more thoroughly. This would be beneficial because it allows for resolving the field inside the structures better, especially in media with high conductivity. Such an implementation can be based on several parts of the algorithm that has been presented in this thesis.

Due to the issues regarding the effective permeabilities μ_{33} for the Casimir and Landau-Lifshitz formalisms that was estimated in the previous chapter, their simulations should be investigated more closely. It would also be interesting to plot the effective permittivities $\epsilon(\omega, \mathbf{k})$ for the dielectric and conducting annulus.

References

[1] J. D. Jackson *"Classical Electrodynamics"* Wiley, Third edition, 1999. ISBN: 0-471-30932-X

[2] V. G. Veselago *"The electrodynamics of substances with simultaneously negative values of ϵ and μ"*, Soviet Physics Uspekhi, vol. 10, p. 509, January 1968 URL : https://www3.nd.edu/$\tilde$djena/ee358/veselago_original_paper.pdf

[3] J. Skaar *"Elektromagnetisme"* Kompendium in course TFE4120, August 1 2012.

[4] D. K. Cheng *"Field and Wave Electromagnetics"*, Addison Wesley, Second edition, 1989. ISBN : 0-201-52820.

[5] B. E. A. Saleh, M. C. Teich *"Fundamentals of Photonics"*, Wiley, Second edition, 2007. ISBN : 978-0-471-35832-9

[6] M. G. Silveirinha *"Metamaterial homogenization approach with application to the characterization of microstructured composites with negative parameters"*, Physical Review B 75, 115104, March 5 2007. doi: 10.1103/PhysRevB.75.115104 URL : http://journals.aps.org/prb/abstract/10.1103/PhysRevB.75.115104

[7] F. Capolino, M. G. Silveirinha *"Chapter 10: Nonlocal Homogenization Theory of Structured Materials"* in *"Theory and Phenomena of Metamaterials"*, CRC Press, 2009. doi: 10.1201/9781420054262.ch10 URL : http://www.crcnetbase.com/doi/pdf/10.1201/9781420054262.ch10

[8] G. Russakoff *"A Derivation of the macroscopic Maxwell equations"* Am. J. Phys, 38, 1188, 1970. doi: 10.1119/1.1976000 URL : http://scitation.aip.org/docserver/fulltext/aapt/journal/ajp/38/10/1.1976000.pdf?expires=1463569404&id=id&accname=2120809&checksum=F5A0A1B3AD63B301801E18FB077BC4AB

[9] L. D. Landau, E. M. Lifshitz, L. P. Pitaevskii *"Electrodynamics of Continuous Media"*, Course of Theoretical Physics, vol. 8, Pergamon Press, 1984. ISBN : 978-0-08-030275-1

[10] D. R. Smith, W. J. Padilla, D. C. Vier, S. C. Nemat-Nasser, S. Schultz *"Composite Medium with Simultaneously Negative Permeability and Permittivity"* Physical Review Letters number 18, 4184, vol. 84, 1 May 2000. doi: http://dx.doi.org/10.1103/PhysRevLett.84.4184 URL : http://journals.aps.org/prl/abstract/10.1103/PhysRevLett.84.4184

[11] E. Kreyszig *"Advanced Engineering Mathematics"* John Wiley & Sons, Inc., 9th edition, 2006. ISBN : 978-0471-72897-9

[12] G. S. Agarwal, D. N. Pattanayak, and E. Wolf *"Electromagnetic fields in spatially dispersive media"* Physical Review B 10, 1447, 15 August 1974. doi: http://dx.doi.org/10.1103/PhysRevB.10.1447 URL : http://journals.aps.org/prb/abstract/10.1103/PhysRevB.10.1447

[13] J. B. Pendry *"Negative Refraction Makes a Perfect Lens"* Physical Review Letters number 18, 3966, vol. 85, 30 October 2000. doi: https://doi.org/10.1103/PhysRevLett.85.3966 URL : http://journals.aps.org/prl/abstract/10.1103/PhysRevLett.85.3966

[14] C. Kittel *"Introduction to Solid State Physics"* John Wiley & Sons, Inc., 8th edition, 2005. ISBN : 978-0471-41526-8

[15] J. Skaar *"Floquet Theory with Sources"*, Note, February 2016

[16] J.B. Pendry , A.J. Holden , D.J. Robbins , W.J. Stewart *"Magnetism from conductors and enhanced nonlinear phenomena"* IEEE Transactions on Microwave Theory and Techniques, vol. 47, issue 11, November 1999. doi: 10.1109/22.798002 URL : http://ieeexplore.ieee.org/document/798002/?arnumber=798002&tag=1

[17] R. Rumph *"Lecture 17 (CEM) – Maxwell's Equations in Fourier Space"* URL : https://www.youtube.com/watch?v=hWSMHcc3CxQ\&spfreload=1, Downloaded 22.02.16

[18] R. Rumph *"Lecture 18 (CEM) – Plane Wave Expansion Method"* URL : https://www.youtube.com/watch?v=2ACDQSGpQVo, Downloaded 22.02.16

[19] Mathworks Documentation *"fft - Fast Fourier transform"* URL : http://se.mathworks.com/help/matlab/ref/fft.html, Downloaded 07.03.16

[20] Mathworks Documentation *"fft2 - 2-D fast Fourier transform"* URL : https://se.mathworks.com/help/matlab/ref/fft2.html

[21] Mathworks Documentation *"fftshift - Shift zero-frequency component to center of spectrum"* URL : http://se.mathworks.com/help/matlab/ref/fftshift.html, Downloaded 07.03.16

[22] Mathworks Documentation *"linsolve - Solve linear system of equations"* URL : http://se.mathworks.com/help/matlab/ref/linsolve.html?refresh=true, Downloaded 18.05.16

[23] C. A. Dirdal, private communication, November 2016

[24] T. S. Rappaport *"Wireless Communications Principles and Practice"* Prentice Hall PTR Inc., 2nd edition, 2002. ISBN :0-13-042232-0

[25] A. Andryieuski, S. M. Kuznetsova, and A. V. Lavrinenko *"Applicability of point-dipoles approximation to all-dielectric metamaterials"* Physical Review B 92, July 7 2015. doi: 10.1103/PhysRevB.92.035114 URL : http://journals.aps.org/prb/pdf/10.1103/PhysRevB.92.035114

[26] J. Skaar, private communication, December 2016

[27] TIBTECH innovations , *"Properties table of Stainless steel, Metals and other Conductive materials"* URL : http://www.tibtech.com/conductivity.php

[28] S. Linden, C. Enkrich, M. Wegener, J. Zhou, T. Koschny, C. M. Soukoulis *"Magnetic Response of Metamaeterials at 100 Terahertz"* Science Magazine, vol. 306, issue 5700, pp. 1351-1353, 19 November 2004. doi : 10.1126/science.1105371 URL : http://science.sciencemag.org/content/306/5700/1351

[29] M. A. Ordal, L. L. Long, R. J. Bell, S. E. Bell, R. R. Bell, R. W. Alexander, Jr., and C. A. Ward *"Optical properties of the metals Al, Co, Cu, Au, Fe, Pb, Ni, Pd, Pt, Ag, Ti, and W in the infrared and far infrared"* Applied Optics, vol. 22, issue 7, pp. 1099-1119, October 12 1982. doi : https://doi.org/10.1364/AO.22.001099 URL : `https://www.osapublishing.org/ao/abstract.cfm?id=26571`

[30] M. Kadic, T. Bckmann, R. Schittny and M. Wegener *"Metamaterials beyond electromagnetism"* IOP Science : Reports On Progress in Physics, vol. 76, 5 November 2013. doi: 10.1088/0034-4885/76/12/126501

[31] R. Fleury, F. Monticone, and A. Alù *"Invisibility and Cloaking: Origins, Present, and Future Perspectives"* Phys. Rev. Applied 4, 037001, 1 September 2015. doi : https://doi.org/10.1103/PhysRevApplied.4.037001 URL : `http://journals.aps.org/prapplied/abstract/10.1103/PhysRevApplied.4.037001`

[32] J. B. Pendry, D. Schurig, D. R. Smith *"Controlling Electromagnetic Fields"* Science Magazine, vol. 312, issue 5781, pp. 1780-1782, 23 June 2006. doi : 10.1126/science.1125907 URL : `http://science.sciencemag.org/content/312/5781/1780.full.pdf+html`

[33] B. Gajic *"Signalbehandling og Kommunikasjon - Illustrert guide med eksempler."* Course Book in TTT4110, Institutt for elektronikk og telekommunikasjon Norges tekniske-naturvitenskapelige universitet, May 2013

[34] Dictionary.com *"Define meta-"* `http://www.dictionary.com/browse/meta-`, Downloaded 06.01.17

Appendix A Matrices

$$\overline{\overline{\mathbf{\Gamma}}}_{n=3} = \begin{bmatrix} \epsilon_{0,0} & \epsilon_{-1,0} & \epsilon_{-2,0} & \epsilon_{0,-1} & \epsilon_{-1,-1} & \epsilon_{-2,-1} & \epsilon_{0,-2} & \epsilon_{-1,-2} & \epsilon_{-2,-2} \\ \epsilon_{1,0} & \epsilon_{0,0} & \epsilon_{-1,0} & \epsilon_{1,-1} & \epsilon_{0,-1} & \epsilon_{-1,-1} & \epsilon_{1,-2} & \epsilon_{0,-2} & \epsilon_{-1,-2} \\ \epsilon_{2,0} & \epsilon_{1,0} & \epsilon_{0,0} & \epsilon_{2,-1} & \epsilon_{1,-1} & \epsilon_{0,-1} & \epsilon_{2,-2} & \epsilon_{1,-2} & \epsilon_{0,-2} \\ \epsilon_{0,1} & \epsilon_{-1,1} & \epsilon_{-2,1} & \epsilon_{0,0} & \epsilon_{-1,0} & \epsilon_{-2,0} & \epsilon_{0,-1} & \epsilon_{-1,-1} & \epsilon_{-2,-1} \\ \epsilon_{1,1} & \epsilon_{0,1} & \epsilon_{-1,1} & \epsilon_{1,0} & \epsilon_{0,0} & \epsilon_{-1,0} & \epsilon_{1,-1} & \epsilon_{0,-1} & \epsilon_{-1,-1} \\ \epsilon_{2,1} & \epsilon_{1,1} & \epsilon_{0,1} & \epsilon_{2,0} & \epsilon_{1,0} & \epsilon_{0,0} & \epsilon_{2,-1} & \epsilon_{1,-1} & \epsilon_{0,-1} \\ \epsilon_{0,2} & \epsilon_{-1,2} & \epsilon_{-2,2} & \epsilon_{0,1} & \epsilon_{-1,1} & \epsilon_{-2,1} & \epsilon_{0,0} & \epsilon_{-1,0} & \epsilon_{-2,0} \\ \epsilon_{1,2} & \epsilon_{0,2} & \epsilon_{-1,2} & \epsilon_{1,1} & \epsilon_{0,1} & \epsilon_{-1,1} & \epsilon_{1,0} & \epsilon_{0,0} & \epsilon_{-1,0} \\ \epsilon_{2,2} & \epsilon_{1,2} & \epsilon_{0,2} & \epsilon_{2,1} & \epsilon_{1,1} & \epsilon_{0,1} & \epsilon_{2,0} & \epsilon_{1,0} & \epsilon_{0,0} \end{bmatrix} \tag{161}$$

Figure 32: Two-dimensional Convolution Matrix $\overline{\overline{\mathbf{\Gamma}}}$ for $n = 3$.

Appendix B Article

Higher order terms and locality in metamaterial homogenization

Christopher A. Dirdal,[1] Hans Olaf Hågenvik,[1] Haakon Aamot Haave,[1] and Johannes Skaar[1]

[1] *Department of Electronic Systems, NTNU-Norwegian University of Science and Technology, NO-7491 Trondheim, Norway*

(Dated: January 6, 2017)

The higher order terms in the expansion of the macroscopic polarization, above the electrical quadrupole, are commonly neglected in metamaterial homogenization due to their typically small magnitudes. We show that they nevertheless are generally significant when second order spatial dispersive effects, such as the magnetic response, are considered. In this respect, they are generally equally important as the polarization, magnetization and quadrupole terms, and should not be neglected. The article discussions are facilitated by both analytical approaches and numerical simulations using the plane wave expansion method for the case of a distributed plane wave source. In addition, a special case is examined where the inclusion of these higher order terms leads to effective permittivity and permeability parameters which are in some sense maximally local.

PACS numbers: 78.67.Pt, 78.20.Ci, 78.20.-e, 42.25.Bs, 41.20.Jb, 42.70.-a,42.70.Qs, 41.20.-q

I. INTRODUCTION

The structural freedom in metamaterials have spurred renewed interest into homogenization theories. These are theories that allow for the formulation of *effective* macroscopic Maxwell's equations in structured media from the *exact* microscopic ones. The macroscopic equations have effective plane wave solutions in materials with complex structures, where dimensions are well below the wavelength. Despite the similarities between conventional and metamaterial homogenization, it has become evident that certain differences need to be taken into consideration [1–9]; in particular, the importance of spatial dispersion. In this paper we would like to add another characteristic feature of metamaterial homogenization to the list: That higher order terms in the expansion of macroscopic polarization, *above the electric quadrupole*, generally have physical significance with respect to the magnetic response of the system, despite often being far smaller in magnitude than the lower orders. Hence, some of the underlying assumptions regarding the non-importance of the electrical quadrupole *and higher order terms* in both classical [10–13] and more recent [2, 3, 8, 9] treatments on homogenization, should in some cases be reconsidered when applied to metamaterials.

Faced with the wide variety of proposed homogenization theories in literature, it seems reasonable to make classical formulations by Landau-Lifshitz, Casimir, Russakoff and Jackson [10–14] our starting point, which have parallels among more recent metamaterial treatments such as [2, 8]. The article is structured in the following manner: In Sec. II we present the needed background on the homogenization procedure and the multipoles of the macroscopic polarization according to Russakoff-Jackson homogenization [12, 13]. Section III then presents the needed background on the constitutive relations between the macroscpic fields and multipole quantities, as well as the effective permeability and permittivity functions of the Casimir and Landau-Lifshitz formulations [11, 14]. Both of these sections lead up to Sec. IV where we demonstrate how the higher order terms, *above the electric quadrupole*, may be of general importance. Analytical results and simulations are shown. Finally Sec. V, as a side-remark, presents an interesting case where the inclusion of the higher order terms leads to increased locality of the effective permittivity and permeability.

II. HOMOGENIZATION AND MULTIPOLES

The microscopic Maxwell's equations are

$$\nabla \times \mathbf{e}(\mathbf{r}) = i\omega \mathbf{b}(\mathbf{r}), \tag{1a}$$

$$\nabla \times \frac{\mathbf{b}(\mathbf{r})}{\mu_0} = -i\omega\epsilon_0 \mathbf{e}(\mathbf{r}) + \mathbf{j}(\mathbf{r}) + \mathbf{J}_{\text{ext}}(\mathbf{r}), \tag{1b}$$

$$\nabla \cdot \mathbf{e}(\mathbf{r}) = \frac{\varrho(\mathbf{r}) + \rho_{\text{ext}}(\mathbf{r})}{\epsilon_0}, \tag{1c}$$

$$\nabla \cdot \mathbf{b}(\mathbf{r}) = 0, \tag{1d}$$

where $\mathbf{e}(\mathbf{r})$ and $\mathbf{b}(\mathbf{r})$ represent the microscopic electric field and magnetic flux density, respectively, $\mathbf{j}(\mathbf{r})$ and $\varrho(\mathbf{r})$ represent the induced current and charge densities, respectively, and $\mathbf{J}_{\text{ext}}(\mathbf{r})$ and $\rho_{\text{ext}}(\mathbf{r})$ represent the source current and charge densities. Harmonic fields with angular frequency ω have been assumed, and the $\mathrm{e}^{-i\omega t}$ dependence is suppressed. For simplicity, we will throughout this article consider structures consisting of non-magnetic inclusions. While generalization is not very complicated, the simplifications lead to more transparent expressions. The medium is assumed to be passive (or in thermal equilibrium in the absence of the field under study [11]), i.e., we exclude gain media.

The homogenization method described in Russakoff [12] and Jackson [13] can be applied relatively straightforwardly to the case of metamaterials, replacing molecules by metamaterial cells. The cells can be those resulting from a partition of the metamaterial into small volumes (compared to the spatial variation of the source). For the special case where the metamaterial is a periodic structure, the cells are chosen to be the smallest unit cells. The Russakoff-Jackson formulation of effective, macro-

scopic fields relies on an averaging procedure of the form

$$\langle F(\mathbf{r})\rangle = \int f(\mathbf{r}')F(\mathbf{r}-\mathbf{r}')\mathrm{d}^3r', \tag{2}$$

where F is the function to be averaged, and $f(\mathbf{r})$ is an arbitrary test function that varies slowly over the size of a cell (and may extend over several such cells) [12, 13]. We now specialize to periodic metamaterials, and consider only a single spatial Fourier component of the source, i.e.,

$$\mathbf{J}_{\mathrm{ext}} = \bar{\mathbf{J}}_{\mathrm{ext}}\mathrm{e}^{i\mathbf{k}\cdot\mathbf{r}}, \tag{3a}$$

$$\rho_{\mathrm{ext}} = \overline{\rho}_{\mathrm{ext}}\mathrm{e}^{i\mathbf{k}\cdot\mathbf{r}}, \tag{3b}$$

where $\bar{\mathbf{J}}_{\mathrm{ext}}$ and $\overline{\rho}_{\mathrm{ext}}$ are constant. Then the averaging procedure (2) can be written

$$\langle F(\mathbf{r})\rangle = \bar{F}\mathrm{e}^{i\mathbf{k}\cdot\mathbf{r}}, \tag{4a}$$

where

$$\bar{F} = \frac{f(\mathbf{k})}{V}\int_V F(\mathbf{r})\mathrm{e}^{-i\mathbf{k}\cdot\mathbf{r}}\mathrm{d}^3r, \tag{4b}$$

and the integral is taken over the volume of a unit cell V of the periodic medium (see for example [3]). In arriving at this expression we have made use of the fact that the microscopic fields are Bloch waves of the form

$$F(\mathbf{r}) = U_F(\mathbf{r})\mathrm{e}^{i\mathbf{k}\cdot\mathbf{r}}, \tag{5}$$

where $U_F(\mathbf{r})$ has the same periodicity as the metamaterial. Moreover, we have assumed that the test function in (2) is band-limited, or more precisely, its Fourier transform $f(\mathbf{k})$ is required to vanish outside the first Brillouin zone. This is approximately the case for any sufficiently smooth function $f(\mathbf{r})$ which extends over several unit cells. The operation (4b) essentially represents the spatial average of the periodic modulation $U_F(\mathbf{r})$. In the remainder of this article, we will consider small $\mathbf{k}$'s, well inside the first Brillouin zone. Moreover, we choose the test function such that $f(\mathbf{k}) \approx 1$ there. Then the averaging procedure (4) corresponds to that utilized in Refs. [2, 8].

Application of the averaging procedure (4) to (1a)-(1b), and using the fact that $\mathbf{e}\mathrm{e}^{-i\mathbf{k}\cdot\mathbf{r}}$ and $\mathbf{b}\mathrm{e}^{-i\mathbf{k}\cdot\mathbf{r}}$ are periodic give macroscopic Maxwell's equations

$$i\mathbf{k}\times\mathbf{E} = i\omega\mathbf{B}, \tag{6a}$$

$$i\mathbf{k}\times\frac{\mathbf{B}}{\mu_{\mathbf{0}}} = -i\omega\epsilon_0\mathbf{E} - i\omega\langle\mathbf{p}\rangle + \mathbf{J}_{\mathrm{ext}}, \tag{6b}$$

having identified $\mathbf{j} = -i\omega\mathbf{p}$ and defined macroscopic fields $\mathbf{E} = \langle\mathbf{e}\rangle$ and $\mathbf{B} = \langle\mathbf{b}\rangle$. The effective electromagnetic response of the system is contained in the induced current $-i\omega\langle\mathbf{p}\rangle$, which we shall now expand into multipoles [8, 15]. With the expansion $\exp(-i\mathbf{k}\cdot\mathbf{r}) \approx 1 - i\mathbf{k}\cdot\mathbf{r} - (\mathbf{k}\cdot\mathbf{r})^2/2 + O(k^3)$ we obtain from (4) (to the second order in k)

$$\langle\mathbf{p}\rangle = \frac{\mathrm{e}^{i\mathbf{k}\cdot\mathbf{r}}}{V}\int_V \mathbf{p}\mathrm{e}^{-i\mathbf{k}\cdot\mathbf{r}}\mathrm{d}^3r \tag{7}$$

$$= \frac{\mathrm{e}^{i\mathbf{k}\cdot\mathbf{r}}}{V}\cdot\left(\int_V\mathbf{p}\mathrm{d}^3r - i\mathbf{k}\cdot\int_V\mathbf{r}\mathbf{p}\mathrm{d}^3r - \frac{1}{2}\int_V(\mathbf{k}\cdot\mathbf{r})^2\mathbf{p}\mathrm{d}^3r\right)$$

$$\equiv \mathbf{P} - \frac{\mathbf{k}\times\mathbf{M}}{\omega} - i\mathbf{k}\cdot\mathbf{Q} + \mathbf{R}, \tag{8}$$

where

$$\mathbf{P} = \frac{\mathrm{e}^{i\mathbf{k}\cdot\mathbf{r}}}{V}\int_V\mathbf{p}\mathrm{d}^3r, \tag{9a}$$

$$\mathbf{M} = -\frac{i\omega}{2}\frac{\mathrm{e}^{i\mathbf{k}\cdot\mathbf{r}}}{V}\int_V\mathbf{r}\times\mathbf{p}\mathrm{d}^3r, \tag{9b}$$

$$\mathbf{Q} = \frac{1}{2}\frac{\mathrm{e}^{i\mathbf{k}\cdot\mathbf{r}}}{V}\int_V(\mathbf{r}\mathbf{p}+\mathbf{p}\mathbf{r})\mathrm{d}^3r, \tag{9c}$$

$$\mathbf{R} = -\frac{1}{2}\frac{\mathrm{e}^{i\mathbf{k}\cdot\mathbf{r}}}{V}\int_V(\mathbf{k}\cdot\mathbf{r})^2\mathbf{p}\mathrm{d}^3r. \tag{9d}$$

and we have decomposed the tensor $\mathbf{r}\mathbf{p}$ into its antisymmetric and symmetric parts,

$$\begin{aligned}\mathbf{k}\cdot\mathbf{r}\mathbf{p} &= \mathbf{k}\cdot(\mathbf{r}\mathbf{p}-\mathbf{p}\mathbf{r})/2 + \mathbf{k}\cdot(\mathbf{r}\mathbf{p}+\mathbf{p}\mathbf{r})/2\\ &= -\mathbf{k}\times\mathbf{r}\times\mathbf{p}/2 + \mathbf{k}\cdot(\mathbf{r}\mathbf{p}+\mathbf{p}\mathbf{r})/2.\end{aligned} \tag{10}$$

In addition to the polarization vector $\mathbf{P}$, magnetization vector $\mathbf{M}$, and quadrupole tensor $\mathbf{Q}$, we have included an extra term $\mathbf{R}$ which denotes the so-called *higher order terms* discussed in the introduction, corresponding to electric octupole and magnetic quadrupole. In the following, we will often combine $\mathbf{M}$ and $\mathbf{Q}$ into a combined tensor $\mathbf{Q}^{\mathrm{tot}}$:

$$\mathbf{Q}^{\mathrm{tot}} = \frac{\mathrm{e}^{i\mathbf{k}\cdot\mathbf{r}}}{V}\int_V\mathbf{r}\mathbf{p}\mathrm{d}^3r, \tag{11}$$

such that

$$i\mathbf{k}\cdot\mathbf{Q}^{\mathrm{tot}} = \frac{\mathbf{k}\times\mathbf{M}}{\omega} + i\mathbf{k}\cdot\mathbf{Q}. \tag{12}$$

III. CONSTITUTIVE RELATIONS

The aim of a homogenization procedure is often to arrive at effective parameters or tensors ϵ and μ that describe the effective electromagnetic response of a linear metamaterial. In the so-called Casimir formulation,

$$\epsilon'(\omega,\mathbf{k})\epsilon_0\mathbf{E} = \epsilon_0\mathbf{E} + \mathbf{P}, \tag{13a}$$

$$[1-\mu'^{-1}(\omega,\mathbf{k})]\mathbf{B} = \mu_0\mathbf{M}. \tag{13b}$$

The Casimir formulation thus places $\langle\mathbf{p}\rangle$ *partially* in a permittivity $\epsilon'(\omega,\mathbf{k})$ and *partially* in $1-\mu'^{-1}(\omega,\mathbf{k})$, where $\mu'(\omega,\mathbf{k})$ is a permeability. Evidently the terms $-i\mathbf{k}\cdot\mathbf{Q}$

and $\mathbf{R}$ in (8) have been excluded in this definition, although sometimes $i\mathbf{k}\cdot\mathbf{Q}$ is included in the permittivity [14].

Another possible effective parameter definition is [11]

$$\epsilon_0\epsilon(\omega,\mathbf{k})\mathbf{E} = \epsilon_0\mathbf{E} + \langle\mathbf{p}\rangle, \tag{14}$$

where *all* of $\langle\mathbf{p}\rangle$, including $\mathbf{Q}$ and $\mathbf{R}$, is described by a total permittivity $\epsilon(\omega,\mathbf{k})$. This is called the Landau-Lifshitz formulation, and was used e.g. by Silveirinha [2]. We shall proceed with the Landau-Lifshitz formulation, and return to the Casimir formulation later on.

In a linear medium, we can express multipole densities (9) with constitutive relations

$$P_i = \epsilon_0\chi_{ij}E_j + \xi_{ikj}k_kE_j + \eta_{iklj}k_kk_lE_j, \tag{15a}$$
$$Q^{\text{tot}}_{ik} = i\zeta_{ikj}E_j + i\gamma_{iklj}k_lE_j, \tag{15b}$$
$$R_i = \psi_{iklj}k_kk_lE_j, \tag{15c}$$

where summation over repeated indices is implied. In (15) we have included the necessary orders of k such that $\langle\mathbf{p}\rangle$ is second order in k upon their insertion in (8). Magneto-electric coupling is included in terms of the tensor elements ξ_{ikj} and ζ_{ikj}. From (8), (14) and (15) we obtain

$$\begin{aligned}\epsilon_{ij}(\omega,\mathbf{k}) - \delta_{ij} = \chi_{ij} + (\xi_{ikj} + \zeta_{ikj})k_k/\epsilon_0 \\ + (\psi_{iklj} + \gamma_{iklj} + \eta_{iklj})k_kk_l/\epsilon_0.\end{aligned} \tag{16}$$

While it may be convenient to have only a single constitutive tensor $\epsilon(\omega,\mathbf{k})$, it is often desirable to express the magnetic response more explicitly by introducing a permeability tensor. It is well known that the permeability is related to the second order term in (16) [2, 11]. Observe that the macroscopic quantities $\mathbf{B}$ and $\mathbf{E}$ are left invariant upon the transformation

$$-i\omega\langle\mathbf{p}\rangle \to -i\omega\hat{\mathbf{P}} + i\mathbf{k}\times\hat{\mathbf{M}}, \tag{17}$$

where the new polarization $\hat{\mathbf{P}}$ and magnetization $\hat{\mathbf{M}}$ are arbitrarily chosen. We can express the left hand side in terms of the non-local tensor $\epsilon(\omega,\mathbf{k})$ by (14), and the right hand side in terms of two new tensors ϵ and $1-\mu^{-1}$, in order to obtain

$$\epsilon(\omega,\mathbf{k}) = \epsilon - \frac{c^2}{\omega^2}\mathbf{k}\times[1-\mu^{-1}]\times\mathbf{k}. \tag{18}$$

Here, we have used $\hat{\mathbf{M}} = \mu_0^{-1}(1-\mu^{-1})\mathbf{B}$ and (6a). If we choose the coordinate system such that $\mathbf{k} = k\hat{\mathbf{x}}$, then (18) may be expressed

$$\epsilon(\omega,\mathbf{k}) = \epsilon + \frac{k^2c^2}{\omega^2}\begin{bmatrix}0 & 0 & 0\\ 0 & (1-\mu^{-1})_{33} & -(1-\mu^{-1})_{32}\\ 0 & -(1-\mu^{-1})_{23} & (1-\mu^{-1})_{22}\end{bmatrix}. \tag{19}$$

We now assume a non-gyrotropic medium[1], such that the first order term in (16) vanishes. Comparing (19) with (16) lets us find

$$1-\mu^{-1} = \omega^2\mu_0\cdot \tag{20}$$
$$\begin{bmatrix}\cdot & \cdot & \cdot\\ \cdot & (\psi_{3113}+\gamma_{3113}+\eta_{3113}) & -(\psi_{3112}+\gamma_{3112}+\eta_{3112})\\ \cdot & -(\psi_{2113}+\gamma_{2113}+\eta_{2113}) & (\psi_{2112}+\gamma_{2112}+\eta_{2112})\end{bmatrix},$$

if we choose to put $\epsilon_{22} = 1+\chi_{22}$, $\epsilon_{33} = 1+\chi_{33}$, $\epsilon_{23} = \chi_{23}$, and $\epsilon_{32} = \chi_{32}$. The missing entries in (20) are a result of the fact that $\mathbf{B}$ is transverse, $\mathbf{k}\cdot\mathbf{B} = 0$, and that only the transversal part of $\hat{\mathbf{M}}$ contributes to the induced current.

In principle the magnetization and therefore permeability can be defined in an infinite number of ways, by including any given part of the transversal, induced current. However, the above identification is somewhat natural, as the magnetization term includes all transversal, induced current, except a part possibly induced by the longitudinal component of the electric field. Eq. (20) is a generalization of the relation in Ref. [2]. Note that the Casimir permeability is related to part of the γ_{ikjl} tensor, and may therefore also be viewed as a second order spatial dispersion effect.

IV. IMPORTANCE OF HIGHER ORDER TERMS

The tensors ψ, γ and η relate to $\mathbf{R}$, $\mathbf{Q}^{\text{tot}}$ and $\mathbf{P}$, respectively, in the manner shown in (15). As seen in (16) these contribute on an equal footing to the second order effects of $\epsilon(\omega,\mathbf{k})$ [6], which may be interpreted as describing the magnetic response of the system according to (20). While it is known that the quadrupole tensor $\mathbf{Q}$ may be significant [4, 5], we shall now show that $\mathbf{R}$ too is generally physically important.

Despite the common practice of neglecting $\mathbf{R}$, and therefore ψ, in the multipole expansion (8), the tensors ψ, $\gamma/2$ and η often turn out to be on the same order of magnitude for metamaterial structures. Before demonstrating this from numerical simulations, we may first gain some further intuition by considering (9) and (11)

[1] For non-gyrotropic media, i.e., when there exists a center of symmetry, we have $\epsilon(\omega,-\mathbf{k}) = \epsilon(\omega,\mathbf{k})$ [10, 11], which implies that odd-order terms in (16) must be zero. Note that there is no way to distinguish between ξ_{ikj} and ζ_{ikj} in the expression for $\epsilon_{ij}(\omega,\mathbf{k})$; only the sum appears. In other words, even though the microscopic physics may be dependent on these tensors separately, only the sum matters for the macroscopic fields $\mathbf{E}$ and $\mathbf{B}$. A similar comment is valid when considering $\psi_{iklj}+\gamma_{iklj}+\eta_{iklj}$; only the sum matters macroscopically. We could for instance therefore choose to put $\psi_{iklj} = \eta_{iklj} = 0$ and include their contribution in γ_{iklj}, without altering $\mathbf{E}$ and $\mathbf{B}$.

for a plane-wave dependence of the field[2]

$$\mathbf{e}(\mathbf{r}) = \overline{E}\mathrm{e}^{i\mathbf{k}\cdot\mathbf{r}}\hat{\mathbf{y}}, \tag{21}$$

and $\mathbf{k} = k\hat{\mathbf{x}}$. The following relationship may then be observed

$$\frac{2R_2}{k^2E_2} = i\frac{\partial}{\partial k}\left\{\frac{Q_{21}^{\mathrm{tot}}}{E_2}\right\} = \frac{\partial^2}{\partial k^2}\left\{\frac{P_2}{E_2}\right\}, \tag{22}$$

which gives

$$\psi_{2112} = -\frac{\gamma_{2112}}{2} = \eta_{2112} \tag{23}$$

when compared with (15). Here ψ_{2112} is proportional with the quantity R_2/E_2, while γ_{2112} is related to the first order k-dependence of the quantity $Q_{21}^{\mathrm{tot}}/E_2$, and η_{2112} is related with the second order k-dependence of the quantity P_2/E_2. With this in mind we may qualify the physical importance of $\mathbf{R}$. From (8) and (9) it is evident that the magnitude of $\mathbf{R}$ may not be significant in comparison to the terms associated with $\mathbf{P}$, $\mathbf{M}$ and $\mathbf{Q}$, since $\mathbf{R}$ results from a higher order term of the exponential in $\mathbf{k}\cdot\mathbf{r}$. Nevertheless, this does not mean that it is insignificant when the *second order effects* of $\epsilon(\omega,\mathbf{k})$ (i.e. the magnetic response) are concerned, as seen from (22)-(23). Before moving on, note that since $\mathbf{k}\perp\mathbf{p}(\mathbf{r})$ due to (21), one finds using (10) that

$$\frac{\mathbf{k}\times\mathbf{M}}{\omega} = i\mathbf{k}\cdot\mathbf{Q}, \tag{24}$$

revealing that $\mathbf{M}$ and $\mathbf{Q}$ contribute equally to γ_{iklj} in (15b).

Let us now consider ψ_{2112}, γ_{2112} and η_{2112} for a metamaterial consisting of periodically arranged dielectric cylinders in vacuum. These parameters give the component μ_{33} according to (20). The microscopic dielectric function $\varepsilon(\mathbf{r})$ in a unit cell is displayed in Fig. 1a. Solving the multiple unknowns in (15) generally requires multiple equations. We therefore calculate $\mathbf{E}$, $\mathbf{P}$, $\mathbf{Q}^{\mathrm{tot}}$, and $\mathbf{R}$ by solving $\mathbf{p} = \epsilon_0(\varepsilon(\mathbf{r})-1)\mathbf{e}$ for two choices of $\bar{\mathbf{J}}_{\mathrm{ext}}$, perpendicular and parallel to $\mathbf{k}$, respectively. Utilizing the Floquet property of the source (3) and field (5), a plane wave expansion method can be used to solve the wave equation

$$\nabla\times\nabla\times\mathbf{e} - \frac{\omega^2}{c^2}\varepsilon(\mathbf{r})\mathbf{e} = i\omega\mu_0\mathbf{J}_{\mathrm{ext}}, \tag{25}$$

by inserting Fourier series representations of $\mathbf{e}(\mathbf{r})$, $\varepsilon(\mathbf{r})$, and $\mathbf{J}_{\mathrm{ext}}(\mathbf{r})$. Solutions for the microscopic field $\mathbf{e}(\mathbf{r})$ are then readily found numerically for a given number of Fourier coefficients in the series representations. In order to extract the coefficient parameters in (15), the field quantities $\mathbf{E}$, $\mathbf{P}$, $\mathbf{Q}^{\mathrm{tot}}$, and $\mathbf{R}$ are calculated for three values of k so that first and second order derivatives wrt. k of appropriate quantities can be obtained. By application of this method to the dielectric cylinder in Fig. 1a, the parameter values displayed in Table I are obtained. Here we use normalized parameters: Frequency $\omega a/c = 0.2\pi$ and wavevector $\mathbf{k}a = 0.2\hat{\mathbf{x}}$. We have used $91\times 91 = 8281$ spatial harmonics. We observe that ψ_{2112}, $\gamma_{2112}/2$ and η_{2112} are all on the same order of magnitude, similar to what was found in (23). Using a finite number of spatial harmonics corresponds to performing a *low-pass filtering* of Fig. 1a. The selection of spatial harmonics is performed by a truncation and subsequent application of a Blackman-Harris window in the Fourier domain. Thus, the *actual* structure corresponding to the parameter values in Table I is found by inverse-Fourier transforming the finite coefficient series representation of $\varepsilon(\mathbf{r})$, as given in Fig. 1b: An annulus with slightly rounded edges.

$\psi_{2112}/\epsilon_0 a^2$	-0.060
$\gamma_{2112}/\epsilon_0 a^2$	0.19
$\eta_{2112}/\epsilon_0 a^2$	-0.048

TABLE I: Parameter values in (15) for dielectric annulus.

Using (20) we may calculate

$$\begin{aligned} 1-\mu_{33}^{-1} &= \left(\frac{\omega a}{c}\right)^2\left(\frac{\psi_{2112}}{\epsilon_0 a^2}+\frac{\gamma_{2112}}{\epsilon_0 a^2}+\frac{\eta_{2112}}{\epsilon_0 a^2}\right) \\ &= 0.0345, \end{aligned} \tag{26}$$

for the periodic cylinder metamaterial having inserted the simulation values. Eq. (26) allows us to observe the physical importance of $\mathbf{R}$: Since the parameter ψ_{2112} is on the same order of magnitude as η_{2112} and $\gamma_{2112}/2$, one cannot neglect $\mathbf{R}$ without incurring significant error. Also note that the second order term of $\mathbf{P}$ should not be neglected.

Consider Fig. 2, which shows the real and imaginary part of the microscopic polarization $\mathbf{p}(\mathbf{r})$ in the dielectric annulus. We may interpret the imaginary and real parts as originating individually from the first and second terms in the expansion of the source (3) for $ka \ll 1$, respectively:

$$\mathbf{J}_{\mathrm{ext}} \approx \bar{\mathbf{J}}_{\mathrm{ext}} + i\mathbf{k}\cdot\mathbf{r}\bar{\mathbf{J}}_{\mathrm{ext}} + O(k^2). \tag{27}$$

For the values in Table I the source amplitude $\bar{\mathbf{J}}_{\mathrm{ext}}$ has been chosen to be real, and from (25) one observes that if both $\mathbf{J}_{\mathrm{ext}}$ and $\varepsilon(\mathbf{r})$ are real, then $\mathbf{e}(\mathbf{r})$ and $\mathbf{p}(\mathbf{r}) = \epsilon_0(\varepsilon(\mathbf{r})-1)\mathbf{e}(\mathbf{r})$ are imaginary. Hence Fig. 2b corresponds with the first, constant source term in the expansion (27). Similarly, the field distribution in Fig. 2a thus arises from the second, nonconstant source term, and is less dominant due to $ka \ll 1$. From (4) and (9)

[2] The wave equation (25) reveals that this solution is approached for a source $\mathbf{J}_{\mathrm{ext}} = \bar{J}_{\mathrm{ext}}\mathrm{e}^{ikx}\hat{\mathbf{y}}$ in the limit $\omega \ll ck$. Alternatively, the solution is approached for high frequencies where the permittivity tends to unity.

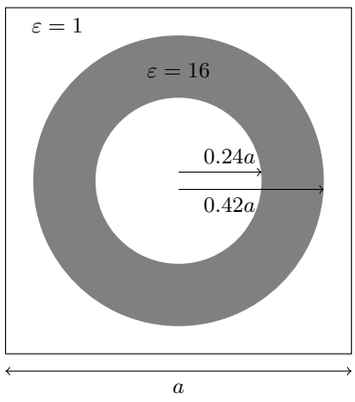

(a)

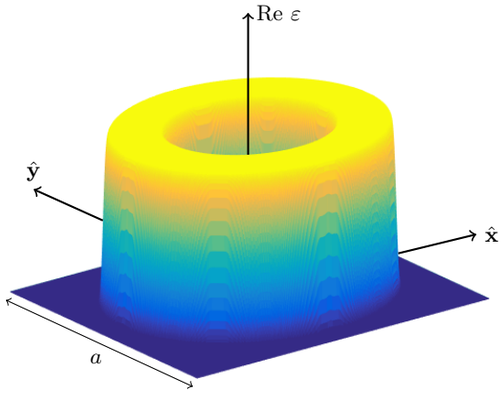

(b)

FIG. 1: (a) Dielectric annulus in vacuum with microscopic permittivity $\varepsilon = 16$. (b) Inverse Fourier transform of finite series representation of $\varepsilon(\mathbf{r})$, having used 91×91 coefficients. As a result of having used a finite number of coefficients, the edges become smoothened, corresponding to low-pass filtering of (a).

it therefore follows that $\mathbf{E}$ and $\mathbf{P}$ are dominated by their imaginary parts, and it follows from (15) that the parameters $\psi_{2112}, \gamma_{2112}$ and η_{2112} are then dominated by their *real* parts for the dielectric annulus.

In metamaterial applications it is most often of interest to work with inclusions made of conducting materials, rather than purely dielectric structures such as those considered so far. To model this we consider a complex microscopic permittivity

$$\varepsilon = 1 + i16, \tag{28}$$

within the same ring structure as pictured in Fig. 1a. Applying otherwise the same parameters as those leading to Table I, now yields the numerical values of Table II.

Now that ε is complex, the real and imaginary parts of the microscopic polarization $\mathbf{p}(\mathbf{r})$ each arise from a *combination* of the source terms $\overline{\mathbf{J}}_{\text{ext}}$ and $i\mathbf{k}\cdot\mathbf{r}\overline{\mathbf{J}}_{\text{ext}}$, as

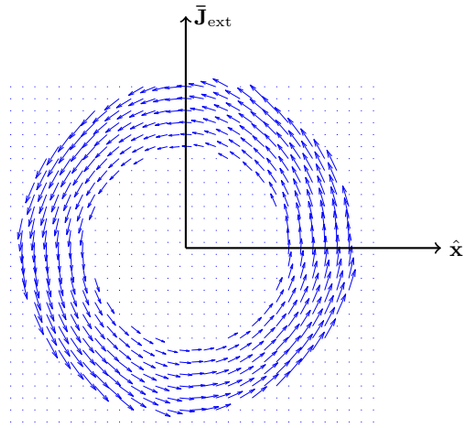

(a) Re $\mathbf{p}(\mathbf{r})$

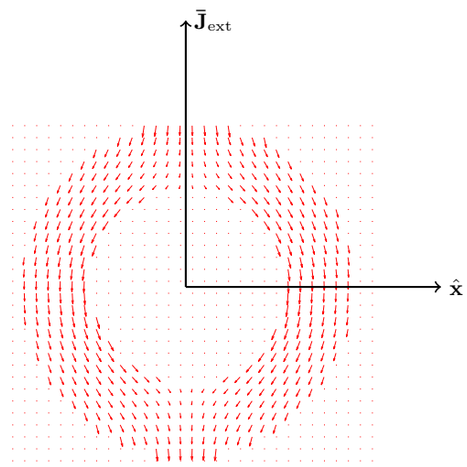

(b) Im $\mathbf{p}(\mathbf{r})$

FIG. 2: Real and imaginary parts of the microscopic polarization $\mathbf{p}(\mathbf{r})$ in the dielectric annulus in Fig. 1. The vectors in (b) have been minimized by a factor 50 for comparison with (a); i.e. the imaginary part of $\mathbf{p}(\mathbf{r})$ dominates.

$\psi_{2112}/\epsilon_0 a^2$	$-0.066 - i0.048$
$\gamma_{2112}/\epsilon_0 a^2$	$0.011 + i0.17$
$\eta_{2112}/\epsilon_0 a^2$	$-0.055 - i0.023$

TABLE II: Parameter values in (15) for a (poorly) conducting annulus of the same geometry as that pictured in Fig. 1.

may be seen from (25). Hence Re $\mathbf{p}(\mathbf{r})$ and Im $\mathbf{p}(\mathbf{r})$ are roughly on the same order of magnitude, and therefore so are the real and imaginary parts of $\psi_{2112}, \gamma_{2112}/2$ and η_{2112}.

Assuming dimensions $a \geq 1\mu$m, the relation $\varepsilon = 1 + i\sigma/\epsilon_0\omega$ reveals that the parameter choice (28) and the given normalized frequency correspond with $\sigma \leq$

$2.7 \cdot 10^4$ Sm^{-1}. This conductivity is not very large. In the limit that $\sigma \to \infty$, however, we know that the electrostatic field vanishes within the conducting ring, leaving only that part of the field distribution which comes from the nonconstant source term $i\mathbf{k}\cdot\mathbf{r}\bar{\mathbf{J}}_{\mathrm{ext}}$; i.e. a polarization resembling that of Fig. 2a. Such a cylinder-symmetric distribution of $\mathbf{p}(\mathbf{r})$ yields $\mathbf{R} = 0$ in (9d), and hence we expect $\psi_{2112} = 0$. More generally, for ideal conductors and $\mathbf{k} = k\hat{\mathbf{x}}$, we expect that the $\mathbf{R}$-term generally remains important, but that it looses importance as the degree of mirror-symmetry about the yz-plane increases.

V. INCREASED LOCALITY FOR CASIMIR FORMULATION

We conclude this article with some side remarks regarding the influence of the higher order terms on the locality of the effective parameters. Local parameters ϵ and μ are desirable, since they enable the use of Fresnel equations to describe the behavior of finite samples or layered samples. The permittivity and permeability resulting from the Landau-Lifshitz formulation are therefore appealing, since they in some sense are maximally local[3]. In the Casimir formulation, however, the parameters ϵ' and μ' according to (13) are generally highly nonlocal. In this section, we will examine a special case where *modified* Casimir parameters can nevertheless be made equally local by including the higher order terms $\mathbf{Q}$ and $\mathbf{R}$ in ϵ' and μ', and choosing an appropriate coordinate origin.

A coordinate transformation $\mathbf{r} \to \tilde{\mathbf{r}} = \mathbf{r} - \mathbf{r}_0$, causes the multipole quantities in (8) to mix: Considering for instance the polarization and magnetization vectors, they mix according to

$$\tilde{\mathbf{P}} = [1 - i\mathbf{k}\cdot\mathbf{r}_0 - \frac{1}{2}(\mathbf{k}\cdot\mathbf{r}_0)^2]\mathbf{P}, \tag{29a}$$

$$\tilde{\mathbf{M}} = [1 - i\mathbf{k}\cdot\mathbf{r}_0][\mathbf{M} + i\omega\frac{\mathbf{r}_0\times\mathbf{P}}{2}], \tag{29b}$$

where we have kept necessary orders of k such that $\langle\mathbf{p}\rangle$ is second order in k upon their insertion in (8). By combining (13a) and (29a), and noting that $\mathbf{E}$ is invariant under the coordinate transformation, the Casimir permittivity elements, *after* coordinate transformation, is expressed

$$\tilde{\epsilon}'_{ij} - \delta_{ij} = [1 - ik_l r_{0l} - \frac{1}{2}(k_l r_{0l})^2](\epsilon'_{ij} - \delta_{ij}). \tag{30}$$

[3] In particular, for non-gyrotropic, weakly spatially dispersive media, where $\epsilon(\omega, \mathbf{k})$ only contains zeroth and second order terms in k, as much as possible of the induced current are represented by a local μ (20). Under certain circumstances (if the second order term of $\langle\mathbf{p}\rangle$ is perpendicular to $\mathbf{k}$, and this term is independent of the longitudinal part of $\mathbf{E}$), all induced current is described by the permeability. This will e.g. be the case for the 1D example below.

Analogous steps lead to an expression for a coordinate-shifted Casimir permeability $1 - \tilde{\mu}'^{-1}_{ij}$. Since the parameters $\tilde{\epsilon}'_{ij}$ and $1 - \tilde{\mu}'^{-1}_{ij}$ vary with the coordinate shift $\mathbf{r_0}$ as seen in (30), it is in some cases possible to choose a coordinate origin in which the first order k-dependence, if any, is cancelled. Coordinate shifts may therefore help in making the parameters more local, as will be observed in the example below.

A special case for which the Casimir parameters can be made maximally local, in the sense mentioned earlier, is obtained by including $\mathbf{Q}$ and $\mathbf{R}$ in modified versions of (13) of the following manner[4]

$$\epsilon_0(\epsilon' - 1)\mathbf{E} = \mathbf{P} - i\mathbf{k}\cdot\mathbf{Q}, \tag{31a}$$

$$\frac{\mathbf{k}\times(1 - \mu'^{-1})\mathbf{B}}{\mu_0\omega} = \frac{\mathbf{k}\times\mathbf{M}}{\omega} - \mathbf{R}, \tag{31b}$$

while assuming the plane wave solution of the microscopic field considered in (21) with $\mathbf{k} = k\hat{\mathbf{x}}$ (realistic fields will be considered below in a simulation). We then find

$$\epsilon'_{22} = 1 + \chi_{22} + \frac{k}{\epsilon_0}\left(\xi_{212} + \frac{\zeta_{212}}{2}\right) + \frac{k^2}{\epsilon_0}\left(\eta_{2112} + \frac{\gamma_{2112}}{2}\right), \tag{32a}$$

$$(1 - \mu'^{-1}_{33}) = \mu_0\omega^2\left(\frac{\zeta_{212}}{2k} + \psi_{2112} + \frac{\gamma_{2112}}{2}\right), \tag{32b}$$

where we have used (12) and (24) in (15b) to express $\mathbf{Q}$ and $\mathbf{M}$ in terms of the parameters ζ_{212} and γ_{2112}. If we assume $\xi_{212} = -\zeta_{212} = 0$ (no magnetoelectric coupling), and make use of (23), we obtain $\mathbf{k}$-independent parameters within the frame of second order dispersion treated in this article: $\epsilon'_{22} = 1 + \chi_{22}$ and $1 - \mu'^{-1}_{33} = 0$. In other words, the Casimir parameters have become even more local due to the inclusion of contributions from $\mathbf{Q}$ and $\mathbf{R}$ in the definitions (31).

Let us now apply the modified Casimir parameters (31) to a realistic system: Consider a 1D metamaterial consisting of periodically alternating layers (a unit cell of which is displayed in Fig. 3) for frequency $\omega a/c = 0.009$, wavevector $\mathbf{k}a = 0.01\hat{\mathbf{x}}$, and equal layer thicknesses. The source $\mathbf{J}_{\mathrm{ext}}$ and field $\mathbf{e}(\mathbf{r})$ point along $\hat{\mathbf{y}}$, and thus $\mathbf{M}$ and $\mathbf{Q}$ contribute equally to γ_{iklj} since $\mathbf{k} \perp \mathbf{p}$, in accordance with (24). Instead of the plane wave expansion method described earlier, the simplicity of the system allows us to find an exact solution to the wave equation (25) in terms of a matrix approach making use of the boundary conditions and the Bloch property of the fields. The results of the simulation are presented in Table III, where we observe that ψ_{2112}, $\gamma_{2112}/2$ and η_{2112} follow (23). In

[4] Note that these expressions apply to the case where $\mathbf{R} \perp \mathbf{k}$, i.e., when it is possible to describe the entire $\mathbf{R}$-contribution in terms of $1 - \mu'^{-1}$.

terms of the scaled parameters we may express (32) as

$$\epsilon'_{22} = 1 + \chi_{22} + (ka)\left(\frac{\xi_{212}}{a\epsilon_0} + \frac{\zeta_{212}}{2a\epsilon_0}\right) + (ka)^2\left(\frac{\eta_{2112}}{\epsilon_0 a^2} + \frac{\gamma_{2112}}{2\epsilon_0 a^2}\right),$$
$$(1 - {\mu'_{33}}^{-1}) = \left(\frac{\omega a}{c}\right)^2\left(\frac{\zeta_{212}}{2(ka)\epsilon_0 a} + \frac{\psi_{2112}}{\epsilon_0 a^2} + \frac{\gamma_{2112}}{2\epsilon_0 a^2}\right) \quad (33)$$

Inserting the simulation values in the above relation reveals that the magnitudes of ξ_{212} and ζ_{212} are negligible. This is due to the choice of coordinate origin in the unit cell (Fig. 3): It corresponds to that r_0 which gives a zero first order derivative of (30) for $k = 0$, when assuming (21). A slight shift of the coordinate origin away from $r_0 = 0.75a$ renders $\xi_{212} = -\zeta_{212}$ significant (e.g. if the coordinate origin is located at $0.76a$ one obtains $\xi_{212} = -\zeta_{212} = -0.075i$).

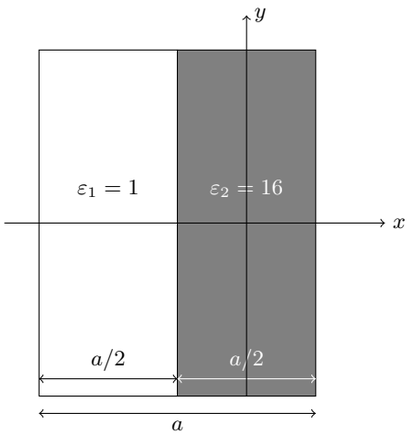

FIG. 3: Unit cell of a layered medium (1D metamaterial) which extends infinitely to the left and right

χ	7.50
$\xi/\varepsilon_0 a$	$i4.75 \cdot 10^{-9}$
$\zeta/\varepsilon_0 a$	$-i3.76 \cdot 10^{-17}$
$\psi/\varepsilon_0 a^2$	-0.0782
$\gamma/\varepsilon_0 a^2$	0.1563
$\eta/\varepsilon_0 a^2$	-0.0782

TABLE III: Parameter values in (15) for the 1D metamaterial displayed in Fig. 3.

Comparing the modified Casimir parameters (32) with the Landau-Lifshitz parameters ϵ_{22} and $1 - \mu_{33}^{-1}$ defined by (20),

$$\epsilon_{22} = 1 + \chi_{22}, \quad (34a)$$
$$(1 - \mu_{33}^{-1}) = \mu_0\omega^2(\psi_{2112} + \gamma_{2112} + \eta_{2112}), \quad (34b)$$

reveals that $\epsilon'_{22} = \epsilon_{22}$ and ${\mu'_{33}}^{-1} = \mu_{33}^{-1}$ when (23) and $\xi_{212} = -\zeta_{212} = 0$ apply. In other words, when we evaluate the Landau-Lifshitz and modified Casimir permeabilities they give identical values in this case (*almost identical* in the case of the layered metamaterial of Fig. 3). If we consider the Landau-Lifshitz parameter as the benchmark for local parameters, the modified Casimir parameter has in this sense become maximally local.

Although (32) and (34) yield identical results in the above case, they have different expressions. This indicates that the manner in which we have included $\mathbf{Q}$ and $\mathbf{R}$ into modified Casimir parameters is not unique.

VI. CONCLUSION

When concerned with spatial dispersive effects of the second order in k (i.e. magnetic response), it has been shown that the higher order multipoles *above* the electrical quadrupole are significant. They generally contribute with the same magnitude as do the polarization, magnetization and electrical quadrupole multipoles, and should therefore not be neglected, despite the higher order multipoles themselves generally being of smaller magnitude. This has been demonstrated in simulations on metamaterials consisting of periodic arrays of dielectric or conducting cylinders, and analytical findings have been provided in the special case where plane wave fields can be assumed. The plane wave expansion method in the case of a distributed plane wave source has been used to provide the relevant simulation results. A case example has been given where maximally local Casimir parameters are achieved by the inclusion of the higher order multipoles.

To facilitate our discussions we have utilized the classical scheme of Russakoff-Jackson homogenization, and effective parameter formulations by Landau-Lifshitz, and Casimir.

[1] A. P. Vinogradov and A. V. Aivazyan, Phys. Rev. E **60**, 987 (1999).
[2] M. G. Silveirinha, Phys. Rev. B **75**, 115104 (2007).
[3] M. G. Silveirinha, in *Metamaterials Handbook: Theory and phenomena of metamaterials*, edited by F. Capolino (CRC Press, London, 2009) Chap. 10.

[4] D. J. Cho, F. Wang, X. Zhang, and Y. R. Shen, Phys. Rev. B **78**, 121101 (2008).
[5] J. Petschulat, C. Menzel, A. Chipouline, C. Rockstuhl, A. Tünnermann, F. Lederer, and T. Pertsch, Phys. Rev. A **78**, 043811 (2008).
[6] C. Simovski and S. Tretyakov, in *Metamaterials Handbook: Theory and Phenomena of Metamaterials*, edited by F. Capolino (CRC Press, London, 2009) Chap. 2.
[7] A. Alù, Phys. Rev. B **83**, 081102 (2011).
[8] A. Alù, Phys. Rev. B **84**, 075153 (2011).
[9] A. D. Yaghjian, A. Alù, and M. G. Silveirinha, Photonics and Nanostructures - Fundamentals and Applications **11**, 374 (2013).
[10] V. Agranovich and V. Ginzburg, *Crystal optics with spatial dispersion, and excitons:*, Springer series in solid-state sciences (Springer-Verlag, 1984).
[11] L. D. Landau, E. M. Lifshitz, and L. P. Pitaevskii, *Electrodynamics of continuous media* (Pergamon Press, Oxford, 1984).
[12] G. Russakoff, Am. J. Phys. **38**, 1188 (1970).
[13] J. D. Jackson, *Classical electrodynamics*, 3rd ed. (Wiley, New York, 1999).
[14] A. P. Vinogradov, Physics-Uspekhi **45**, 331 (2002).
[15] J. van Bladel, *Electromagnetic fields* (IEEE Press, Hoobken, NJ, 2007).

Appendix C MATLAB Code

The code for the one- and two-dimensional PWEM, simulating $\mathcal{O}(k^2)$ terms of $\langle \mathbf{p} \rangle$ and the code for simulating the effective permeability μ are given below. Helper functions are also attached.

C.1 Functions for simulating parameters η, γ and ψ for both 2D- and 1D systems

```
function [eta,gamma,psi,casimir] = solveTensorPar(geometry,origo,a
    ,f,n,kxstart,kxstop,kystart,kystop,it,deltax,deltay)
% geometry: permittivity of structure
% a: unit cell characteristic length
% f: frequency
% n: n.o. harmonics in PWEM
% kstart: k starting scan value
% kstop: k stopping scan value
% it: resolution in k (> 2)
% deltax: shift along x axis
% deltay: shift along y axis
% Variable "geometry" must be a nxn matrix where n is an odd
    number.


% Definitions
[row,col] = size(geometry);
eps0 = 8.854187817e-12;

% Only iterate over one k-component at the time.
deltakx = (kxstop-kxstart)/it;
deltaky = (kystop-kystart)/it;

% if (kystop == 0)
%     deltak = (kxstop-kxstart)/it;
% else
%     deltak = (kystop-kystart)/it;
% end

res = a/col;
x = -deltax:res:(a-res-deltax);
y = -deltay:res:(a-res-deltay);
%
switch origo
    case 'bl'
        chi = (geometry -1);

    case 'br'
        chi = rot90((geometry-1),2);
end

%chi = rot90((geometry-1),3);

%  if (kystop == 0)
%      chi = rot90((geometry-1),3);
%  elseif (kxstop == 0)
%      %chi = transpose((geometry-1));
%      chi = geometry-1;
%  end


% Allocating memory for vector components
Ex = zeros(it,2);
Ey = zeros(it,2);
Px = zeros(it,2);
```

```
Py = zeros(it,2);
Qxx = zeros(it,2);
Qyx = zeros(it,2);
Qxy = zeros(it,2);
Qyy = zeros(it,2);
Rxkx = zeros(it,2);
Rykx = zeros(it,2);
Rxky = zeros(it,2);
Ryky = zeros(it,2);
Mz = zeros(it,2);
kvals = zeros(it);


Qxxint = zeros(row,col);
Qyxint = zeros(row,col);
Qxyint = zeros(row,col);
Qyyint = zeros(row,col);
Rxkxint = zeros(row,col);
Rykxint = zeros(row,col);
Rxkyint = zeros(row,col);
Rykyint = zeros(row,col);
Exint = zeros(row,col);
Eyint = zeros(row,col);
Mzint = zeros(row,col);

% Config 1 : k = kx , u = uy
for m = 1:it
    kx = kxstart + (deltakx*m)
    %ky = 0;
    ky = kystart + (deltaky*m)

    if (kystop == 0)
        % Determine periodic part of microscopic electric field
           for kx = 1, uy
        % = 1
        [Exn,Eyn,exn,eyn] = solve2DPar(geometry,'bl',a,f,n,kx
           ,0,0,(1*exp(complex(0,-0.5*kx))),0);
         kvals(m) = kx;
    elseif (kxstop == 0)
        % Determine periodic part of microscopic electric field
           for ky = 1, ux
        % = -1
        [Exn,Eyn,exn,eyn] = solve2DPar(geometry,'br',a,f,n,0,ky
           ,-(1*exp(complex(0,-0.5*ky))),0,0);
        %[Exn,Eyn] = solve2DPar(geometry,a,f,n,0,ky,1,0);
         kvals(m) = ky;
    end

    px = zeros(row,col);
    py = zeros(row,col);
    % Determine microscopic polarization
    for i1 = 1:row
        for j1 = 1:col
            px(i1,j1) = Exn(i1,j1)*eps0*chi(i1,j1);
            py(i1,j1) = Eyn(i1,j1)*eps0*chi(i1,j1);
        end
    end
    % Determine integrands P,Q and R
    for q = 1:row
        for r = 1:col
           Exint(q,r) = Exn(q,r).*exp(-1i*((kx*x(r)) + (ky*y(q))))
              ;
           Eyint(q,r) = Eyn(q,r).*exp(-1i*((kx*x(r)) + (ky*y(q))))
              ;
%            Exint = exn;
%            Eyint = eyn;
```

```
114
115 %             Qxxint(q,r) = px(q,r)*x(q);
116 %             Qyxint(q,r) = py(q,r)*x(q);
117 %
118 %             Qxyint(q,r) = px(q,r)*y(r);
119 %             Qyyint(q,r) = py(q,r)*y(r);
120 %
121 %             Rxkxint(q,r) = px(q,r)*x(q)*x(q)*kx*kx;
122 %             Rykxint(q,r) = py(q,r)*x(q)*x(q)*kx*kx;
123 %
124 %             Rxkyint(q,r) = px(q,r)*y(r)*y(r)*ky*ky;
125 %             Rykyint(q,r) = py(q,r)*y(r)*y(r)*ky*ky;
126
127             Qxxint(q,r) = px(q,r)*x(r);
128             Qyxint(q,r) = py(q,r)*x(r);
129
130             Qxyint(q,r) = px(q,r)*y(q);
131             Qyyint(q,r) = py(q,r)*y(q);
132
133             Rxkxint(q,r) = px(q,r)*x(r)*x(r)*kx*kx;
134             Rykxint(q,r) = py(q,r)*x(r)*x(r)*kx*kx;
135
136             Rxkyint(q,r) = px(q,r)*y(q)*y(q)*ky*ky;
137             Rykyint(q,r) = py(q,r)*y(q)*y(q)*ky*ky;
138
139             Mzint(q,r) = ((py(q,r)*x(r)) - (px(q,r)*y(q)));
140         end
141     end
142     % Integrate w.r.t. dxdy
143     Ex(m,1) = (sum(sum(Exint))*(res^2))/(a^2);
144     Ey(m,1) = (sum(sum(Eyint))*(res^2))/(a^2);
145     Px(m,1) = (sum(sum(px))*(res^2))/(a^2);
146     Py(m,1) = (sum(sum(py))*(res^2))/(a^2);
147     Qxx(m,1) = (sum(sum(Qxxint*(res^2)/(a^2))));
148     Qyx(m,1) = (sum(sum(Qyxint*(res^2)/(a^2))));
149     Qxy(m,1) = (sum(sum(Qxyint*(res^2)/(a^2))));
150     Qyy(m,1) = (sum(sum(Qyyint*(res^2)/(a^2))));
151     Rxkx(m,1) = -(sum(sum(Rxkxint)*(res^2)))/(2*a*a);
152     Rykx(m,1) = -(sum(sum(Rykxint)*(res^2)))/(2*a*a);
153     Rxky(m,1) = -(sum(sum(Rxkyint)*(res^2)))/(2*a*a);
154     Ryky(m,1) = -(sum(sum(Rykyint)*(res^2)))/(2*a*a);
155
156     Mz(m,1) = -(complex(0,0.5*2*pi*f))*sum(sum(Mzint)*(res^2))
            *(1/(a*a));
157 end
158
159 fprintf('Config. 1 complete. \n')
160
161 % Px
162 % Py
163 % Qxx
164 % Qyx
165 % Rx
166 % Ry
167 %
168
169 m = 1;
170
171 % Config 2: k = kx, u = ux
172 for m = 1:it
173     kx = kxstart + (deltakx*m)
174     %ky = 0;
175     ky = kystart + (deltaky*m)
176
177
178     if (kystop == 0)
```

```
179         % Determine periodic part of microscopic electric field
                for kx = 1, ux
180         % = 1
181         [Exn,Eyn,exn,eyn] = solve2DPar(geometry,'bl',a,f,n,kx
                ,0,(1*exp(complex(0,-0.5*kx))),0,0);
182         kvals(m) = kx;
183     elseif (kxstop == 0)
184         % Determine periodic part of microscopic electric field
                for ky = 1, uy
185         % = 1
186         [Exn,Eyn,exn,eyn] = solve2DPar(geometry,'br',a,f,n,0,ky
                ,0,(1*exp(complex(0,-0.5*ky))),0);
187         kvals(m) = ky;
188     end
189
190     px = zeros(row,col);
191     py = zeros(row,col);
192     % Determine microscopic polarization
193     for i1 = 1:row
194         for j1 = 1:col
195             px(i1,j1) = Exn(i1,j1)*eps0*chi(i1,j1);
196             py(i1,j1) = Eyn(i1,j1)*eps0*chi(i1,j1);
197         end
198     end
199     % Determine integrands P,Q and R
200     for q = 1:col
201         for r = 1:col
202            Exint(q,r) = Exn(q,r).*exp(-1i*((kx*x(r)) + (ky*y(q))))
                   ;
203            Eyint(q,r) = Eyn(q,r).*exp(-1i*((kx*x(r)) + (ky*y(q))))
                   ;
204 %            Exint = exn;
205 %            Eyint = eyn;
206
207 %            Qxxint(q,r) = px(q,r)*x(q);
208 %            Qyxint(q,r) = py(q,r)*x(q);
209 %
210 %            Qxyint(q,r) = px(q,r)*y(r);
211 %            Qyyint(q,r) = py(q,r)*y(r);
212 %
213 %            Rxkxint(q,r) = px(q,r)*x(q)*x(q)*kx*kx;
214 %            Rykxint(q,r) = py(q,r)*x(q)*x(q)*kx*kx;
215 %
216 %            Rxkyint(q,r) = px(q,r)*y(r)*y(r)*ky*ky;
217 %            Rykyint(q,r) = py(q,r)*y(r)*y(r)*ky*ky;
218
219            Qxxint(q,r) = px(q,r)*x(r);
220            Qyxint(q,r) = py(q,r)*x(r);
221
222            Qxyint(q,r) = px(q,r)*y(q);
223            Qyyint(q,r) = py(q,r)*y(q);
224
225            Rxkxint(q,r) = px(q,r)*x(r)*x(r)*kx*kx;
226            Rykxint(q,r) = py(q,r)*x(r)*x(r)*kx*kx;
227
228            Rxkyint(q,r) = px(q,r)*y(q)*y(q)*ky*ky;
229            Rykyint(q,r) = py(q,r)*y(q)*y(q)*ky*ky;
230
231            Mzint(q,r) = ((py(q,r)*x(r))- (px(q,r)*y(q)));
232         end
233     end
234     % Integrate w.r.t. dxdy
235     Ex(m,2) = (sum(sum(Exint))*(res^2))/(a^2);
236     Ey(m,2) = (sum(sum(Eyint))*(res^2))/(a^2);
237     Px(m,2) = (sum(sum(px))*(res^2))/(a^2);
238     Py(m,2) = (sum(sum(py))*(res^2))/(a^2);
```

```
239     Qxx(m,2) = (sum(sum(Qxxint*(res^2)/(a^2))));
240     Qyx(m,2) = (sum(sum(Qyxint*(res^2)/(a^2))));
241     Qxy(m,2) = (sum(sum(Qxyint*(res^2)/(a^2))));
242     Qyy(m,2) = (sum(sum(Qyyint*(res^2)/(a^2))));
243     Rxkx(m,2) = -(sum(sum(Rxkxint)*(res^2)))/(2*a*a);
244     Rykx(m,2) = -(sum(sum(Rykxint)*(res^2)))/(2*a*a);
245     Rxky(m,2) = -(sum(sum(Rxkyint)*(res^2)))/(2*a*a);
246     Ryky(m,2) = -(sum(sum(Rykyint)*(res^2)))/(2*a*a);
247
248     Mz(m,2) = -(complex(0,0.5*2*pi*f))*sum(sum(Mzint)*(res^2))
            *(1/(a*a));
249 end
250
251 fprintf('Config. 2 complete. \n')
252
253 % Allocating P constants
254 kappaP = zeros(it,1);
255 tauP = zeros(it,1);
256 phiP = zeros(it,1);
257 thetaP = zeros(it,1);
258
259 % Allocating Q constants
260 kappaQ = zeros(it,1);
261 tauQ = zeros(it,1);
262 phiQ = zeros(it,1);
263 thetaQ = zeros(it,1);
264
265 % Allocating R constants
266 kappaR = zeros(it,1);
267 tauR = zeros(it,1);
268 phiR = zeros(it,1);
269 thetaR = zeros(it,1);
270
271 % Allocating M constants
272 kappaM = zeros(it,1);
273 tauM = zeros(it,1);
274 phiM = zeros(it,1);
275 thetaM = zeros(it,1);
276
277 fprintf('Solving Linear Systems \n')
278
279 for g = 1:it
280     A = [Ex(g,1),Ey(g,1);Ex(g,2),Ey(g,2)];
281
282     % linsolve for P
283
284     X1 = linsolve(A,[Px(g,1); Px(g,2)]);
285     kappaP(g) = X1(1);
286     tauP(g) = X1(2);
287
288     X2 = linsolve(A,[Py(g,1); Py(g,2)]);
289     phiP(g) = X2(1);
290     thetaP(g) = X2(2);
291
292     clear X1
293     clear X2
294
295     % linsolve for Q
296
297     if (kystop == 0)
298         X1 = linsolve(A,[Qxx(g,1); Qxx(g,2)]);
299         kappaQ(g) = X1(1);
300         tauQ(g) = X1(2);
301
302         X2 = linsolve(A,[Qyx(g,1); Qyx(g,2)]);
303         phiQ(g) = X2(1);
```

```
304         thetaQ(g) = X2(2);
305
306         clear X1
307         clear X2
308
309         X3 = linsolve(A,[Mz(g,1); Mz(g,2)]);
310         thetaM(g) = X3(2);
311
312     elseif (kxstop == 0)
313         X1 = linsolve(A,[Qxy(g,1); Qxy(g,2)]);
314         kappaQ(g) = X1(1);
315         tauQ(g) = X1(2);
316
317         X2 = linsolve(A,[Qyy(g,1); Qyy(g,2)]);
318         phiQ(g) = X2(1);
319         thetaQ(g) = X2(2);
320
321         clear X1
322         clear X2
323     end
324
325     % linsolve for R
326
327     if (kystop == 0)
328         X1 = linsolve(A,[Rxkx(g,1); Rxkx(g,2)]);
329         kappaR(g) = X1(1);
330         tauR(g) = X1(2);
331
332         X2 = linsolve(A,[Rykx(g,1); Rykx(g,2)]);
333         phiR(g) = X2(1);
334         thetaR(g) = X2(2);
335
336         clear X1
337         clear X2
338     elseif (kxstop == 0)
339         X1 = linsolve(A,[Rxky(g,1); Rxky(g,2)]);
340         kappaR(g) = X1(1);
341         tauR(g) = X1(2);
342
343         X2 = linsolve(A,[Ryky(g,1); Ryky(g,2)]);
344         phiR(g) = X2(1);
345         thetaR(g) = X2(2);
346
347         clear X1
348         clear X2
349     end
350
351 end
352
353 % Calculate parameters for given configuration
354
355 if (kystop == 0)
356     % Current evaluation is for determining eta_2112 , gamma_2112
        and psi_2112.
357     disp('Parameters: _2112')
358
359 %     %logarithm part
360 %     deltakxlog10 = log10(deltakx);
361 %     etavec3 = log10(thetaP)/(2*deltakxlog10^2);
362 %     gammavec3 = log10(thetaQ)/(deltakxlog10);
363 %     psivec2 = zeros(it,1);
364 %     for o = 1:it
365 %         psivec2(o) = log10(thetaR(o)/((kvals(o))^2));
366 %     end
367 %     etavec2 = diff(etavec3,2);%/(2*(deltakx^2)); %*((kxstop-
    kxstart)/(it-1))
```

```
%     gammavec2 = diff(gammavec3);%/(1i))/(deltakx);
%
%     etavec = 10.^etavec2;
%     gammavec = 10.^gammavec2;
%     psivec = 10.^psivec2;

    etavec = diff(thetaP,2)/(2*(deltakx^2)); %*((kxstop-kxstart)/(
        it-1))
    gammavec = diff(thetaQ/(1i))/(deltakx);
    Cgammavec = diff(thetaM/(1i))/(deltakx);
    psivec = zeros(it,1);
    for o = 1:it
        psivec(o) = thetaR(o)/((kvals(o))^2);
    end
elseif (kxstop == 0)
    %Current evaluation is for determining eta_1221 , gamma_1221
        and psi_1221.
    disp('Parameters : _1221')
    etavec = diff(kappaP,2)/(2*(deltaky^2)); %*((kystop-kystart)/(
        it-1))
    gammavec = diff(kappaQ/(1i))/(deltaky);
    psivec = zeros(it,1);
    for o = 1:it
        psivec(o) = kappaR(o)/((kvals(o))^2);
    end
end

eta = etavec(floor(it/2))/eps0;
gamma = gammavec(floor(it/2))/eps0;
psi = psivec(floor(it/2))/eps0;

% Casimir gamma
casimir = -Cgammavec(floor(it/2))/(eps0*2*pi*f);

% etavec
% -gammavec
% psivec

% Ex
% Ey
% Px
% Py
% Qxx
% Qyx
% Rx
% Ry

%kappaP
%tauP
%phiP
%thetaP
%kappaQ
%tauQ
%phiQ
%thetaQ
%kappaR3
%tauR
%phiR
%thetaR

end
```

```
function [eta,gamma,psi] = solve1DConstants(geometry,a,f,n,kstart,
    kstop,it,deltax)
% Calculates eta, gamma and psi from equation 34 in article
% geometry: structure matrix
```

```
% a: unit cell length
% f: frequency
% kstart, kstop: range of k-values
% it: number of iterations in k-value range
% deltax: shift along x axis
[row,col] = size(geometry);
eps0 = 8.854187817e-12;
%chi = (geometry(floor(row/2),:))-1;
deltak = (kstop-kstart)/it;
res = a/col;
%x = -(a-deltax):res:deltax-res;
x = -deltax:res:(a-res-deltax);
%x = (deltax):res:(a-deltax-res);

chi = (geometry(1,:))-1;


P = zeros(1,it);
M = zeros(1,it);
R = zeros(1,it);
E = zeros(1,it);
kvalues = zeros(1,it);

for i = 1:it
    k = kstart + (i*deltak)

    emicro = solve1D(geometry,a,f,n,k);

    pIntegrand = zeros(1,col);
    mIntegrand = zeros(1,col);
    rIntegrand = zeros(1,col);
    eIntegrand = zeros(1,col);

    for j = 1:col
        pIntegrand(j) = eps0*emicro(j)*chi(j)/(a);
        mIntegrand(j) = pIntegrand(j)*x(j)*(1i*2*pi*f)/(2);
        rIntegrand(j) = pIntegrand(j)*x(j)*x(j)*((k^2))/(2);
        %
        eIntegrand(j) = emicro(j).*exp(-1i*k*x(j))/(a);
    end

    E(i) = (sum(eIntegrand*res));
    %
    P(i) = (sum(pIntegrand*(res)));
    M(i) = -(sum(mIntegrand*(res)));
    R(i) = -(sum(rIntegrand*(res)));
    kvalues(i) = k;
%     E(i)
%     P(i)
%     M(i)
%     R(i)
end

etavec = zeros(1,it);
gammavec = zeros(1,it);
psivec = zeros(1,it);

for q = 1:it
etavec(q) = (P(q))/(E(q));
gammavec(q) = - (2*(M(q))/((2*pi*f)*E(q)));
psivec(q) = (2*(R(q))/((kvalues(q).^2)*E(q)));
end


etavecd = diff(etavec/(deltak^2),2);%/(deltak);
%etavecd2 = diff(etavecd1/deltak);%/(deltak);
```

```
70 gammavecd = diff(gammavec/deltak);%/(deltak);
71
72 eta = etavecd(floor(it/2))/2;
73 gamma = -gammavecd(floor(it/2));
74 psi = psivec(floor(it/2))/2;
75
76 %figure(4)
77 %plot(kstart:(deltak):kstop - (3*deltak),real(etavecd2),'-or')
78 %figure(5)
79 %plot(kstart:(deltak):kstop - (2*deltak),real(gammavecd),'-ob')
80 %figure(6)
81 %plot(kstart:(deltak):kstop - (deltak),real(psivec),'-oy')
82
83 %plot(0:it-3,etavec,'b');
84 %hold on
85 %plot(0:it-2,gammavec,'r');
86 %hold on
87 %plot(0:it-1,R,'y');
88 %hold off
89
90 end
```

C.2 Functions for 2D PWEM algorithms

```
function [Exnum,Eynum,exnum,eynum] = solve2DPar(geometry,origo,a,f
    ,n,kx,ky,uxgiven,uygiven,pad)
tic
% Difference from solve1D is that u is given as argument.
% Geometry matrix should have dimensions > 200x200.

% The origo input parameter rotates the unit cell according to the
% coordinate system of the Fourier transform and ensures that the
    factor
% exp(ikr) is multiplied correctly into solution matrix.

% Use origo = 'bl' for standard simualtion with u = uy and k = kx.

% Make n odd
if(mod(n,2) == 0)
    n = n+1;
end

% Create constants
omega = 2*pi*f;
c = 3*(10^8);
uzero = 4*pi*(10^(-7));
sigma = ((omega/(c))^2);
phi = complex(0,omega*uzero);
eps0 = 8.854187817e-12;

% Create Source
if nargin == 10
    ux = zeros(n^2,1);
    uy = zeros(n^2,1);
    ux(floor(((n^2)/2)+1),1) = uxgiven;
    uy(floor(((n^2)/2)+1),1) = uygiven;
else
    ux(floor(((n^2)/2)+1),1) = 1;
    uy(floor(((n^2)/2)+1),1) = 1;
end

% Create w and k
[w,k] = makeVectors2d(a,n);
if nargin == 10
    k = ones(n^2,2);
    k(:,1) = kx;
    k(:,2) = ky;
end

% Creating square matrix and otp matrices
sq = curlOperator2d(w,k);
[Tx,Ty,TxTy] = outerproduct(w,k);

switch origo
    case 'bl'
        %nTest = n-20 % assuming function call with n = 51
        epsilon = convmat(geometry,n,n,1,pad);
    case 'br'
        % Rotate oppositely to adjust for axis-mirroring
        epsilon = convmat(rot90(geometry,2),n,n,1,0);
    case 'tr'
        epsilon = convmat(geometry,n,n,1,0);
    case 'tl'
        % Rotate oppositely to adjust for axis-mirroring
        epsilon = convmat(rot90(geometry,2),n,n,1,0);
end

% Create A,D and C = B matrices
```

```
A = sq-Tx-(sigma*epsilon);
D = sq-Ty-(sigma*epsilon);
CB = -(TxTy);

% Solve coupled Matrix equation set
coefficients = [A,CB;CB,D];
source = phi*[ux;uy];
Vs = linsolve(coefficients,source);
Vx = Vs(1:(n^2));
Vy = Vs(((n^2)+1):((n^2)+(n^2)));

% Convert from solution vectors to solution matrices
Vxtemp = zeros(n,n);
Vytemp = zeros(n,n);
for q = 1:n
   Vxtemp(q,1:n) = Vx(((((n+1)-q)*n)-(n-1)):(((n+1)-q)*n));
   Vytemp(q,1:n) = Vy(((((n+1)-q)*n)-(n-1)):(((n+1)-q)*n));
end


% Rotate solution matrices
Vxout = rot90(Vxtemp,3);
Vyout = rot90(Vytemp,3);


% Pad with zeros and take ifft. Expadnum,Eypadnum is used for
% calculating effective permittivity. Expad, Eypad is used for
   plotting.
[nx,ny] = size(geometry);

res = a/nx;
% restTEST = a/(2*nx);
%
% nxTEST = (nx*2)+1;
% nyTEST = (nx*2)+1;

padx = nx - n;
pady = ny - n;

% padxTEST = (nxTEST) - n;
% padyTEST = (nyTEST) - n;

realx = 0:res:(a-(1*res));
realy = 0:res:(a-(1*res));

% TESTx = 0:resTEST:(a-resTEST);
% TESTy = 0:resTEST:(a-resTEST);

Expadnum = padarray(Vxout,[(floor(padx/2)) (floor(pady/2))]);
[rows,cols] = size(Expadnum);
exnum = rows*cols*(ifftn(ifftshift(Expadnum)));

Eypadnum = padarray(Vyout,[(floor(padx/2)) (floor(pady/2))]);
[rows,cols] = size(Eypadnum);
eynum = rows*cols*(ifftn(ifftshift(Eypadnum)));


% ExpadnumTEST = padarray(Vxout,[(floor(padxTEST/2)) (floor(
   padyTEST/2))]);
% [rows,cols] = size(ExpadnumTEST);
% exnumTEST = rows*cols*(ifftn(ifftshift(Expadnum)));
%
% EypadnumTEST = padarray(Vyout,[(floor(padxTEST/2)) (floor(
   padyTEST/2))]);
% [rows,cols] = size(EypadnumTEST);
% eynumTEST = rows*cols*(ifftn(ifftshift(Eypadnum)));
```

```
126
127 Exnum = zeros(nx,ny);
128 Eynum = zeros(nx,ny);
129
130 % ExnumTEST = zeros(nxTEST,nyTEST);
131 % EynumTEST = zeros(nxTEST,nyTEST);
132
133 % Adjust axes and origo in any pair of solution matrices such that
      origo is
134 % in top left corner. Adjust signs for coordinate transform.
135 switch origo
136     case 'bl'
137
138     case 'br'
139
140     case 'tr'
141         exnum = rot90(exnum,1);
142         eynum = rot90(eynum,1);
143 %         exnumTEST = rot90(exnum,1);
144 %         eynumTEST = rot90(eynum,1);
145
146     case 'tl'
147         exnum = rot90(exnum,2);
148         eynum = rot90(eynum,2);
149 %         exnumTEST = rot90(exnum,2);
150 %         eynumTEST = rot90(eynum,2);
151 end
152
153
154 for it1 = 1:nx
155     for it2 = 1:ny
156         Exnum(it1,it2) = exnum(it1,it2)*exp(1i*((kx*realx(it2)) +
              (ky*realy(it1))));
157         Eynum(it1,it2) = eynum(it1,it2)*exp(1i*((kx*realx(it2)) +
              (ky*realy(it1))));
158     end
159 end
160
161 % for it1 = 1:(nxTEST)
162 %     for it2 = 1:(nyTEST)
163 %         ExnumTEST(it1,it2) = exnumTEST(it1,it2)*exp(1i*((kx*
      TESTx(it2)) + (ky*TESTy(it1))));
164 %         EynumTEST(it1,it2) = eynumTEST(it1,it2)*exp(1i*((kx*
      TESTx(it2)) + (ky*TESTy(it1))));
165 %     end
166 % end
167 % figure(1)
168 % imshow(real(Eynum))
169 % figure(2)
170 % imshow(imag(Eynum))
171
172 % Calculate P
173
174 px = zeros(199,199);
175 py = zeros(199,199);
176 % pxTEST = zeros(nxTEST,nyTEST);
177 % pyTEST = zeros(nxTEST,nyTEST);
178
179 chi = (geometry -1);
180
181 for i1 = 1:ny
182     for j1 = 1:nx
183         px(i1,j1) = Exnum(i1,j1)*eps0*chi(i1,j1);
184         py(i1,j1) = Eynum(i1,j1)*eps0*chi(i1,j1);
185     end
186 end
```

```
% figure(1)
% plot(0:298,real(Exnum(:,150)),'b',0:298,imag(Exnum(:,150)),'r')
% figure(2)
% plot(0:298,real(Eynum(:,150)),'b',0:298,imag(Eynum(:,150)),'r')


% figure(1)
% plot(0:498,real(Exnum(250,:)),'b',0:498,imag(Exnum(250,:)),'r')
% figure(2)
% plot(0:498,real(Eynum(250,:)),'b',0:498,imag(Eynum(250,:)),'r')

% figure(3)
% plot(0:198,real(Exnum(100,:)),'b',0:198,imag(Exnum(100,:)),'r')
% figure(4)
% plot(0:198,real(Eynum(100,:)),'b',0:198,imag(Eynum(100,:)),'r')

% figure(2)
% subplot(2,2,1)
% plot(0:998,real(Exnum(500,:)),'b',0:998,imag(Exnum(500,:)),'r')
% title('Ex along x-axis')
% subplot(2,2,2)
% plot(0:998,real(Eynum(500,:)),'b',0:998,imag(Eynum(500,:)),'r')
% title('Ey along x-axis')
%
% subplot(2,2,3)
% plot(0:998,real(Exnum(:,500)),'b',0:998,imag(Exnum(:,500)),'r')
% title('Ex along y-axis')
% subplot(2,2,4)
% plot(0:998,real(Eynum(:,500)),'b',0:998,imag(Eynum(:,500)),'r')
% title('Ey along y-axis')

plotres = a/499;
plotaxis = 0:(plotres):(a-plotres);

% figure(5)
% subplot(2,2,1)
% plot(plotaxis,real(Exnum(250,:)),'b',plotaxis,imag(Exnum(250,:))
    ,'r')
% title('Ex along x-axis')
% subplot(2,2,2)
% plot(plotaxis,real(Eynum(250,:)),'b',plotaxis,imag(Eynum(250,:))
    ,'r')
% title('Ey along x-axis')
%
% subplot(2,2,3)
% plot(plotaxis,real(Exnum(:,250)),'b',plotaxis,imag(Exnum(:,250))
    ,'r')
% title('Ex along y-axis')
% subplot(2,2,4)
% plot(plotaxis,real(Eynum(:,250)),'b',plotaxis,imag(Eynum(:,250))
    ,'r')
% title('Ey along y-axis')

% figure(1)
% subplot(2,2,1)
% plot(0:498,real(Exnum(250,:)),'b',0:498,imag(Exnum(250,:)),'r')
% title('Ex along x-axis')
% subplot(2,2,2)
% plot(0:498,real(Eynum(250,:)),'b',0:498,imag(Eynum(250,:)),'r')
% title('Ey along x-axis')
%
% subplot(2,2,3)
% plot(0:498,real(Exnum(:,250)),'b',0:498,imag(Exnum(:,250)),'r')
% title('Ex along y-axis')
% subplot(2,2,4)
% plot(0:498,real(Eynum(:,250)),'b',0:498,imag(Eynum(:,250)),'r')
```

```
% title('Ey along y-axis')


% figure(2)
% subplot(2,2,1)
% plot(0:498,real(px(249,:)),'b',0:498,imag(px(249,:)),'r')
% title('Px along x-axis')
% subplot(2,2,2)
% plot(0:498,real(py(249,:)),'b',0:498,imag(py(249,:)),'r')
% title('Py along x-axis')
%
% subplot(2,2,3)
% plot(0:498,real(px(:,249)),'b',0:498,imag(px(:,249)),'r')
% title('Px along y-axis')
% subplot(2,2,4)
% plot(0:498,real(py(:,249)),'b',0:498,imag(py(:,249)),'r')
% title('Py along y-axis')

% figure(6)
% subplot(2,2,1)
% plot(plotaxis,real(px(250,:)),'b',plotaxis,imag(px(250,:)),'r')
% title('Px along x-axis')
% subplot(2,2,2)
% plot(plotaxis,real(py(250,:)),'b',plotaxis,imag(py(250,:)),'r')
% title('Py along x-axis')
%
% subplot(2,2,3)
% plot(plotaxis,real(px(:,250)),'b',plotaxis,imag(px(:,250)),'r')
% title('Px along y-axis')
% subplot(2,2,4)
% plot(plotaxis,real(py(:,250)),'b',plotaxis,imag(py(:,250)),'r')
% title('Py along y-axis')

% x = 0:2:(cols-1);
% y = 0:2:(rows-1);
%
% %Plot Re[P]
% figure(23)
% quiver(x,y,real(px((x)+1,(y)+1)),real(py((x)+1,(y)+1)),'b');
% legend('Re(P)')
% set(gca,'position',[0.138 0.2 0.72 0.72]);
% set(gca,'FontName', 'times');
% set(gca,'FontSize', 16);
% set(gca,'FontWeight','normal')
% set(get(gca,'children'),'LineWidth',0.1);
% print fisk -deps
%
% %Plot Im[P]
% figure(24)
% quiver(x,y,imag(px(x+1,y+1)),imag(py(x+1,y+1)),'r');
% legend('Im(P)')
% set(gca,'position',[0.138 0.2 0.72 0.72]);
% set(gca,'FontName', 'times');
% set(gca,'FontSize', 16);
% set(gca,'FontWeight','normal')
% set(get(gca,'children'),'LineWidth',0.1);
% print fisk -deps



% Expad = padarray(Vxout,[5 5]);
% [rows,cols] = size(Expad);
% Ex = rows*cols*(ifft2(ifftshift(Expad)));
%
% Eypad = padarray(Vyout,[5 5]);
% [rows,cols] = size(Eypad);
```

```
% Ey = rows*cols*(ifft2(ifftshift(Eypad)));

%{
% Calculate D
Dx = zeros(nx,ny);
Dy = zeros(nx,ny);


for i = 1:nx
    for j = 1:ny
        Dx(i,j) = rot90(geometry(i,j))*Exnum(i,j);
        Dy(i,j) = rot90(geometry(i,j))*Eynum(i,j);
    end
end
%}
%%%% Plotting %%%%
% Only the desired plots should be plotted for efficiency. Comment
% all other figures that are not interesting. There are 12
   different
% figures.

%Plot real part of Structure
%figure(1)
%meshz(real(geometry))
%set(gca,'position',[0.138 0.2 0.72 0.72]);
%set(gca,'FontName', 'times');
%set(gca,'FontSize', 16);
%set(gca,'FontWeight','normal')
%set(get(gca,'children'),'LineWidth',0.1);
%title('Re[Structure]')
%xlabel('x axis')
%ylabel('y axis')
%zlabel('Re[\epsilon(x,y)]')
%print fisk -deps

% Plot imag part of Structure (for conductors)
%figure(2)
%meshz(imag(geometry))
%set(gca,'position',[0.138 0.2 0.72 0.72]);
%set(gca,'FontName', 'times');
%set(gca,'FontSize', 16);
%set(gca,'FontWeight','normal')
%set(get(gca,'children'),'LineWidth',0.1);
%title('Im[Structure]')
%xlabel('x axis')
%ylabel('y axis')
%zlabel('Im[\epsilon(x,y)]')
%print fisk -deps

% Plot E as vector field
% x = 0:2:(cols-1);
% y = 0:2:(rows-1);

%Plot Re[E]
% figure(3)
% quiver(x,y,real(Exnum((x)+1,(y)+1)),real(Eynum((x)+1,(y)+1)),'b
   ');
% legend('Re(E)')
% set(gca,'position',[0.138 0.2 0.72 0.72]);
% set(gca,'FontName', 'times');
% set(gca,'FontSize', 16);
% set(gca,'FontWeight','normal')
% set(get(gca,'children'),'LineWidth',0.1);
% print fisk -deps
%
% %Plot Im[E]
```

```
% % figure(4)
% % quiver(x,y,imag(Exnum(x+1,y+1)),imag(Eynum(x+1,y+1)),'r');
% % legend('Im(E)')
% % set(gca,'position',[0.138 0.2 0.72 0.72]);
% % set(gca,'FontName', 'times');
% % set(gca,'FontSize', 16);
% % set(gca,'FontWeight','normal')
% % set(get(gca,'children'),'LineWidth',0.1);
% % print fisk -deps
% % %Plot D as vector field
% % xnum = 0:10:nx-1;
% % ynum = 0:10:ny-1;
%{
% Plot Re[D]
figure(5)
quiver(xnum,ynum,real(Dx(xnum+1,ynum+1)),real(Dy(xnum+1,ynum+1)),'
    Color',[0,0.6,0.5]); %,'Color',[0,0.6,0.5]
legend('Re(D)')
set(gca,'position',[0.138 0.2 0.72 0.72]);
set(gca,'FontName', 'times');
set(gca,'FontSize', 16);
set(gca,'FontWeight','normal')
set(get(gca,'children'),'LineWidth',0.1);
print fisk -deps

% Plot Im[D]
figure(6)
quiver(xnum,ynum,imag(Dx(xnum+1,ynum+1)),imag(Dy(xnum+1,ynum+1)),'
    Color',[0.6,0.6,0.5]);
legend('Im(D)')
set(gca,'position',[0.138 0.2 0.72 0.72]);
set(gca,'FontName', 'times');
set(gca,'FontSize', 16);
set(gca,'FontWeight','normal')
set(get(gca,'children'),'LineWidth',0.1);
print fisk -deps

% Plot All components f = Ex, Ey, Dx, Dy as f(x,y).

[spatDx, spatDy] = size(Dx);

figure(7)
meshz(0:(a/spatDx):a,0:(a/spatDy):a,real(Dx))
xlabel('x-axis')
ylabel('y-axis')
set(gca,'position',[0.138 0.2 0.72 0.72]);
set(gca,'FontName', 'times');
set(gca,'FontSize', 18);
set(gca,'FontWeight','normal')
set(get(gca,'children'),'LineWidth',0.1);
zlabel('Re[Dx]')
print fisk -deps

figure(8)
meshz(0:(a/spatDx):a,0:(a/spatDy):a,imag(Dx))
xlabel('x-axis')
ylabel('y-axis')
set(gca,'position',[0.138 0.2 0.72 0.72]);
set(gca,'FontName', 'times');
set(gca,'FontSize', 18);
set(gca,'FontWeight','normal')
set(get(gca,'children'),'LineWidth',0.1);
zlabel('Im[Dx]')
print fisk -deps
%}
  [spatx,spaty] = size(Exnum);
```

```
%
% figure(9)
% meshz(0:(a/spatx):a,0:(a/spaty):a,real(Exnum))
% xlabel('x-axis')
% ylabel('y-axis')
% set(gca,'position',[0.138 0.2 0.72 0.72]);
% set(gca,'FontName', 'times');
% set(gca,'FontSize', 18);
% set(gca,'FontWeight','normal')
% set(get(gca,'children'),'LineWidth',0.1);
% zlabel('Re[Ex]')
% print fisk -deps
%
% figure(10)
% meshz(0:(a/spatx):a,0:(a/spaty):a,imag(Exnum))
% xlabel('x-axis')
% ylabel('y-axis')
% set(gca,'position',[0.138 0.2 0.72 0.72]);
% set(gca,'FontName', 'times');
% set(gca,'FontSize', 18);
% set(gca,'FontWeight','normal')
% set(get(gca,'children'),'LineWidth',0.1);
% zlabel('Im[Ex]')
% print fisk -deps
%
% figure(11)
% subplot(1,2,1)
% meshz(0:(a/spatx):a,0:(a/spaty):a,real(Eynum))
% xlabel('x-axis')
% ylabel('y-axis')
% set(gca,'position',[0.138 0.2 0.72 0.72]);
% set(gca,'FontName', 'times');
% set(gca,'FontSize', 18);
% set(gca,'FontWeight','normal')
% set(get(gca,'children'),'LineWidth',0.1);
% zlabel('Re[Ey]')
% print fisk -deps
%
% figure(12)
% meshz(0:(a/spatx):a,0:(a/spaty):a,imag(Eynum))
% xlabel('x-axis')
% ylabel('y-axis')
% set(gca,'position',[0.138 0.2 0.72 0.72]);
% set(gca,'FontName', 'times');
% set(gca,'FontSize', 18);
% set(gca,'FontWeight','normal')
% set(get(gca,'children'),'LineWidth',0.1);
% zlabel('Im[Ey]')
% print fisk -deps
toc
end
```

```
function E = solve2DTrans(geometry,a,f,n,kx,ky,uz)

% Difference from solve1D is that u is given as argument.
% Geometry matrix should have dimensions > 200x200.
tic

%%%%% Make n odd %%%%%
if(mod(n,2) == 0)
    n = n+1;
end

%%%%% Creating Source %%%%%
if nargin == 7
    u = zeros(n^2,1);
```

```
    u(floor(((n^2)/2)+1),1) = uz;
else
    u = zeros(n^2,1);
    u(floor(((n^2)/2)+1),1) = 1;
end

%%%%% Creating Constants %%%%%
omega = 2*pi*f;
c = 3*(10^8);
uzero = 4*pi*(10^(-7));
sigma = ((omega/(c))^2);
phi = complex(0,omega*uzero);

%%%%% Creating Vectors %%%%%
[w,k] = makeVectors2d(a,n);
if nargin == 7
    k = ones(n^2,2);
    k(:,1) = kx;
    k(:,2) = ky;
end

%%%%% Creating Matrices %%%%%
sq = curlOperator2d(w,k);

epsilon = convmat(geometry,n,n,1);
leftside = sq-(sigma*epsilon);
Vz = phi*(leftside\u);
Vtemp = zeros(n,n);

% Convert from solution vector to solution matrix
for q = 1:n
   Vtemp(q,1:n) = Vz(((((n+1)-q)*n)-(n-1)):(((n+1)-q)*n));
end

Vout = rot90(Vtemp,3);

% Pad with zeros and take ifft.
Epad = padarray(Vout,[100 100]); % Pad with zeros
[rows,cols] = size(Epad);
E = rows*cols*(ifft2(ifftshift(Epad)));

meshz(imag(E))
end
```

```
function [w,k] = makeVectors2d(a,n)
% Assuming quadratic unit cells

w = zeros(n.^2,2);
k = (1/sqrt(2))*(0.01/a)*ones(n.^2,2);
wx = zeros(1,n);
wy = zeros(1,n);

for i = -floor(n/2):1:floor(n/2)
   wx(i+floor(n/2)+1) = (2*pi)/(a)*i;
   wy(i+floor(n/2)+1) = (2*pi)/(a)*i;
end

for p = 1:(n)
    for j = 1:(n)
        w(j + (n*(p-1)),1) = wx(p);
        w(j + (n*(p-1)),2) = wy(j);
    end
end
%w
% for o = 1:(n^2)
% end
```

```
end
```

```
function sq = curlOperator2d(w,k)
% w = [wx,wy] k = [kx,ky], both comlumn vectors
[row,col] = size(w);
sq = zeros(row,row);

tx = w(:,1)+k(:,1);
ty = w(:,2)+k(:,2);

if (col == 2)
for i = 1:row
    sq(i,i) = ((tx(i))^2) + ((ty(i))^2);
end
end
end
```

```
function [Txsq,Tysq,TxTy] = outerproduct(w,k)
[nsq,dim] = size(w);

T = w+k;
TxTy = zeros(nsq,nsq);
Txsq = zeros(nsq,nsq);
Tysq = zeros(nsq,nsq);

Txsqvec = (T(:,1).^2);
Tysqvec = (T(:,2).^2);

% Txsqvec = (T(:,1)*T(:,1));
% Tysqvec = (T(:,2)*T(:,2));
for i = 1:nsq
   TxTy(i,i) = T(i,1)*T(i,2);
   Txsq(i,i) = Txsqvec(i);
   Tysq(i,i) = Tysqvec(i);
end
end
```

C.3 Functions for 1D PWEM algorithm

```
function Ek = solve1D(geometry,a,f,n,knew)
%tic
%%%%% Make n odd %%%%%
if(mod(n,2) == 0)
    n = n+1;
end

%%%%% Creating Source %%%%%
u = zeros(n,1);
u(floor(n/2)+1) = 1;

%%%%% Creating Constants %%%%%
omega = 2*pi*f;
c = 1/(sqrt((pi*4e-7)*(8.85e-12)));
uzero = 4*pi*(10^(-7));
sigma = ((omega/(c))^2);
phi = complex(0,omega*uzero);

%%%%% Creating Vectors %%%%%
[w,k] = makeVectors(a,n);

if nargin == 5
    k = knew*ones(n,1);
end

%%%%% Creating Matrices %%%%%
sq = curlOperator(w+k);
epsilon = convmat(geometry,n,1,1);
% A is the fftshifted FT of geometry.

%%%%% Calculating Matrix Equation %%%%%
leftside = sq-(sigma*epsilon);
V = phi*(leftside\u);
%%%%% Transform back to r-domain %%%%%

[row,col] = size(geometry);

varexp = (col-n)/2;
%varexp = 99950;
Vnew = [zeros(varexp,1); V; zeros(varexp,1)];
Vnewshift = ifftshift(Vnew);
Vnewshiftfft = (length(Vnewshift))*ifft(Vnewshift);
E = double(Vnewshiftfft);
% varexp is the padding length on each side of vector, and
% adjusts number of points in output vector.
% i. e. if E should have 25000 points, then varexp = (25000-n)/2.

%%%%% Determine E with k-dependence %%%%%

axis = 0:((2*varexp)+n-1);
axis = reshape(axis,length(axis),1);
factor = varexp + (n/2);

[newrow,newcol] = size(E);

res = a/newrow;

newaxis = 0:res:(a-res);

%Ek = E.*exp(1i*(k(1)/(factor))*axis);
Ek = zeros(1,newcol);

for q = 1:newrow
    Ek(q) = E(q)*exp(1i*k(1)*newaxis(q));
```

```
end
%%%%% Plot Structure, E and Ek %%%%%

% Plot Structure
%figure(1)
%h = area(geometry);
%h.FaceColor = [0 0.5 0.5];
%set(gca,'position',[0.138 0.2 0.72 0.72]);
%set(gca,'FontName', 'times');
%set(gca,'FontSize', 16);
%set(gca,'FontWeight','normal')
%set(get(gca,'children'),'LineWidth',1);
%title('Structure')
%xlabel('x axis')
%ylabel('\epsilon(x)')
%set(gca,'XLim',[0 4e4])  % x-omr?de som skal vises
%set(gca,'YLim',[0 40])
%legend('Permittivity')
%print fisk -deps

% % Plot E*exp(-ikr)
% figure(5)
% plot(0:((2*varexp)+n-1),real(E),'b',0:((2*varexp)+n-1),imag(E),'
    r');
% set(gca,'position',[0.138 0.2 0.72 0.72]);
% set(gca,'FontName', 'times');
% set(gca,'FontSize', 16);
% set(gca,'FontWeight','normal')
% set(get(gca,'children'),'LineWidth',2);
% title('E-field in Structure')
% xlabel('Scaled x axis')
% ylabel('E * exp(-ikx)')
% legend('Re(E)','Im(E)')
% print fisk -deps

%Plot E
figure(6)
plot(newaxis,real(Ek),'b',newaxis,imag(Ek),'r'); %,newaxis,imag(Ek
    ),'r'
set(gca,'position',[0.138 0.2 0.72 0.72]);
set(gca,'FontName', 'times');
set(gca,'FontSize', 16);
set(gca,'FontWeight','normal')
set(get(gca,'children'),'LineWidth',2);
title('E-field in Structure with k dependence')
xlabel('Scaled x axis')
ylabel('E')
legend('Re(E)','Im(E)') %,'Im(E)'
print fisk -deps
%toc
end
```

```
function [w,k] = makeVectors(a,n)
% This function calculates the vectors w and k for the matrix
    equation.
% a is the length of the unit cell in r-space.
% n is the length of the vectors w and k.
if(mod(n,2) == 0)
    n = n+1;
end
kt(1:n) = 0.01/a;

wt = zeros(1,n);

for i = -floor(n/2):1:floor(n/2)
   wt(i+floor(n/2)+1) = ((2*pi)/(a))*i;
```

```
end
k = transpose(kt); % transposing column vector into row vector
w = transpose(wt); % transposing column vector into row vector
end
```

```
function squared = curlOperator(T)
% This function creates the matrix curl operator with the vectors
    w and k.
% Input T = w+k
% squared is a nxn matrix with (w+k)^2 along the diagonal.
n = length(T);
squared = eye(n); % Creating identity matrix
for i = 1:n
    for j = 1:n
       if (i == j)
           squared(i,j) = T(i).^2;
       end
    end
end
end
```

C.4 Function for creating 1D and 2D convolution matrices with and without windowing

```
function C = convmat(A,P,Q,R,pad)
% CONVMAT  Rectangular convolution matrix C for both 1D and 2D PWEM algorithms.
% Convolution matrix algorithm based on : https://www.youtube.com/watch?v=hWSMHcc3CxQ
% Video made by Dr. Raymond Rumpf.
% A input is structure (vector or matrix)
% P,Q,R are number of spatial harmonics along each dimension (x,y,z)
% For 1D : P = n, Q = R = 1 , For 2D : P = Q = n, R = 1

% Change row vector into column vector
[dimx,dimy] = size(A);
if (dimx == 1)
   A = reshape(A,dimy,dimx);
end

[Nx,Ny,Nz] = size(A);
NH = P*Q*R; % Total number of spatial harmonics

% Shifting the indices to be distributed around zero.

p = [-floor(P/2): + floor(P/2)]; % indices along x
q = [-floor(Q/2): + floor(Q/2)]; % indices along y
r = [-floor(R/2): + floor(R/2)]; % indices along z

p0 = 1 + floor(Nx/2);
q0 = 1 + floor(Ny/2);
r0 = 1 + floor(Nz/2);

if (pad == 0)
    A = fftshift(fftn(A)/(Nx*Ny*Nz));
%     p0 = 1 + floor(Nx/2);
%     q0 = 1 + floor(Ny/2);
%     r0 = 1 + floor(Nz/2);
    hammingwindow = window2((2*P)-1,(2*Q)-1,@blackmanharris);
    pad
else
    ATest = fftshift(fftn(A)/(Nx*Ny*Nz));
    Pfictive = P - pad;
    Qfictive = Q - pad;

    Plp = ((2*Pfictive)-1);
    Qlp = ((2*Qfictive)-1);

    Atest = ATest((p0-floor(Plp/2)):(p0+floor(Plp/2)),(q0-floor(Qlp/2)):(q0+floor(Qlp/2))); % Low-pass filter as if n = Pfictive = Qfictive
    A = padarray(Atest,[pad pad]); % Pad to obtain "n = 51"
    p0 = 1 + floor(((2*P)-1)/2);
    q0 = 1 + floor(((2*Q)-1)/2);
    hammingwindowTEMP = window2(Plp,Qlp,@blackmanharris);
    hammingwindow = padarray(hammingwindowTEMP,[pad pad]);
    pad
end
size(A);
size(hammingwindow);
%hammingwindow = window2((P+2),(Q+2),@hamming);
%hammingwindow = window2((2*P)-1,(2*Q)-1,@blackmanharris);


% Compute array indices of center harmonic
```

```
% p0 = 1 + floor(Nx/2);
% q0 = 1 + floor(Ny/2);
% r0 = 1 + floor(Nz/2);

p0w = 1 + floor(((2*P)-1)/2);
q0w = 1 + floor(((2*Q)-1)/2);

for rrow = 1:R; % R = 1 in 2D case
for qrow = 1:Q; % Q = 1 in 1D case
for prow = 1:P;
    row = ((rrow-1)*P*Q) + ((qrow-1)*P) + prow;
    for rcol = 1:R; % R = 1 in 2D case
    for qcol = 1:Q; % Q = 1 in 1D case
    for pcol = 1:P;
        col = ((rcol-1)*P*Q) + ((qcol-1)*P) + pcol;
        pfft = p(prow)- p(pcol);
        qfft = q(qrow)- q(qcol);
        rfft = r(rrow)- r(rcol);
        indx = p0w + pfft;
        indy = q0w + qfft;
        factor = hammingwindow(indx,indy,1);
        %factor = 1;
        C(row,col) = A(p0 + pfft,q0 + qfft,r0 + rfft)*factor;
        %C(row,col) = A(p0test + pfft,q0test + qfft,r0 + rfft)*
            factor;
        % Zero order harmonics are placed along diagonal of matrix
    end
    end
    end
end
end
end
%C
end
```

C.5 Function for simulating effective permeability μ according to Casimir and Landu-Lifshitz formalisms

```
function [RJmu,LLmu,Eta,Gamma,Psi,Casimir] = effectiveMu(
    omegastart,omegastop,step,structure,a)
uzero = 4*pi*(10^(-7));
% Calculation of effective mu according to Russakoff-Jackson (
    Casimir) and
% Landau-Lifshitz formalism
clight = 3e8;
RJmu = zeros(step,1);
LLmu = zeros(step,1);

Eta = zeros(step,1);
Gamma = zeros(step,1);
Psi = zeros(step,1);
Casimir = zeros(step,1);

omegares = (omegastop-omegastart)/step;

for it = 1:step
    omega = it*omegares;
    it
    [eta,gamma,psi,casimir] = solveTensorPar(structure,'bl',1,((
        omega)/(2*pi)),41,0,0.3,0,0,3,0.5,0.5);

    Eta(it) = eta;
    Gamma(it) = gamma;
    Psi(it) = psi;
    Casimir(it) = casimir;

    RJU = casimir;
    LLU = eta+gamma+psi;

    RJmu(it) = (1)/(1-(omega*omega*a*a*(1/(clight*clight))*RJU));
    LLmu(it) = (1)/(1-(omega*omega*a*a*(1/(clight*clight))*LLU));

end
end
```